TABLE 2
Mean Artifact Scores in End-Diastolic and End-Systolic Phases with Half and Segmental Reconstruction Algorithms

Reconstruction Algorithm and Artifact	Heart Rate (beats/min)												
	40	45	50	55	60	65	70	75	80	85	90	95	100
	End-Diastolic Phase												
Half reconstruction algorithm													
Blurring artifact	0.0	0.0	0.0	0.0	0.5	1.0	1.5	1.0	1.0	1.0	2.0	2.5	3.0
Stair-step artifact	0.0	0.0	0.0	0.0	0.0	1.0	1.5	0.0	0.0	1.0	1.5	1.5	2.0
Segmental reconstruction algorithm													
Blurring artifact	0.0	0.0	0.0	0.0	0.5	0.0	0.0	1.0	1.0	0.0	0.0	0.0	1.0
Stair-step artifact	0.0	0.0	0.0	0.0	0.0	0.0	0.0	0.0	0.0	0.0	0.0	0.0	0.0
	End-Systolic Phase												
Half reconstruction algorithm													
Blurring artifact	0.0	0.5	1.0	1.5	1.5	2.5	2.5	3.0	3.0	3.0	3.5	4.0	4.0
Stair-step artifact	0.0	0.0	0.0	0.0	0.0	1.0	2.0	1.5	0.0	1.0	1.5	2.0	2.0
Segmental reconstruction algorithm													
Blurring artifact	0.0	0.5	1.0	0.5	1.5	1.0	1.5	1.5	3.0	2.0	0.5	1.0	2.0
Stair-step artifact	0.0	0.0	0.0	0.0	0.0	0.0	0.5	0.0	0.0	0.0	0.0	0.0	0.0

institutional review board approved this retrospective study. Informed consent was not required.

Multi–Detector Row CT and Image Interpretation

The CT scanner and scanning protocol used to examine patients were the same as those used in the phantom studies. The estimated effective radiation dose was 7.4 mSv. All patients received 100–150 mL of nonionic contrast agent through an intravenous antecubital catheter infused with a flow rate of 3.0–3.5 mL/sec without any premedication. The scanning delay was set with an automatic triggering system (SureStart; Toshiba) (37). As soon as the signal density level in the ascending aorta, which was monitored in real time, reached a predefined threshold of 150 HU, the patient was automatically instructed to maintain a breath hold; at this time, CT data and an ECG trace were obtained. Both a half and a segmental reconstruction algorithm were also applied in human studies. With the ECG trace, retrospective reconstruction was performed for acquisition of phase images starting from early systole (0% of the R-R interval) and ending at the end of diastole (95% of the R-R interval) by using 5% increasing steps; thus, 20 heart phases were obtained. One short-axis image and two long-axis cine images were created with these reconstructed data by using the same software that was used in phantom experiments. The end-diastolic and end-systolic phases were visually determined with these cine images. Short-axis images of the two phases, which covered the whole heart (10-mm section thickness), were used for functional analysis.

CT images were analyzed by an experienced observer (S.K.) without any clinical information. Manual adjustments of endocardial and epicardial borders of each short-axis image were performed. As previously described, papillary muscles were regarded as being part of the LV cavity (10,18). Subsequently, end-diastolic volume (EDV), end-systolic volume (ESV) (both were measured in milliliters), and LV mass (measured in grams) were calculated on the basis of the Simpson rule. LV mass was calculated as a product of the specific gravity of the myocardium (ie, 1.05 g/cm^3) and integrated LV myocardial area (10). Finally, the percentage of EF was calculated with EDV and ESV data (38).

Interobserver Variability of CT Measurements

Because the repeatability of multi–detector row CT measurements is relevant to the amount of agreement, interobserver variability was tested by comparing measurements obtained by two experienced observers (S.K., H.T.) at different times and without any clinical information by using data sets obtained in the first 20 patients.

MR Imaging and Image Interpretation

MR imaging was performed with a 1.5-T whole-body imager (Symphony; Siemens, Erlangen, Germany), with multiple surface coils connected to phased-array receivers. Breath-hold cine MR imaging was performed with the segmented steady-state free precession sequence (13–15). Imaging parameters were as follows: repetition time msec/echo time msec, 3.6/1.8; flip angle, 70°; seven to 15 lines per segment; matrix, 208 × 256; and field of view, 340 × 340. Cine MR images of 10–12 contiguous sections with 10-mm section thickness were obtained in the short-axis plane, covering the entire LV from the base to the apex, to acquire three-dimensional LV data (18,19).

MR images were analyzed by an observer (E.T., with 10 years of experience) without any clinical information but with the aid of commercially available software (Argus; Siemens). Image analysis was followed with manual correction of the LV border, as with multi–detector row CT. Subsequently, various functional parameters were measured with the same method.

Echocardiography and Image Interpretation

For two-dimensional echocardiography, patients underwent imaging in the left lateral decubitus position by using a commercially available system (Sonos 5500; Hewlett-Packard, Palo Alto, Calif). Images were obtained by an observer (M.O., with 8 years of experience) using a 3.5-MHz transducer in the parasternal (long- and short-axis) and apical (two- and four-chamber views) planes and were saved in cine loop format. EF was calculated by the same observer, who was blinded to other information obtained with two- and four-chamber images, and who used the previously validated biplanar Simpson rule (1,2,38–41).

ECG-gated SPECT and Image Interpretation

Each patient underwent exercise thallium 201 (^{201}Tl) SPECT, as described previously (18,42). At the peak exercise level, approximately 74 MBq of ^{201}Tl was injected intravenously. Approximately 10 minutes after the termination of exercise, initial SPECT was performed. Approximately 3–4 hours after termination of the initial examination, an additional 37 MBq of ^{201}Tl was injected, and reinjection SPECT was performed. ECG-gated SPECT images were obtained with a dual-head gamma camera (Millennium; GE Medical Systems, Milwaukee, Wis) equipped with low-energy thin section collimation (30 projections over 180°, eight frames per cardiac cycle, 60 seconds per projection). Two energy windows were used (ie, 30% windows centered on the 70- and 167-keV peaks). ECG-gated perfusion SPECT images were prefiltered with Butterworth filter (order, five; voxel size, 7.2 mm; cutoff frequency, 0.40 cycles per pixel) (18). A zoom factor of 1.28 was used. Data were reconstructed by using a filtered back-projection technique with no attenuation or scatter correction. The EF was automatically calculated with reinjection SPECT images by using the Germano algorithm (3,18,19,43).

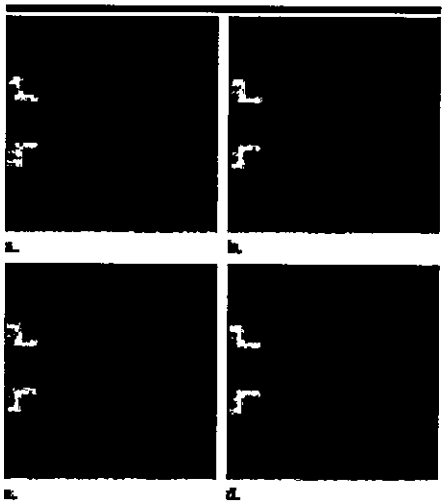

Figure 2. End-diastolic and end-systolic vertical long-axis CT scans of a phantom were reconstructed with half and segmental reconstruction algorithms at a heart rate of 95 beats per minute. (a) End-diastolic and (b) end-systolic vertical long-axis CT scans obtained with half approach. (c) End-diastolic and (d) end-systolic vertical long-axis CT scans obtained with segmental approach. Severe artifacts were observed with a half approach, especially in the end-systolic phase, while no severe artifacts were observed with a segmental approach. Artifacts of reconstructed images obtained with a half approach were so severe that determination of the myocardial outline was difficult.

Statistical Analysis

Data are expressed as mean ± standard deviation. Evaluation of agreement between artifact scores of the phantom was performed by using κ statistics. Systemic error and the degree of agreement of global functional parameters obtained with multi–detector row CT and MR imaging were assessed according to the method described by Bland and Altman (44). Systemic error and the degree of agreement of EF, as calculated with echocardiography and MR imaging data and ECG-gated SPECT and MR imaging data, respectively, were assessed with the same method. The degree of agreement between the two methods was determined as the mean difference (bias), standard deviation of the differences, limits of agreement (mean ± 2 standard deviations), standard error of the mean difference, and 95% confidence interval of the mean difference. A one-sample t test at the 5% significance level was used to determine whether the resulting difference from zero, as an under- or overestimation with multi–detector row CT, was significant. F ratios were used to describe the equality of the standard deviation of difference of EF values obtained with multi–detector row CT with a segmental reconstruction algorithm and MR imaging to EF values obtained with echocardiography and MR imaging and EF values obtained with ECG-gated SPECT and MR imaging.

In a second analysis, linear regression analysis was used to compare the functional values obtained with multi–detector row CT, echocardiography, and ECG-gated SPECT with MR imaging. F ratios were used to describe the equality of standard error of estimates of EF between the correlation of multi–detector row CT with a segmental reconstruction algorithm and MR imaging, between echocardiography and MR imaging, and between ECG-gated SPECT and MR imaging. A P value of less than .05 was considered to indicate statistical significance.

RESULTS

Phantom Studies

The results of phantom studies are shown in Table 2. The κ value for evaluation of agreement between the blurring artifact scores was 0.58, while that between the stair-step artifacts was 0.73. Various artifacts were observed in patients with higher heart rates (≥65 beats per minute) who were evaluated with a half reconstruction algorithm; no substantial artifacts were found in patients evaluated with a segmental reconstruction algorithm, except in those with a heart rate of 80 beats per minute. In patients with higher heart rates (≥65 beats per minute), artifacts of reconstructed images obtained with a half reconstruction algorithm were generally so severe that determination of the myocardial outline was difficult (Fig 2).

Human Studies

No substantial motion artifact was observed, even in patients with a high heart

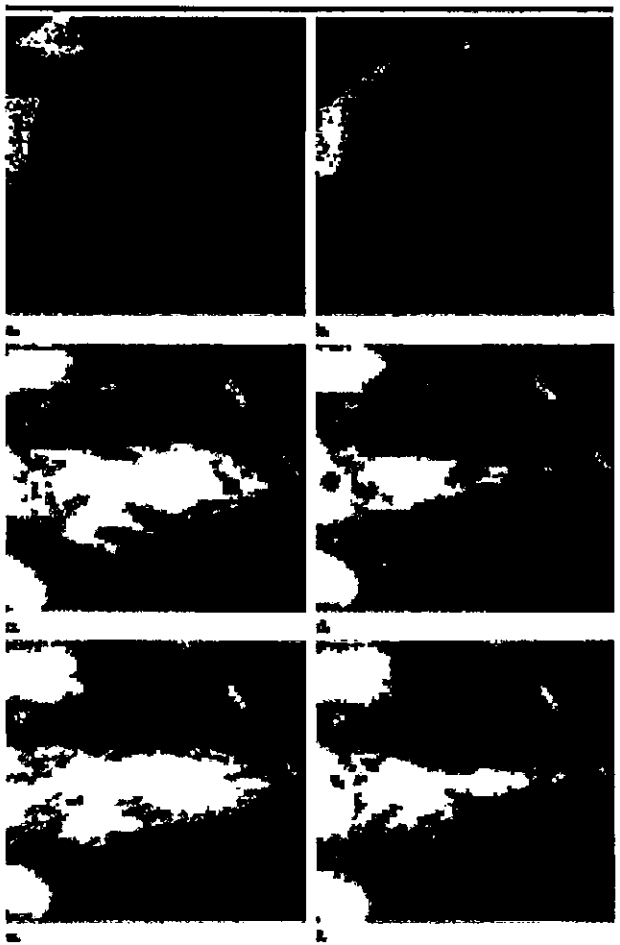

Figure 3. End-diastolic and end-systolic short-axis and vertical long-axis CT scans were reconstructed with a segmental reconstruction algorithm in a patient with a heart rate of 98 beats per minute. (a) Typical end-diastolic and (b) corresponding end-systolic short-axis CT scans. (c) End-diastolic and (d) end-systolic vertical long-axis CT scans. Epicardial (black line in a and b) and endocardial (white line in a and b) tracings exclude epicardial fat and include papillary muscles within ventricular cavity. No severe artifact was found on these scans. End-diastolic and end-systolic vertical long-axis scans were also reconstructed with a half reconstruction algorithm in the same patient. (e) End-diastolic and (f) end-systolic vertical long-axis CT scans. Artifacts of reconstructed images obtained with a half reconstruction algorithm were more severe than those obtained with a segmental approach. Of note, the end systolic size of the LV cavity appeared larger on scans obtained with a half approach than on scans obtained with a segmental approach. Angina pectoris was diagnosed in this patient.

rate, when a segmental reconstruction approach was used. On the other hand, artifacts were generally more severe on reconstructed images obtained with a half approach than on images obtained with a segmental approach if the heart rate was higher (Fig 3).

A summary of data obtained with multi–detector row CT, echocardiography, ECG-gated SPECT, and MR imaging is presented in Tables 3–5. Results of the Bland-Altman analysis are shown in Tables 6–8 and Figures 4–6. Bland-Altman analysis revealed no significant degree of directional measurement bias when data obtained with multi–detector row CT and segmental reconstruction algorithm were compared with data obtained with MR imaging (n = 50). No significant difference of the mean difference from 0 was found for any parameter (n = 50). On the other hand, significant overestimation of ESV ($P < .01$) and underestimation of EF ($P < .001$) were observed with a half approach (n = 50). In terms of EF, the standard deviation of difference between multi–detector row CT with a segmental reconstruction algorithm and MR imaging was significantly less than that between echocardiography and MR imaging (n = 41, $P < .001$) or that between ECG-gated SPECT and MR imaging (n = 27, $P < .001$).

The results of linear regression analysis are shown in Tables 9–11. The data (EF, EDV, ESV, and LV mass) obtained with multi–detector row CT were closely correlated with the data obtained with MR imaging (n = 50). In terms of EF, the standard error of the estimate between multi–detector row CT with a segmental reconstruction algorithm and MR imaging was significantly smaller than that between echocardiography and MR imaging (n = 41, $P < .001$) or that between ECG-gated SPECT and MR imaging (n = 27, $P < .001$).

Interobserver Variability of CT Measurements

An interobserver variability of 8.6% for EF, 7.3% for EDV, 9.6% for ESV, and 10.4% for LV mass was found with the half reconstruction algorithm. On the other hand, an interobserver variability of 5.7% for EF, 6.9% for EDV, 7.0% for ESV, and 9.3% for LV mass was found with the segmental reconstruction algorithm. These results revealed small interobserver variability among the multi–detector row CT measurements.

DISCUSSION

Our results demonstrate that the LV values, including EF, EDV, ESV, and LV mass, obtained with multi–detector row CT and a segmental reconstruction algorithm correlated and agreed with those obtained with MR imaging over a wide range of heart rates. Moreover, functional analysis with multi–detector row CT and a segmental reconstruction algorithm was more accurate than analysis performed with two-dimensional echocardiography or ECG-gated SPECT.

Among the many factors that may affect the accuracy of LV functional measurements with multi–detector row CT, the main limitation is the fact that temporal resolution is worse with multi–detector row CT than with MR imaging (ap-

TABLE 3
LV Measurements with Multi–Detector Row CT and MR Imaging in 50 Patients

Modality and Algorithm	LV EF (%)	EDV (mL)	ESV (mL)	LV Mass (g)
Multi–detector row CT				
Half reconstruction algorithm	46.5 ± 14.4 (12–70)	153.5 ± 59.4 (81–342)	86.2 ± 53.7 (31–263)	142.2 ± 61.7 (60–347)
Segmental reconstruction algorithm	50.1 ± 16.2 (12–76)	153.7 ± 59.5 (85–322)	81.7 ± 55.8 (27–262)	141.1 ± 56.9 (76–326)
MR imaging	51.3 ± 16.1 (12–78)	154.0 ± 64.3 (63–334)	80.6 ± 57.8 (25–257)	138.6 ± 53.9 (67–316)

Note.—Data are mean ± standard deviation. Data in parentheses are the range.

TABLE 4
LV EF in 41 Patients

Modality	LV EF (%)
Echocardiography	54.6 ± 16.7 (15–86)
Multi–detector row CT with segmental reconstruction algorithm	50.7 ± 16.0 (12–76)
MR imaging	51.8 ± 15.9 (12–78)

Note.—Data are mean ± standard deviation. Data in parentheses are the range.

TABLE 5
LV EF in 27 Patients

Modality	LV EF (%)
ECG-gated SPECT	39.6 ± 17.5 (12–74)
Multi–detector row CT	43.1 ± 15.9 (12–75)
MR imaging	43.3 ± 15.0 (12–67)

Note.—Data are mean ± standard deviation. Data in parentheses are the range.

TABLE 6
Multi–Detector Row CT and MR Imaging in 50 Patients

Algorithm and Statistics	LV EF (%)	EDV (mL)	ESV (mL)	LV Mass (g)
Half reconstruction algorithm				
Bias*	−4.7 ± 6.0	−0.49 ± 18.2	5.5 ± 12.4	3.6 ± 19.9
Limits of agreement†	12.0	36.3	24.8	39.8
95% CI	1.7	5.0	3.4	5.5
Standard error of the mean difference	0.8	2.6	1.8	2.8
Regression line	y = −0.11 × +0.8	y = −0.08 × +12.1	y = 0.075 × +11.8	y = 0.14 × −16.0
Segmental reconstruction algorithm				
Bias*	−1.2 ± 4.6	−0.35 ± 15.2	1.1 ± 8.6	2.5 ± 15.0
Limits of agreement†	9.3	30.5	17.3	30.0
95% CI	1.3	4.2	2.4	4.2
Standard error of the mean difference	0.7	2.2	1.2	2.1
Regression line	y = 0.005 × −1.5	y = −0.079 × +11.7	y = −0.036 × +4.0	y = 0.057 × −5.4

Note.—Bland-Altman analysis revealed significant overestimation of ESV ($P < .01$) and underestimation of EF ($P < .001$) in a half approach compared with MR imaging. No significant degree of directional measurement bias was observed in any of the comparisons of multi–detector row CT with a segmental reconstruction algorithm and MR imaging data. No significant difference of the mean difference from 0 was found for any parameter with a segmental approach. CI = confidence interval.
* Data are mean ± standard deviation.
† Two standard deviations.

TABLE 7
EF Difference between Multi–Detector Row CT and MR Imaging and between Echocardiography and MR Imaging

Statistics	Multi–Detector Row CT and MR Imaging (%)	Echocardiography and MR Imaging (%)
Bias*	−1.1 ± 4.1	2.6 ± 9.3
Limits of agreement†	8.2	18.6
95% CI	1.3	2.9
Standard error of the mean difference	0.6	1.5
Regression line	y = 0.007 × −1.5	y = 0.41 × +0.38

Note.—The standard deviation of difference between multi–detector row CT and MR imaging was significantly less than that between echocardiography and MR imaging ($P < .001$). CI = confidence interval.
* Data are mean ± standard deviation.
† Two standard deviations.

TABLE 8
EF Difference between Multi–Detector Row CT and MR Imaging and between ECG-gated SPECT and MR Imaging

Statistics	Multi–Detector Row CT and MR Imaging (%)	ECG-gated SPECT and MR Imaging (%)
Bias*	−0.2 ± 3.7	−3.6 ± 9.9
Limits of agreement†	7.4	19.8
95% CI	1.4	3.7
Standard error of the mean difference	0.7	1.9
Regression line	y = 0.062 × − 2.8	y = 0.17 × −10.8

Note.—The standard deviation of difference between multi–detector row CT and MR imaging was significantly less than that between ECG-gated SPECT and MR imaging ($P < .001$). CI = confidence interval.
* Data are mean ± standard deviation.
† Two standard deviations.

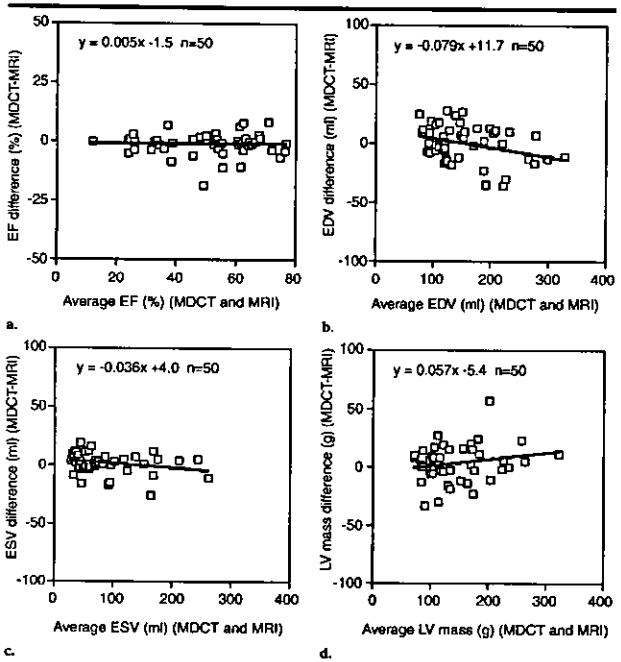

Figure 4. Graphs created with Bland-Altman analysis of (a) LV EF, (b) EDV, (c) ESV, and (d) LV mass, as measured with multi–detector row CT *(MDCT)* with a segmental reconstruction algorithm and MR imaging in 50 patients. Graphs show close agreement between multi–detector row CT and MR imaging. The slopes of the regression lines were not significantly different from 0. No significant differences of the mean difference from 0 were found.

proximately 50 msec). A single helical CT study with a temporal resolution of 400 msec (4) and recent multi–detector row CT studies with a temporal resolution of 125–250 msec performed with a half or biphasic reconstruction algorithm showed close correlation with cineventriculography (32) and MR imaging (33) studies, in terms of EF. Because of the limited temporal resolution, however, systolic images, especially those obtained in patients with a higher heart rate, were shown to be of lower quality (32,33). Additionally, ESV was overestimated, while EDV was not significantly different (4). As a result, underestimation of EF was noted in these studies. In our study, artifacts of reconstructed images obtained with a half approach (temporal resolution of 250 msec) were generally severe if the heart rate was high. In addition, overestimation of ESV and underestimation of EF were observed when a half approach was applied. Juergens et al (32) suggested that data reconstruction algorithms that use segmental data from several heartbeats will likely allow optimization of the analysis of cardiac function with multi–detector row CT. In fact, our phantom experiments demonstrated that a segmental reconstruction algorithm, in which several sets of heartbeat data were used, was more appropriate than a half reconstruction algorithm in terms of reducing motion artifacts, especially in patients with high heart rates.

In the current human studies, no substantial motion artifact was observed, even in patients with a high heart rate, when a segmental reconstruction approach was used. In addition, the various LV functional values obtained with multi–detector row CT and a segmental reconstruction method were shown to correlate and agree with those obtained with MR imaging, which was in agreement with the findings of the preliminary study of Halliburton et al (34). Of note, the standard deviation of EF difference between multi–detector row CT with a segmental approach and MR imaging was significantly less than that between echocardiography and MR imaging or ECG-gated SPECT and MR imaging. Thus, functional analysis with multi–detector row CT and a segmental approach was considered more accurate than functional analysis with two-dimensional echocardiography or ECG-gated SPECT. Previous reports (1,2) suggest that two-dimensional echocardiography is a poor modality to use in the assessment of LV volume and function when ventricular geometry is not uniform. ECG-gated SPECT is also limited when large LV perfusion defects exist (45) or the heart is small (46).

In general, a segmental reconstruction algorithm is effective in shortening the temporal resolution and reducing motion artifacts. At a certain heart rate, however, temporal resolution is not improved, even with a segmental reconstruction approach.

For example, in patients with a heart rate of 80 beats per minute, a temporal resolution of 250 msec is not improved—even with a segmental reconstruction algorithm—which results in increased artifacts in our phantom study. Thus, the functional assessment of certain heart rates may still be less than ideal. A more rapid rotation time (approximately 0.4 seconds per rotation) has been attained with multi–detector row CT (23,34), which will make it possible to shorten and stabilize the temporal resolution with a segmental approach. As a result, functional assessment with multi–detector row CT will be further improved.

Our results reveal good repeatability among multi–detector row CT measurements, especially with a segmental approach, which indicates that determination of LV border with multi–detector row CT and a segmental approach is accurate and reliable. In fact, we did not encounter substantial difficulties due to motion artifacts when determining the LV border, even in patients with a high heart rate. Although there was no significant difference between the mean value of various functional parameters as determined with multi–detector row CT and MR imaging, the Bland-Altman plot reveals wide limits of agreement. In addition, temporal resolution of a segmental reconstruction algorithm is dependent on heart rate, which is not the case with MR imaging. These findings suggest that LV functional measurements obtained with multi–detector row CT and MR imaging may not be interchangeable.

Recent reports show that the use of a β-blocker is effective in lowering heart rates and reducing motion artifacts (31). According to the literature, however, a β-blocker decreases heart rates by an average of only 8 beats per minute (31). In addition, Vogl et al (22) reported that use of a β-blocker did not produce any effect in some patients. Thus, use of a β-blocker is not always effective in the reduction of motion artifacts. In addition, premedication is troublesome in clinical settings, because careful observation and a prolonged stay are required (23); therefore, β-blockers were not routinely used in our institution. Instead, a segmental reconstruction algorithm has been used to improve temporal resolution when the heart rate is high. A segmental approach may not be useful in the precise assessment of coronary arteries, however, especially when the R-R interval is irregular. At present, there is no definitive solution when the heart rate is high and irregular (23). In addition, the use of a β-blocker changes the LV function (47). Thus, functional parameters, with the exception of LV mass, can be unreliable after such premedication. To obtain functional data as added information, use of a β-blocker is unacceptable.

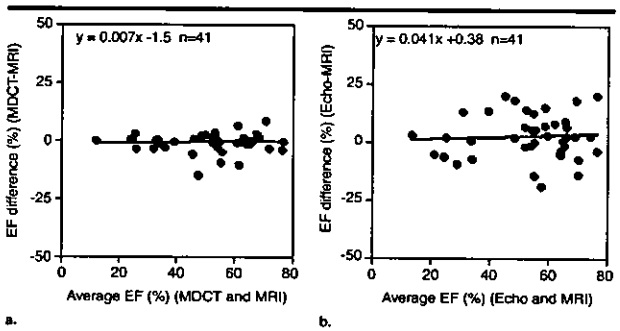

Figure 5. Graphs created with Bland-Altman analysis of LV EF in 41 patients, as measured with (a) multi–detector row CT *(MDCT)* with a segmental reconstruction algorithm and MR imaging or (b) echocardiography and MR imaging. Graphs clearly show that the dispersion between multi–detector row CT and MR imaging was significantly less than that between echocardiography and MR imaging ($P < .001$).

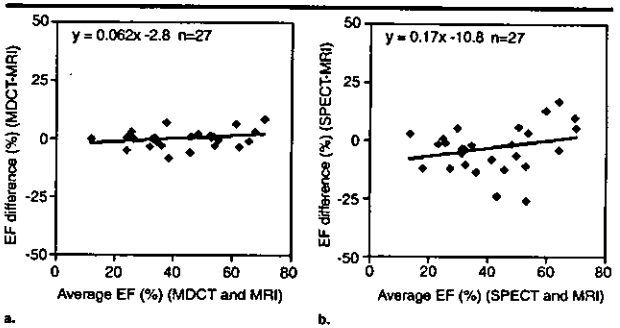

Figure 6. Graphs created with Bland-Altman analysis of LV EF in 27 patients, as measured with (a) multi–detector row CT *(MDCT)* with a segmental reconstruction algorithm and MR imaging or (b) ECG-gated SPECT and MR imaging. Graphs clearly show that the dispersion between multi–detector row CT and MR imaging was significantly less than that between ECG-gated SPECT and MR imaging ($P < .001$).

Radiation dose reduction is clinically important. A large helical pitch, reduced tube current, increased number of detector rows, and faster rotation time can be used to reduce the radiation dose. For example, a larger helical pitch will lead to reduced radiation exposure. When the helical pitch is greater, however, the temporal resolution with a segmental approach becomes worse, which may decrease data fidelity not only for multi–detector row CT coronary information but also for functional analysis. Reduced tube current would serve to directly reduce radiation exposure. Reduced tube current will, however, cause increased image noise. For these reasons, a larger helical pitch or reduced tube current should be avoided (30). Recently, a multi–detector row CT scanner equipped with more detector rows and a faster rotation time has been introduced, resulting in reduction of the radiation dose. In addition, lowering the tube current during unneeded phases of the cycle (48) is effective for radiation dose reduction.

TABLE 9
Linear Regression Analysis between Multi-Detector Row CT and MR Imaging in 50 Patients

Algorithm and Statistics	LV EF	EDV	ESV	LV Mass
Half reconstruction algorithm				
Correlation coefficient	0.93	0.96	0.98	0.95
Standard error of estimates	5.4	17.0	11.4	19.7
Regression line	$y = 0.83x + 3.8$	$y = 0.89x + 17.1$	$y = 0.91x + 13.0$	$y = 1.09x - 8.7$
Segmental reconstruction algorithm				
Correlation coefficient	0.96	0.97	0.99	0.96
Standard error of estimates	4.4	14.0	8.4	15.4
Regression line	$y = 0.97x + 0.5$	$y = 0.90x + 15.6$	$y = 0.96x + 4.9$	$y = 1.01x - 1.1$

Note.—Values obtained with multi-detector row CT were closely correlated with those obtained with MR imaging.

TABLE 10
Linear Regression Analysis for EF between Echocardiography and MR Imaging and between Multi-Detector Row CT with a Segmental Reconstruction Algorithm and MR Imaging in 41 Patients

Statistics	Multi-Detector Row CT and MR Imaging	Echocardiography and MR Imaging
Correlation coefficient	0.95	0.84
Standard error of estimates	5.0	9.2
Regression line	$y = 0.92x + 2.4$	$y = 0.84x + 10.5$

Note.—Standard error of estimates between multi-detector row CT and MR imaging was significantly less than that between echocardiography and MR imaging ($P < .001$).

TABLE 11
Linear Regression Analysis for EF between ECG-Gated SPECT and MR Imaging and between Multi-Detector Row CT with a Segmental Reconstruction Algorithm and MR Imaging in 27 Patients

Statistics	Multi-Detector Row CT and MR Imaging	ECG-gated SPECT and MR Imaging
Correlation coefficient	0.97	0.83
Standard error of estimates	3.6	8.8
Regression line	$y = 1.04x - 1.7$	$y = 0.97x - 2.2$

Note.—Standard error of estimates between multi-detector row CT and MR imaging was significantly smaller than that between ECG-gated SPECT and MR imaging ($P < .001$).

Unfortunately, this strategy may influence the reliability of functional analysis.

The use of multi-detector row CT solely in the assessment of cardiac function does not appear reasonable because of the radiation exposure. It is important, however, that a functional analysis can be conducted by using data obtained with noninvasive coronary imaging without an increase in cost, volume of contrast agent administered, or radiation dose. We believe that multi-detector row CT will be useful in the comprehensive evaluation of coronary arteries and resting LV function.

A limitation of the F test may be the possible violation of the independence assumption, since the variances are about measures taken on the same subject. The critical F values were used for comparison purposes, and statistical significance was not necessarily implied.

In conclusion, the various LV functional parameters of multi-detector row CT with a segmental reconstruction algorithm obtained by using data from several heartbeats correlated and agreed with those obtained with MR imaging. Moreover, the functional analysis with multi-detector row CT with a segmental reconstruction algorithm was more accurate than that with two-dimensional echocardiography or ECG-gated SPECT.

References

1. Buck T, Hunold P, Wentz KU, Tkalec W, Nesser HJ, Erbel R. Tomographic three-dimensional echocardiographic determination of chamber size and systolic function in patients with left ventricular aneurysm. Circulation 1997; 96:4286–4297.
2. Qin JX, Jones M, Shiota T, et al. Validation of real-time three-dimensional echocardiography for quantifying left ventricular volumes in the presence of a left ventricular aneurysm: in vitro and in vivo studies. J Am Coll Cardiol 2000; 36:900–907.
3. Bavelaar-Croon CD, Kayser HW, van der Wall EE, et al. Left ventricular function: correlation of quantitative gated SPECT and MR imaging over a wide range of values. Radiology 2000; 217:572–575.
4. Mochizuki T, Murase K, Higashino H, et al. Two- and three-dimensional CT ventriculography: a new application of helical CT. AJR Am J Roentgenol 2000; 174: 203–208.
5. Lessick J, Sideman S, Azhari H, Marcus M, Grenadier E, Beyar R. Regional three-dimensional geometry and function of left ventricles with fibrous aneurysms: a cine-computed tomography study. Circulation 1991; 84:1072–1086.
6. Lipton MJ, Higgins CB, Farmer D, Boyd DP. Cardiac imaging with a high-speed cine-CT scanner: preliminary results. Radiology 1984; 152:579–582.
7. Lipton MJ, Farmer DW, Killebrew EJ, et al. Regional myocardial dysfunction: evaluation of patients with prior myocardial infarction with fast CT. Radiology 1985; 157:735–740.
8. Rees MR, Feiring AJ, Rumberger JA, MacMillan RM, Clark DL. Heart evaluation by cine CT: use of two new oblique views. Radiology 1986; 159:804–806.
9. Higgins CB. Which standard has the gold? (editorial). J Am Coll Cardiol 1992; 19:1608–1609.
10. Pattynama PM, Lamb HJ, van der Velde EA, van der Wall EE, de Roos A. Left ventricular measurements with cine and spin-echo MR imaging: a study of reproducibility with variance component analysis. Radiology 1993; 187:261–268.
11. Bellenger NG, Burgess MI, Ray SG, et al. Comparison of left ventricular ejection fraction and volumes in heart failure by echocardiography, radionuclide ventricography, cardiovascular magnetic resonance; are they interchangeable? Eur Heart J 2000; 21:1387–1396.
12. de Roos A, Kunz P, Lamb H, et al. Magnetic resonance imaging of ischemic heart disease: why cardiac magnetic resonance imaging will play a significant role in the management of patients with coronary artery disease. J Comput Assist Tomogr 1999; 23(suppl 1):S135–S141.
13. Barkhausen J, Ruehm SG, Goyen M, et al. MR evaluation of ventricular function: true fast imaging with steady-state precession versus fast low-angle shot cine MR imaging: feasibility study. Radiology 2001; 219:264–269.
14. Carr JC, Simonetti O, Bundy J, Li D, Pereles S, Finn JP. Cine MR angiography of the heart with segmented true fast imaging with steady-state precession. Radiology 2001; 219:828–834.
15. Miller S, Simonetti OP, Carr J, Kramer U, Finn JP. MR imaging of the heart with cine true fast imaging with steady-state precession: influence of spatial and temporal resolutions on left ventricular functional parameters. Radiology 2002; 223: 263–269.
16. Heusch A, Koch JA, Krogmann ON, Korbmacher B, Bourgeois M. Volumetric analysis of the right and left ventricle in a porcine heart model: comparison of three-dimensional echocardiography, magnetic resonance imaging and angiography. Eur J Ultrasound 1999; 9:245–255.
17. Lorenz CH, Walker ES, Morgan VL, Klein SS, Graham TP Jr. Normal human right and left ventricular mass, systolic function, and gender differences by cine magnetic resonance imaging. J Cardiovasc Magn Reson 1999; 1:7–21.
18. Tadamura E, Kudoh T, Motooka M, et al. Assessment of regional and global left ventricular function by reinjection Tl-201 SPECT and rest Tc-99m sestamibi ECG-gated SPECT. J Am Coll Cardiol 1999; 33: 991–997.
19. Tadamura E, Kudoh T, Motooka M, et al. Use of technetium-99m sestamibi ECG-gated single-photon emission tomography for the evaluation of left ventricular function following coronary artery bypass graft: comparison with three-dimensional magnetic resonance imaging. Eur J Nucl Med 1999; 26:705–712.
20. Nieman K, Oudkerk M, Rensing BJ, et al. Coronary angiography with multi-slice computed tomography. Lancet 2001; 357:599–603.
21. Achenbach S, Giesler T, Ropers D, et al. Detection of coronary artery stenoses by contrast-enhanced, retrospectively electrocardiographically-gated, multislice spiral computed tomography. Circulation 2001; 103:2535–2538.
22. Vogl TJ, Abolmaali ND, Diebold T, et al. Techniques for the detection of coronary atherosclerosis: multi-detector row CT coronary angiography. Radiology 2002; 223:212–220.
23. Nieman K, Cademartiri F, Lemos PA, Raaijmakers R, Pattynama PM, Feyter PJ. Reliable noninvasive coronary angiography with fast submillimeter multislice spiral computed tomography. Circulation 2002; 106:2051–2054.
24. Schroeder S, Kopp AF, Baumbach A, et al. Noninvasive detection and evaluation of atherosclerotic coronary plaques with multislice computed tomography. J Am Coll Cardiol 2001; 37:1430–1435.
25. Horiguchi J, Nakanishi T, Ito K. Quantification of coronary artery calcium using multidetector CT and a retrospective ECG-gating reconstruction algorism. AJR Am J Roentgenol 2001; 177:1429–1435.
26. White RD, Setser RM. Integrated approach to evaluating coronary artery disease and ischemic heart disease. Am J Cardiol 2002; 90:49L–55L.
27. Hong C, Becker CR, Schoepf UJ, Ohnesorge B, Bruening R, Reiser MF. Coronary artery calcium: absolute quantification in nonenhanced and contrast-enhanced multi-detector row CT studies. Radiology 2002; 223:474–480.
28. Willmann JK, Weishaupt D, Lachat M, et al. Electrocardiographically gated multi-detector row CT for assessment of valvular morphology calcification in aortic stenosis. Radiology 2002; 225:120–128.
29. Hong C, Becker CR, Huber A, et al. ECG-gated reconstructed multi-detector row CT coronary angiography: effect of varying trigger delay on imaging quality. Radiology 2001; 220:712–717.
30. Kopp AF, Schroeder S, Kuettner A, et al. Coronary arteries: retrospectively ECG-gated multi-detector row CT angiography with selective optimization of the image reconstruction window. Radiology 2001; 221:683–688.
31. Ropers D, Baum U, Pohle K, et al. Detection of coronary artery stenoses with thin-slice multi-detector row spiral computed tomography and multiplanar reconstruction. Circulation 2003; 107:664–666.
32. Juergens KU, Grude M, Fallenberg EM, et al. Using ECG-gated multidetector CT to evaluate global left ventricular myocardial function in patients with coronary artery disease. AJR Am J Roentgenol 2002; 179:1545–1550.
33. Juergens KU, Grude M, Maintz D, et al. Multi-detector row CT of left ventricular function with dedicated analysis software versus MR imaging: initial experience. Radiology 2004; 230:403–410.
34. Halliburton SS, Boese JM, Flohr TG, Lieber ML, Kuzmiak SA, White RD. Improved volumetric analysis of the left ventricle using cardiac multislice computed tomography (MSCT) with high temporal resolution image reconstruction (abstr). Radiology 2002; 225(P):389.
35. Ota T, Taguchi K. A navigation tool to assist optimal scan protocol of electrocardiogram (ECG)-gated retrospective reconstruction for multislice helical CT (abstr). Radiology 2001; 221(P):690.
36. Flohr T, Ohnesorge B. Heart rate adaptive optimization of spatial and temporal resolution for electrocardiogram-gated multislice spiral CT of the heart. J Comput Assist Tomogr 2001; 25:907–923.
37. Takase K, Sawamura Y, Igarashi K, et al. Demonstration of the artery of Adamkiewicz at multidetector row helical CT. Radiology 2002; 223:39–45.
38. Dirksen MS, Bax JJ, de Roos A, et al. Usefulness of dynamic multislice computed tomography of left ventricular function in unstable angina pectoris and comparison with echocardiography. Am J Cardiol 2002; 90:1157–1160.
39. Schiller NB, Acquatella H, Ports TA, et al. Left ventricular volume from paired biplane two-dimensional echocardiography. Circulation 1979; 60:547–555.
40. Gordon EP, Schnittger I, Fitzgerald PJ, Williams P, Popp RL. Reproducibility of left ventricular volumes by two-dimensional echocardiography. J Am Coll Cardiol 1983; 2:506–513.
41. Otterstad JE, Froeland G, St John SM, Holme I. Accuracy and reproducibility of biplane two-dimensional echocardiographic measurements of left ventricular dimensions and function. Eur Heart J 1997; 18:507–513.
42. Takahashi N, Tamaki N, Tadamura E, et al. Combined assessment of regional perfusion and wall motion in patients with coronary artery disease with technetium-99m tetrofosmin. J Nucl Cardiol 1994; 1:29–38.
43. Germano G, Kiat H, Kavanagh PB, et al. Automatic quantification of ejection fraction from gated myocardial perfusion SPECT. J Nucl Med 1995; 36:2138–2147.
44. Bland JM, Altman DG. Statistical methods for assessing agreement between two methods of clinical measurement. Lancet 1986; 1:307–310.
45. Manrique A, Faraggi M, Vera P, et al. Tl-201 and Tc-99m MIBI gated SPECT in patients with large perfusion defects and left ventricular dysfunction: comparison with equilibrium radionuclide angiography. J Nucl Med 1999; 40:805–809.
46. Mazzanti M, Germano G, Kiat H, et al. Identification of severe and extensive coronary artery disease by automatic measurement of transient ischemic dilation of the left ventricle in dual-isotope myocardial perfusion SPECT. J Am Coll Cardiol 1996; 27:1612–1620.
47. Ool H, Colucci WS. Pharmacological treatment of heart failure. In: Hardmann JG, Limbird LE, Gilman AG, eds. The pharmacological basis of therapeutics. 10th ed. New York, NY: McGraw-Hill, 2001; 913–916.
48. Jakobs TF, Becker CR, Ohnesorge B, et al. Multislice helical CT of the heart with retrospective ECG gating: reduction of radiation exposure by ECG-controlled tube current modulation. Eur Radiol 2002; 12: 1081–1086.

R353Q Polymorphism, Activated Factor VII, and Risk of Premature Myocardial Infarction in Japanese Men

Masakazu Ogawa, MD; Satoshi Abe, MD; Sadatoshi Biro, MD; Masahiko Saigo, MD; Takashi Kihara, MD; Shiro Setoyama, MD**; Tatsuru Matsuoka, MD; Hitoshi Toda, MD; Hiroyuki Torii, MD; Yoshihiko Atsuchi, MD; Yoshifumi Toyama, MD; Shigeki Tateishi, MD; Shinichi Minagoe, MD; Ikuro Maruyama, MD*; Chuwa Tei, MD

Background The association between myocardial infarction (MI) and the R353Q polymorphism of the Factor VII (FVII) gene, which reportedly influences FVII concentrations, activated Factor VII (FVIIa), or FVII antigen (FVIIag), remains controversial.

Methods and Results The present case–control study in 127 Japanese men with their first MI at or before 45 years of age and 150 matched healthy controls was designed to clarify this association in premature MI. R353Q polymorphism was determined by polymerase chain reaction, and plasma concentrations of FVIIa and FVIIag were assayed. The distribution of the RR, RQ, and QQ genotypes with respect to R353Q polymorphism was 117, 10, and 0 in the patients, and 131, 17, and 2 in the controls. The Q allele was negatively associated with premature MI (odds ratio=0.41, p=0.038). The plasma concentration of FVIIa was slightly higher in patients (55.1±40.9 U/L) than in controls (44.8±20.2 U/L), but not significantly (p=0.078); the plasma concentration of FVIIag did not differ between patients (88.7±15.7%) and controls (87.0±9.0%) (p=0.557). Plasma FVIIa concentrations were influenced by R353Q polymorphism (p<0.001).

Conclusions The Q allele may be protective against premature MI. *(Circ J 2004; 68: 520–525)*

Key Words: Coronary risk factor; Factor VII; Genotype; Premature myocardial infarction; R353Q polymorphism

Factor VII (FVII) is the first enzyme in the extrinsic pathway of the blood coagulation system. Activation of the extrinsic coagulation pathway plays a key role in hemostasis[1] and thus FVII contributes to the occurrence of thrombotic events. Although most FVII circulates in plasma in the zymogen form, small but significant amounts of activated FVII (FVIIa) also are present, and appear to serve as a primer for triggering the extrinsic cascade[2–5] The Northwick Park Heart Study suggested that FVII coagulant activity is independently associated with risk of coronary events in middle-aged men[6,7] and several additional studies have linked elevated concentrations of FVII in plasma to coronary heart disease[8–14] Thus, FVII has become recognized as a hemostatic coronary risk factor.

Plasma FVII concentrations are influenced by both genetic and environmental factors. Green et al reported a strong association between a common polymorphism in exon 8 of the FVII gene (R353Q polymorphism) and plasma FVII[15] which has been confirmed by several other studies[8,9,16–23] especially with respect to FVIIa[24] However, the association between R353Q polymorphism of the FVII gene and myocardial infarction (MI) remains controversial. The contribution of the coagulation system to the pathogenesis of MI can be studied most readily in patients with premature MI, who have less atherosclerotic coronary stenosis than elderly patients[25–28]

We performed a case–control study to determine whether plasma FVIIa concentrations and R353Q polymorphism are associated with risk of premature MI.

(Received April 25, 2003; revised manuscript received March 2, 2004; accepted March 8, 2004)

*Departments of Cardiovascular, Respiratory and Metabolic Medicine, and *Laboratory and Molecular Medicine, Graduate School of Medicine, Kagoshima University and **Kagoshima Prefectural Comprehensive Health Center, Kagoshima, Japan*

Mailing address: Satoshi Abe, MD, Department of Cardiovascular, Respiratory and Metabolic Medicine, Graduate School of Medicine, Kagoshima University, 8-35-1 Sakuragaoka, Kagoshima 890-8520, Japan. E-mail: abe@m2.kufm.kagoshima-u.ac.jp

Methods

Study Population

We investigated 129 consecutive Japanese male patients treated as outpatients at Kagoshima Coronary Care Unit Network (2000–2003), with a first MI occurring before the age of 45 years (mean±SD, 40.4±4.5 years old) and giving informed consent. We angiographically confirmed occlusion or significant stenosis of a coronary artery in all patients. Of the 129 patients, 2 patients, one had Kawasaki disease and another had a coronary artery anomaly, were excluded. The remaining 127 patients (premature MI patients) had a mean age of 43.9±5.1 years at study entry, 3.3±3.8 years after initial MI. Coronary angiography showed single-vessel disease in 93 (73.2%), and multivessel disease in 34 (26.8%). Oral anticoagulant agents were administered to 33 patients. Control subjects were 150 consecutive age-matched healthy Japanese men (43.8±5.1 years old at entry), who underwent a medical checkup at Kagoshima Prefectural Comprehensive Health Center and gave informed consent. None of the control subjects had coronary heart disease according to their medical history or electrocardiography, and none took an oral anticoagulant. This study protocol was approved by the Ethics Committee of Kagoshima University.

Table 1 Characteristics of the Premature MI Patients and Control Subjects

Characteristics	Premature MI patients	Control subjects	p value
No.	127	150	
Age at MI, years	40.4±4.5		
Age at study entry, years	43.9±5.1	43.7±5.1	NS
Total number of coronary risk factors*	1.9±0.8	1.4±0.8	<0.001
Hypertension present (%)	17 (13.4)	24 (16.0)	NS
Hypercholesterolemia present (%)	79 (62.2)	66 (44.0)	0.003
Diabetes mellitus present (%)	29 (22.8)	9 (6.0)	<0.001
Smoking history (%)	110 (86.6)	110 (73.3)	0.006

MI, myocardial infarction. Values are means±SD for continuous variables. NS, not significant.
**Total number of coronary risk factors represents the sum of hypertension, hypercholesterolemia, diabetes mellitus, and smoking (maximum, 4).*

Identification of Conventional Coronary Risk Factors

Hypertension, hypercholesterolemia, diabetes mellitus, and smoking history were evaluated as conventional coronary risk factors. Hypertension was defined by a systolic blood pressure at entry of at least 140 mmHg, a diastolic pressure at least 90 mmHg, a past history of hypertension, or receiving antihypertensive medication. Hypercholesterolemia was defined by a serum total cholesterol concentration at entry of at least 220 mg/dl, a past history of hypercholesterolemia, or receiving lipid-lowering medication. Diabetes mellitus was defined by a fasting plasma glucose concentration at entry of at least 126 mg/dl, a past history of diabetes mellitus, or receiving hypoglycemic medications.

Laboratory Measurements and Techniques

Blood sampling was performed gently by 3 expert physicians at study entry. Samples were collected from all subjects between 07.00 and 11.00 h after an overnight fast, and also 20 min later in a separate syringe. Blood samples were centrifuged for 10 min (3,000 G, 4°C) and divided into plasma, serum, and blood cells. Each was dispensed into a plastic tube respectively and frozen at –80°C until analysis. Plasma concentrations of FVIIa and FVII antigen (FVIIag) were measured using a double-antibody enzyme-linked immunosorbent assay (Roche Diagnostics, Basel, Switzerland)[4] and a coagulation time method (Roche Diagnostics), respectively.

Detection of R353Q Polymorphism

R353Q polymorphism was detected as described by Green et al[15] Amplified fragments were digested with 5 U of *MspI* (New England BioLabs, Beverly, MA, USA) and then subjected to electrophoresis on a 2% agarose gel. Fragments of 205 bp (the R allele) and 272 bp (the Q allele) were detected. Genotypes were defined as RR, RQ, and QQ.

Statistical Analysis

Differences in baseline characteristics between the premature MI patients and control subjects were assessed using chi-square test for categorical variables and by unpaired t-test for continuous variables. Because the distributions of the plasma concentrations of FVIIa and FVIIag were skewed, logarithmic transformation was performed. Log FVIIa and log FVIIag were compared between groups by unpaired t-test. To estimate the contribution of various risk factors to the occurrence of premature MI, multivariate logistic regression analysis was performed with FVIIa, FVIIag, hypertension, hypercholesterolemia, diabetes mellitus, and smoking status as independent variables. The frequencies of genotypes in the premature MI and control groups were compared using the chi-square test with the values predicted by Hardy-Weinberg equilibrium. Frequencies of alleles and genotypes (RR genotype vs RQ+QQ genotypes) were compared using the chi-square test between the premature MI and control groups. The odds ratio (OR) was calculated with a 95% confidence interval (95%CI). Multivariate logistic regression analysis including hypertension, hypercholesterolemia, diabetes mellitus, and smoking status was performed to assess the association between the R353Q polymorphism and the occurrence of premature MI. The effect of the Q allele, with the R allele chosen as the reference allele, was analyzed by the introduction of 3 dummy variables (0, 1, and 2) coding respectively for the number of Q alleles. Categorical independent variables (hypertension, hypercholesterolemia, diabetes mellitus, and smoking status) also were coded as dummy variables (0 for absence and 1 for presence). The association of plasma FVIIa and FVIIag concentrations with each genotype was analyzed with one-way analysis of variance.

Values for continuous variables are expressed as means± SD. A p-value of less than 0.05 was considered to be statistical significant. All computations were carried out with the STAT View-J 5.0 (SAS Institute, NC, Cary, USA) or STATA 7.0 (Stata Corporation, College Station, USA).

Results

Characteristics of the Study Population

Characteristics of the premature MI patients and control subjects are shown in Table 1. There was no significant difference in age at entry between the 2 groups. Patients showed significantly higher prevalences of hypercholesterolemia, diabetes mellitus, and smoking than control subjects (p<0.01), and had a greater number of conventional coronary risk factors than control subjects (p<0.001). Family history was recognized in 7.1% of MI patients.

R353Q Polymorphism and Premature MI

The frequencies of the genotypes and alleles of the R353Q polymorphism are shown in Table 2. The distribution of genotypes was virtually identical to that predicted by the Hardy-Weinberg equilibrium, in both the MI patients (p=0.644) and control subjects (p=0.113). Because

Table 2 Plasma FVIIa and FVIIag Concentrations, and the Distribution of Genotypes and Alleles of R353Q Polymorphism of the Factor VII Gene Between the Premature MI Patients and Control Subjects: Risk of Premature MI

Variable	Premature MI patients	Control subjects
FVIIa (U/L)	55.1±40.7	44.8±20.2
FVIIag (%)	88.7±15.7	87.0±9.0
Genotype, no. (%)		
RR	117 (92.1)	131 (87.3)
RQ	10 (7.8)	17 (11.3)
QQ	0 (0)	2 (1.3)
RQ + QQ	10 (7.8)	19 (12.7)
Alleles, no. (%)		
R	244 (96.1)	279 (93.0)
Q	10 (3.9)	21 (7.0)

FVIIa, activated factor VII; FVIIag, factor VII antigen; MI, myocardial infarction.
Values are means±SD for continuous variables.

Table 3 Risk of Premature Myocardial Infarction for R353Q Polymorphism by Multivariate Logistic Regression Analysis

Variable	OR (95% CI)	p value
Q allele	0.41 (0.18–0.95)	0.038
Hypertension	0.86 (0.42–1.76)	NS
Hypercholesterolemia	1.87 (1.13–3.10)	0.016
Diabetes mellitus	5.37 (2.27–12.74)	<0.001
Smoking status	2.43 (1.25–4.70)	0.009

OR, odds ratio; CI, confidence interval.
The multivariate logistic regression analysis included the Q allele of R353Q polymorphism and hypertension, hypercholesterolemia, diabetes mellitus and smoking history. All independent variables were coded as dummy variables (for R353Q polymorphism, 0 for RR, 1 for RQ, and 2 for QQ; for hypertension, hypercholesterolemia, diabetes mellitus, and smoking history: 0 for absence and 1 for presence).

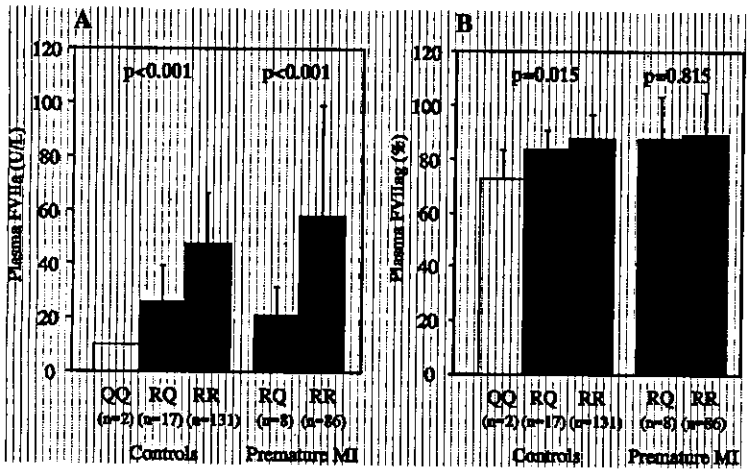

Fig 1. Plasma concentrations of FVIIa (A) and FVIIag (B) according to R353Q polymorphism. QQ, RQ, and RR refer to the respective genotypes. Values are means±SD. FVIIa, activated factor VII; FVIIag, factor VII antigen; MI, myocardial infarction.

the QQ genotype was not seen in premature MI patients, the distribution of genotypes was compared between the RR and the RQ+QQ genotypes. No significant difference in frequency of the RQ+QQ genotype or the Q allele was seen between the 2 groups.

The results of logistic regression analysis including the Q allele, hypertension, hypercholesterolemia, diabetes mellitus, and smoking are shown in Table 3. In the multivariate analysis including the 4 conventional coronary risk factors, the Q allele was significantly associated with the occurrence of premature MI (OR 0.41; p=0.038, r^2=0.01). There were no significant interactions between the Q allele and conventional risk factors.

Ten premature MI patients with the Q allele had 2.7±1.2 conventional risk factors, significantly more (p=0.002) than 19 control subjects with the Q allele (1.5±0.7). All premature MI patients with the Q allele had a history of smoking, and none had hypertension. No significant difference in prevalence of diabetes mellitus or hypercholesterolemia was noted (data not shown).

Plasma FVII and Premature MI

Plasma concentrations of FVIIa and FVIIag were compared between MI patients not receiving anticoagulant agents and control subjects. The plasma FVIIa concentrations in the patients (55.1±40.7 U/L) were slightly higher than those in control subjects (44.8±20.2 U/L), but not significant (p=0.078). Plasma FVIIag concentrations showed no significant difference between the 2 groups (88.7±15.7% vs 87.0±9.0%, p=0.557) (Table 2).

In multivariate logistic regression analysis including plasma concentrations of FVIIa and FVIIag and the presence of hypertension, hypercholesterolemia, diabetes mellitus, and past or present smoking status with respect to

premature MI, plasma FVIIa and FVIIag concentrations showed no significant association with risk of premature MI (p=0.102 and 0.810, respectively).

R353Q Polymorphism and FVII

Plasma concentrations of FVIIa and FVIIag in the various genotypes are compared in Fig 1. In the control subjects, plasma FVIIa concentrations for the QQ, RQ, and RR genotypes were 9.7±0.7 U/L, 26.0±13.2 U/L, and 47.8±12.3 U/L, respectively. Plasma FVIIag concentrations were 72.5±10.6%, 83.6±7.2%, and 87.6±9.0%, respectively. R353Q polymorphism, then, showed significant associations with FVIIa (p<0.001) and FVIIag (p=0.015). In MI patients, plasma FVIIa concentrations for the RQ genotype (21.0±9.8 U/L) were significantly lower (p<0.001) than those with the RR genotype (58.3±41.0 U/L). However, plasma FVIIag concentrations showed no significant difference between the 2 genotypes (87.5±15.7% vs 88.8±15.8%, respectively, p=0.815).

Discussion

The findings of the multivariate logistic regression analysis that included the conventional coronary risk factors of hypertension, hypercholesterolemia, diabetes mellitus, and smoking suggest that R353Q polymorphism is significantly associated with the risk of premature MI in the present study population. Plasma FVIIa concentrations in the patients were slightly higher than those in control subjects, but not significantly. Therefore, the Q allele of R353Q polymorphism might protect against premature MI in Japanese men.

Several studies have suggested that FVII is a coronary risk factor[6–14] but it has not been established by consensus that R353Q polymorphism of the FVII gene is associated with the risk of MI. Therefore, we conducted the present case–control study analyzing FVII genotypes. Although most FVII circulates in the zymogen form, a priming role in triggering the coagulation cascade has been assigned to the smaller amounts of circulating FVIIa[2–5] Because FVIIa is the first active protease in the extrinsic pathway of the coagulation cascade, plasma FVIIa concentrations may be important for determining the occurrence of thrombotic events such as thrombosis after rupture of an atherosclerotic plaque. Kario et al reported that plasma FVIIa concentrations were increased in patients with cardiovascular disease[9] and Philippou et al observed increased FVIIa in patients with acute coronary syndromes[10] However, the increase of FVIIa has not been sufficiently established as a hemostatic coronary risk factor. In our previous study, we found activation of the coagulation cascade, evaluated by the ratio of tissue factor and tissue factor pathway inhibitor in premature MI, but could not confirm the increase of plasma FVIIa[29]

In the present study of premature MI in Japanese men, we observed significant associations for R353Q polymorphism, but not for plasma FVIIa (p=0.078). Many studies have not recognized associations between plasma R353Q polymorphism or FVIIa and cardiovascular disease[23,30–34] The Framingham Heart Study reported that R353Q polymorphism was not significantly associated with cardiovascular disease, and suggested that R353Q polymorphism might be in linkage disequilibrium with other polymorphisms of the FVII gene or with another as-yet-unidentified gene located near the FVII gene[23] Recently, significant associations between polymorphisms of the FVII gene and MI, coronary artery disease, or cardiac events after intervention have been confirmed[35–40] Iacoviello et al suggested that R353Q and the hypervariable region 4 polymorphisms influenced the risk of MI in families with a history of thrombosis[35] Girelli et al reported that there were significantly more heterozygotes and homozygotes for the Q and A2 alleles among those who had not had a MI than among those who had had an infarction (p=0.01 for R353Q)[36] However, there have been no studies showing a significant association between R353Q polymorphism of FVII and premature MI.

Among there are many studies of the polymorphisms of genes and coronary heart disease in Japanese[41–43] as far as we know there have been only 2 studies investigating the genotypes of coagulation factor VII and coronary heart disease. Tamaki et al reported that polymorphisms of factor VII gene were not associated with the risk of MI[34] whereas Shimokata et al found a significant association between FVII polymorphism and coronary artery disease, but not MI[40] Therefore, we are the first to recognize a significant association with the risk of MI in Japanese.

Many studies have reported fewer stenotic atheromatous lesions on the coronary angiograms of younger MI patients compared with the elderly[25–28] Because atherosclerosis plays a reduced role in premature MI, prothrombotic factors become relatively important[27,44–47] Therefore, we selected relatively young Japanese men as study subjects. In the present study, the relation of R353Q polymorphism to the risk of premature MI was significant when considered together with the presence of conventional coronary risk factors. The discrepancy between our results and previous Japanese studies may be caused by the difference in the age of the study subjects. The mean ages of patients in studies by Tamaki et al and Shimokata et al were 59 years and 63 years, respectively. Because the role of FVII in the pathogenesis of MI might be less significant than conventional coronary risk factors in elderly Japanese, the previous 2 Japanese studies that included many elderly patients did not recognize the significant associations between R353Q polymorphism and MI. In contrast to hypercholesterolemia, diabetes mellitus, and smoking, all of which increased risk in this study, the Q allele seemed to be protective against premature MI. In contrast to the present results, when Moor et al and Ardissino et al assessed R353Q polymorphism in young survivors of MI, they found no significant differences in the prevalence of R353Q polymorphism between patients with premature MI and control subjects[8,32] In Taiwan, Li et al reported that R353Q polymorphism was an independent risk predictor of subsequent cardiac events in the young survivors of MI, but there was no difference in the prevalence of this polymorphism between patients and controls[39] The reason for disagreement between these study findings is not clear, but may involve differences of ethnicity and the prevalence of established coronary risk factors in the subjects.

Premature MI patients with the Q allele who otherwise might have had a reduced risk of MI had a significantly greater number of conventional coronary risk factors than control subjects with the Q allele. Recently, Iacoviello et al reported that smoking doubled the risk of MI in subjects with the Q allele[48] In the present study, all premature MI patients with the Q allele were current or former smokers. The Q allele presumably could not counter the increased risk of MI from smoking.

Study Limitations

The study was retrospective in design and had small statistical power (0.28) because of its small scale. We need more than 450 young MI patients to obtain results with sufficient statistical power (type II error <0.20) and we will continue the present study protocol to obtain a sufficient number of patients. Although the distribution of the Q allele in the control subjects was similar to that previously described in Japanese (12.6% by Tamaki et al; 17.6% by Shimokawa et al)[20,21,35,40] the number of controls in our study was also low. Therefore, we cannot establish the FVII gene as the protective factor of MI. Large prospective epidemiologic studies are necessary to clarify the associations between polymorphism of the FVII gene, plasma FVIIa, and risk of MI.

In addition, among several polymorphisms we examined only the R353Q polymorphism of the FVII gene. Other polymorphisms of the FVII gene such as the hypervariable region 4[49] and the decanucleotide insertion/deletion polymorphism,[37,50-52] which is located in the promoter region of the FVII gene and influences its transcription, may have influenced the association. Recently, Peyvandi et al reported that a novel polymorphism in intron 1a of the FVII gene (G73A) might protect against premature MI[53] Therefore, these polymorphisms of the FVII gene also need to be analyzed. Because antiplatelet agents do not have direct effects on the coagulation cascade, we measured factor VII concentrations without interrupting these agents, which were being administered to the majority of cases. To strictly exclude the effects of antiplatelet agents, it is necessary to take blood samples from patients not receiving antiplatelet agents.

In conclusion, R353Q polymorphism of FVII, which importantly influences plasma FVIIa concentrations, may protect against premature MI.

Acknowledgments

We thank Drs Tsuminori Yamashita, Masato Maeda, Hiroshi Kaieda, Tsuyoshi Yamaguchi, Seiki Harada, Hiroyuki Fujisaki, Hideaki Fukunaga, Hirohisa Shono, Toshiko Maki, Tetsuro Muranaga, Kozo Shiraishi, and Kiyotake Arikawa for their kind help. We also thank Ms Noriko Yoshihara and Mr Hirobumi Okamura for measuring the biochemical parameters.

References

1. Fuster V, Corti R, Badimon JJ. Therapeutic targets for the treatment of atherothrombosis in the new millennium: Clinical frontiers in atherosclerosis research. *Circ J* 2002; **66:** 783–790.
2. Seligsohn U, Kasper CK, Osterud B, Rapaport SI. Activated factor VII: Presence in factor IX concentrates and persistence in the circulation after infusion. *Blood* 1979; **53:** 828–837.
3. Nakagaki T, Foster DC, Berkner KL, Kisiel W. Initiation of the extrinsic pathway of blood coagulation: Evidence for the tissue factor dependent autoactivation of human coagulation factor VII. *Biochemistry* 1991; **30:** 10819–10824.
4. Morrissey JH, Macik BG, Neuenschwander PF, Comp PC. Quantitation of activated factor VII levels in plasma using a tissue factor mutant selectively deficient in promoting factor VII activation. *Blood* 1993; **81:** 734–744.
5. Morrissey JH. Tissue factor interactions with factor VII: Measurement and clinical significance of factor VIIa in plasma. *Blood Coagul Fibrinol* 1995; **6:** S14–S19.
6. Meade TW, Mellows S, Brozovic M, Miller GJ, Chakrabarti RR, North WRS, et al. Haemostatic function and ischaemic heart disease: Principal results of the Northwick Park Heart Study. *Lancet* 1986; **2:** 533–537.
7. Meade TW, Ruddock V, Stirling Y, Chakrabarti R, Miller GJ. Fibrinolytic activity, clotting factors, and long-term incidence of ischaemic heart disease in the Northwick Park Heart Study. *Lancet* 1993; **342:** 1076–1079.
8. Moor E, Silveira A, van't Hooft F, Suontaka AM, Eriksson P, Blomback M, et al. Coagulation factor VII mass and activity in young men with myocardial infarction at a young age: Role of plasma lipoproteins and factor VII genotype. *Arterioscler Thromb Vasc Biol* 1995; **15:** 655–664.
9. Kario K, Miyata T, Sakata T, Matsuo T, Kato H. Fluorogenic assay of activated factor VII: Plasma factor VIIa levels in relation to arterial cardiovascular diseases in Japanese. *Arterioscler Thromb* 1994; **14:** 265–274.
10. Philippou H, Adami A, Amersey RA, Stubbs PJ, Lane DA. A novel specific immunoassay for plasma two-chain factor VIIa: Investigation of FVIIa levels in normal individuals and in patients with acute coronary syndromes. *Blood* 1997; **89:** 767–775.
11. Hoffman CJ, Miller RH, Lawson WE, Hultin MB. Elevation of factor VII activity and mass in young adults at risk of ischemic heart disease. *J Am Coll Cardiol* 1989; **14:** 941–946.
12. de Sousa JC, Azevedo J, Soria C, Barros F, Ribeiro C, Parreira P, et al. Factor VII hyperactivity in acute myocardial thrombosis: A relation to the coagulation activation. *Thromb Res* 1988; **51:** 165–173.
13. Redondo M, Warzka HH, Stucki B, Sulzer I, Biasiutti FD, Binder BR, et al. Coagulation factors II, V, VII, and X, prothrombin gene 20210G→A transition, and factor V Leiden in coronary artery disease: High factor V clotting activity is an independent risk factor for myocardial infarction. *Arterioscler Thromb Vasc Biol* 1999; **19:** 1020–1025.
14. Broadhurst P, Kelleher C, Hughes L, Imeson JD, Raftery EB. Fibrinogen, factor VII clotting activity and coronary artery disease severity. *Atherosclerosis* 1990; **85:** 169–173.
15. Green F, Kelleher C, Wilkes H, Temple A, Meade T, Humphries S. A common genetic polymorphism associated with lower coagulation factor VII levels in healthy individuals. *Arterioscler Thromb* 1991; **11:** 540–546.
16. Saha N, Liu Y, Heng CK, Hong S, Low PS, Tay JSH. Association of factor VII genotype with plasma factor VII activity and antigen levels in healthy Indian adults and interaction with triglycerides. *Arterioscler Thromb* 1994; **14:** 1923–1927.
17. de Maat MPM, Green F, de Knijff P, Jespersen J, Kluft C. Factor VII polymorphisms in populations with different risks of cardiovascular disease. *Arterioscler Thromb Vasc Biol* 1997; **17:** 1918–1923.
18. Bernardi F, Marchetti G, Pinotti M, Arcieri P, Baroncini C, Papacchini M, et al. Factor VII gene polymorphisms contribute about one third of the factor VII levels variation in plasma. *Arterioscler Thromb Vasc Biol* 1996; **16:** 72–76.
19. Hunault M, Arbini AA, Lopaciuk S, Carew JA, Bauer KA. The Arg353Gln polymorphism reduces the level of cagulation factor VII: In vivo and in vitro studies. *Arterioscler Thromb Vasc Biol* 1997; **17:** 2825–2829.
20. Takamiya O. Genetic polymorphism (Arg353A→Gln) in coagulation factor VII gene and factor VII levels (coagulant activity, antigen and binding ability to tissue factor) in 101 healthy Japanese. *Scand J Clin Lab Invest* 1995; **55:** 211–215.
21. Kario K, Narita N, Matsuo T, Kayaba K, Tsutsumi A, Matsuo M, et al. Genetic determinants of plasma factor VII activity in the Japanese. *Thromb Haemost* 1995; **73:** 617–622.
22. Humphries SE, Lane A, Green FR, Cooper J, Miller GJ. Factor VII coagulant activity and antigen levels in healthy men are determined by interaction between factor VII genotype and plasma triglyceride concentration. *Arterioscler Thromb* 1994; **14:** 193–198.
23. Feng D, Tofler GH, Larson MG, O'Donnell CJ, Lipinska I, Schmitz C, et al. Factor VII gene polymorphism, factor VII levels, and prevalent cardiovascular disease: The Framingham Heart Study. *Arterioscler Thromb Vasc Biol* 2000; **20:** 593–600.
24. Bernardi F, Arcieri P, Bertina RM, Chiarotti F, Corral J, Pinotti M, et al. Contribution of factor VII genotype to activated FVII levels: Differences in genotype frequencies between northern and southern European populations. *Arterioscler Thromb Vasc Biol* 1997; **17:** 2548–2553.
25. Ogawa K, Numao T, Iizuka M, Yanagisawa A, Yoshino H, Ishikawa K, et al. Angiographic and coronary risk factor analyses of Japanese patients with ischemic heart disease before age 40: A multicenter cooperative study. *Jpn Circ J* 1996; **60:** 822–830.
26. Zimmerman FH, Cameron A, Fisher LD, Ng G. Myocardial infarction in young adults: Angiographic characterization, risk factors and prognosis (Coronary Artery Surgery Study Registry). *J Am Coll Cardiol* 1995; **26:** 654–661.
27. Choudhury L, Marsh JD. Myocardial infarction in young patients. *Am J Med* 1999; **107:** 254–261.
28. Yasuda T, Shimizu M, Ino H, Okeie K, Yamaguchi M, Fujino N, et al. Coronary lesion morphology and prognosis in young males with myocardial infarction with or without familial hypercholesterolemia. *Jpn Circ J* 2001; **65:** 247–250.
29. Saigo M, Abe S, Ogawa M, Yamashita T, Biro S, Minagoe S, et al. Imbalance of plasminogen activator inhibitor-1/tissue plasminogen activator and tissue factor/tissue factor pathway inhibitor in young Japanese men with myocardial infarction. *Thromb Haemost* 2001; **86:** 1197–1203.
30. Merlini PA, Ardissino D, Oltrona L, Broccolino M, Coppola R, Mannucci PM. Heightened thrombin formation but normal plasma levels of activated factor VII in patients with acute coronary syndromes. *Arterioscler Thromb Vasc Biol* 1995; **15:** 1675–1679.
31. Heywood DM, Ossei-Gerning N, Grant PJ. Association of factor VII: C levels with environmental and genetic factors in patients with ischaemic heart disease and coronary atheroma characterised by angiography. *Thromb Haemost* 1996; **76:** 161–165.
32. Ardissino D, Mannucci PM, Merlini PA, Duca F, Fetiveau R, Tagliabue L, et al. Prothrombotic genetic risk factors in young survivors of myocardial infarction. *Blood* 1999; **94:** 46–51.
33. Batalla A, Alvarez R, Reguero JR, González P, Alvarez V, Cubero GI, et al. Lack of association between polymorphisms of the coagulation factor VII and myocardial infarction in middle-aged Spanish men. *Int J Cardiol* 2001; **80:** 209–212.
34. Tamaki S, Iwai N, Nakamura Y, Tsujita Y, Kinoshita M. Variation of the factor VII gene and ischemic heart disease in Japanese subjects. *Coron Artery Dis* 1999; **10:** 601–606.
35. Iacoviello L, Di Castelnuovo A, de Knijff P, D'Orazio A, Amore C, Arboretti R, et al. Polymorphisms in the coagulation factor VII gene and the risk of myocardial infarction. *N Engl J Med* 1998; **338:** 79–85.
36. Girelli D, Russo C, Ferraresi P, Olivieri O, Pinotti M, Friso S, et al. Polymorphisms in the factor VII gene and the risk of myocardial infarction in patients with coronary artery disease. *N Engl J Med* 2000; **343:** 774–780.
37. Di Castelnuovo A, D'Orazio A, Amore C, Falanga A, Donati MB, Iacoviello L. The decanucleotide insertion/deletion polymorphism in the promoter region of the coagulation factor VII gene and the risk of familial myocardial infarction. *Thromb Res* 2000; **98:** 9–17.
38. Mrozikiewicz PM, Cascorbi I, Ziemer S, Laule M, Meisel C, Stangl V, et al. Reduced procedural risk for coronary catheter interventions in carriers of the coagulation factor VII–Gln^{353} gene. *J Am Coll Cardiol* 2000; **36:** 1520–1525.
39. Li YH, Chen JH, Guo HR, Tsai WC, Chao TH. Genetic risk factors associated with the prognosis of myocardial infarction in young patients. *Thromb Haemost* 2002; **88:** 694–697.
40. Shimokata K, Kondo T, Ohno M, Takeshita K, Inden Y, Iino S, et al. Effects of coagulation factor VII polymorphisms on the coronary artery disease in Japanese: Factor VII polymorphism and coronary disease. *Thromb Res* 2002; **105:** 493–498.
41. Sawano M, Watanabe Y, Ohmura H, Shimada K, Daida H, Mokuno H, et al. Potentially protective effects of the Ser447–Ter mutation of the lipoprotein lipase gene against the development of coronary artery disease in Japanese subjects via a beneficial lipid profile. *Jpn Circ J* 2001; **65:** 310–314.
42. Takezako T, Zhang B, Serikawa T, Fan P, Nomoto J, Saku K. The D allele of the angiotensin-converting enzyme gene and reperfusion-induced ventricular arrhythmias in patients with acute myocardial infarction. *Jpn Circ J* 2001; **65:** 603–609.
43. Taniguchi I, Yamazaki T, Waganuma K, Kurusu T, Shimazu Y, Takikawa K, et al. The DD genotype of angiotensin-converting enzyme polymorphism is a risk factor for coronary artery disease and coronary stent restenosis in Japanese patients. *Jpn Circ J* 2001; **65:** 897–900.
44. Siscovick DS, Schwartz SM, Rosendaal FR, Psaty BM. Thrombosis in the young: Effect of atherosclerotic risk factors on the risk of myocardial infarction associated with prothrombotic factors. *Thromb Haemost* 1997; **78:** 7–12.
45. Ridker PM, Vaughan DE, Stampfer MJ, Manson JE, Hennekens CH. Endogenous tissue-type plasminogen activator and risk of myocardial infarction. *Lancet* 1993; **341:** 1165–1168.
46. Thompson SG, Kienast J, Pyke SD, Haverkate F, van de Loo JC. Hemostatic factors and the risk of myocardial infarction or sudden death in patients with angina pectoris: European Concerted Action on Thrombosis and Disabilities Angina Pectoris Study Group. *N Engl J Med* 1995; **332:** 635–641.
47. Hamsten A, Wiman B, de Faire U, Blomback M. Increased plasma levels of a rapid inhibitor of tissue plasminogen activator in young survivors of myocardial infarction. *N Engl J Med* 1985; **313:** 1557–1563.
48. Iacoviello L, Di Castelnuovo A, D'Orazio A, Donati MB. Cigarette smoking doubles the risk of myocardial infarction in carriers of a protective polymorphism in the blood coagulation factor VII gene. *Thromb Haemost* 1999; **81:** 658.
49. Marchetti G, Gemmati D, Patracchini P, Pinotti M, Bernardi F. PCR detection of a repeat polymorphism within the F7 gene. *Nucleic Acids Res* 1991; **19:** 4570.
50. Marchetti G, Patracchini P, Papacchini M, Ferrati M, Bernardi F. A polymorphism in the 5' region of coagulation factor VII gene (F7) caused by an inserted decanucleotide. *Hum Genet* 1993; **90:** 575–576.
51. Humphries S, Temple A, Lane A, Green F, Cooper J, Miller G. Low plasma levels of factor VIIc and antigen are more strongly associated with the 10 base pair promoter (–323) insertion than the Glutamine 353 variant. *Thromb Haemost* 1996; **75:** 567–572.
52. Dell'Acqua G, Iacoviello L, D'Orazio A, Di Bitondo R, Di Castelnuovo A, Donati MB. A polymorphic cluster in the 5' region of the human coagulation factor VII gene: Detection, frequency, and linkage disequilibrium. *Thromb Res* 1997; **88:** 445–448.
53. Peyvandi F, Mannucci PM, Bucciarelli P, Zeinali S, Akhavan S, Sacchi E, et al. A novel polymorphism in intron 1a of the human factor VII gene (G73A): Study of a healthy Italian population and of 190 young survivors of myocardial infarction. *Br J Haematol* 2000; **108:** 247–253.

THE JOURNAL OF BIOLOGICAL CHEMISTRY
© 2002 by The American Society for Biochemistry and Molecular Biology, Inc.

Vol. 277, No. 22, Issue of May 31, pp. 19255–19264, 2002
Printed in U.S.A.

Overexpression of Calreticulin Modulates Protein Kinase B/Akt Signaling to Promote Apoptosis during Cardiac Differentiation of Cardiomyoblast H9c2 Cells*

Received for publication, December 26, 2001, and in revised form, March 11, 2002
Published, JBC Papers in Press, March 20, 2002, DOI 10.1074/jbc.M112377200

Kan Kageyama‡§¶, Yoshito Iharat‖¶, Shinji Goto‡, Yoshishige Urata‡, Genji Toda§, Katsusuke Yano§, and Takahito Kondo‡

From the ‡Department of Biochemistry and Molecular Biology in Disease, Atomic Bomb Disease Institute, and the §Third Department of Internal Medicine, Nagasaki University School of Medicine, 1-12-4 Sakamoto, Nagasaki 852-8523, Japan

Calreticulin is a Ca^{2+}-binding molecular chaperone of the lumen of the endoplasmic reticulum. Calreticulin has been shown to be essential for cardiac and neural development in mice, but the mechanism by which it functions in cell differentiation is not fully understood. To examine the role of calreticulin in cardiac differentiation, the calreticulin gene was introduced into rat cardiomyoblast H9c2 cells, and the effect of calreticulin overexpression on cardiac differentiation was examined. Upon culture in a differentiation medium containing fetal calf serum (1%) and retinoic acid (10 nM), cells transfected with the calreticulin gene were highly susceptible to apoptosis compared with controls. In the gene-transfected cells, protein kinase B/Akt signaling was significantly suppressed during differentiation. Furthermore, protein phosphatase 2A, a Ser/Thr protein phosphatase, was significantly up-regulated, implying suppression of Akt signaling due to dephosphorylation of Akt by the up-regulated protein phosphatase 2A via regulation of Ca^{2+} homeostasis. Thus, overexpression of calreticulin promotes differentiation-dependent apoptosis in H9c2 cells by suppressing the Akt signaling pathway. These findings indicate a novel mechanism by which cytoplasmic Akt signaling is modulated to cause apoptosis by a resident protein of the endoplasmic reticulum, calreticulin.

Calreticulin (CRT)[1] is a Ca^{2+}-binding molecular chaperone in the endoplasmic reticulum (ER) (1). It is a highly conserved protein with >90% amino acid identity in mammals, including human, rabbit, rat, and mouse (2). The gene has also been found in insects, nematodes, protozoa, and plants, but not in yeast or prokaryotes (1, 3), suggesting a general function in living cells. CRT is involved in many biological process, including regulation of Ca^{2+} homeostasis and intracellular signaling, cell adhesion, gene expression, and glycoprotein folding (3, 4) and nuclear transport (5).

CRT is well expressed in embryonic rat heart, but its expression is significantly suppressed after birth (6). Cardiac development is believed to be regulated cooperatively by a variety of proteins, including signaling molecules (*e.g.* fibroblast growth factor, transforming growth factor-β, ErbB2/B4, neuregulin, etc.), cell adhesion molecules (*e.g.* vascular cell adhesion molecule, α_4 integrin, and versican), ion channels, and transcription factors (*e.g.* GATA, myocyte enhancer factor-2, HAND, chicken ovalbumin upstream promoter transcription factor II, Nkx2.5, TBX5, NF-ATc, Smad6, Pax3, retinoid X receptor/retinoic acid receptor, TEF-1, WT-1, etc.) (7). Interestingly, CRT gene expression is known to be regulated by a transcription factor (Nkx2.5) that is involved in the regulation of gene expression for cardiac development (8). Recently, it has been shown that CRT is essential for cardiac and neural development in mice (9, 10). CRT-deficient embryonic cells show impaired nuclear import of the transcription factor NF-AT3 (nuclear factor of activated T cells), indicating that CRT functions in cardiac development as a component of the Ca^{2+}/calcineurin/NF-AT/GATA-4 transcription pathway (9). Very recently, it has also been reported that CRT transgenic mice suffer complete heart block and sudden death (11). In that study, it was described that CRT-dependent cardiac block involves impairment of both the L-type Ca^{2+} channel and gap junction connexin-40 and connexin-43. Also observed was a decrease in phosphorylated connexin-43 in CRT transgenic heart, suggesting that the functions of protein kinases are altered via the regulation of Ca^{2+} homeostasis. The study indicates that overexpression of CRT affects not the morphogenesis, but the physiological function of cardiomyoblasts. The overall mechanism of the dephosphorylation of connexin-43 in CRT transgenic heart cells is not known, but may involve the altered regulation of protein kinase pathways. These studies suggest that CRT plays a vital role in cardiac differentiation and function, although how has not been fully clarified.

In this study, we investigated the biological role of CRT using rat cardiomyoblast H9c2 cells transfected with the CRT gene. We show that overexpression of CRT promotes apoptosis during cardiac differentiation and that suppression of protein kinase B/Akt signaling for cell survival is involved in the apoptotic process. We also show that expression of protein phosphatase 2A (PP2A), a Ser/Thr protein phosphatase, is involved in altering the regulation of Akt signaling in H9c2 cells overexpressing CRT via the regulation of Ca^{2+} homeostasis.

MATERIALS AND METHODS

Antibodies and Reagents—Antibodies against CRT, calnexin, and Grp78/BiP were purchased from Stressgen Biotech Corp. (Victoria, British Columbia, Canada). The antibody against the protein phosphatase 1α (PP1α) catalytic subunit (PP1αc) was obtained from Santa Cruz Biotechnology (Santa Cruz, CA). The anti-Akt and anti-phosphorylated Akt (Ser^{473}) antibodies were purchased from Cell Signaling Technology (Beverly, MA). Antibodies against PP2B-Aα (calcineurin) and PP2Cα were from Upstate Biotechnology, Inc. (Lake Placid, NY). The anti-PP2A catalytic subunit α (PP2Aα) antibody was from Transduction Laboratories (Lexington, KY). The reagents used in the study were all high grade and were from Sigma or Wako Pure Chemicals (Osaka, Japan).

Cell Culture—H9c2 cells, a clonal line derived from embryonic rat heart (12, 13), were obtained from American Type Culture Collection (CRL-1446). H9c2 cells and the CRT gene-transfected cells were cultured in Dulbecco's modified Eagle's medium (DMEM) supplemented with 10% fetal calf serum (FCS) in a humidified atmosphere of 95% air and 5% CO_2 at 37 °C. Before reaching confluence, the cells were split, plated at low density in culture dishes containing 10% FCS culture medium, and cultured for 24 h. To induce cardiac differentiation, cells were then cultured in DMEM supplemented with 1% FCS and 10 nM all-*trans*-retinoic acid (RA) according to the method described by Ménard *et al.* (14). The culture medium was replaced every 2 days.

Construction of a CRT Gene Expression Vector—A full-length mouse CRT cDNA was cloned from total RNA of mouse monocyte-derived leukemia RAW264.7 cells by reverse transcription-PCR using SuperScript II RNase H reverse transcriptase (Invitrogen) and AdvantageHF2 *Taq* polymerase (CLONTECH, Palo Alto, CA) with the following primer pair, which was designed on the basis of reported nucleotide sequences (15): Primer S, CCATGCTCCTTTCGGTGCCG; and Primer A, GTGGCCTCTACAGCTCATCC. The amplified DNA fragments were subcloned into a TA cloning vector (pCRII, Invitrogen), and the nucleotide sequences of the PCR product were confirmed by sequencing with an ALFexpress II system (Amersham Biosciences, Buckinghamshire, UK). The CRT cDNA was cloned into plasmid pcDNA3.1 (Invitrogen) under the control of the cytomegalovirus promoter for expression in mammalian cells.

Gene Transfection and Selection of Cells—The mock and CRT gene expression vectors were transfected into H9c2 cells using LipofectAMINE Plus reagent (Invitrogen) according to the manufacturer's protocol. Stable transfectants were screened by culturing with 500 μg/ml G418. The cloned G418-resistant lines were then screened for expression of CRT. Two cell lines (CRT-S2 and CRT-S8) found to express high levels of CRT upon immunoblot analysis (see Fig. 1*A*) were selected and used for the experiments.

Fluorescence Microscopy—Cells (5×10^4/ml) were grown on Lab-Tek chamber slides for 24 h. They were fixed with 4% paraformaldehyde in phosphate-buffered saline (PBS; pH 7.2) and permeabilized for 10 min with PBS containing 0.1% Triton X-100. The cells were then blocked with 1% bovine serum albumin in PBS, incubated with anti-CRT or anti-calnexin antibody for 1 h, and washed with PBS containing 1% bovine serum albumin. The immunoreactive primary antibody was visualized with fluorescein isothiocyanate-conjugated anti-rabbit immunoglobulin (Cappel). After washing, the stained cells were mounted in Vectashield medium. A Zeiss Axioskop2 (Carl Zeiss, Jena, Germany) with epi-illumination for fluorescence was used for fluorescence microscopic analysis.

Cell Proliferation Assay—The proliferation of cultured cells was evaluated by measuring attached live cells photometrically after staining with crystal violet. The cells (3000) were placed in 100 μl of medium/well in 96-well plates and cultured with or without the differentiation treatment. After a specific period, the cells were fixed with 4% paraformaldehyde in PBS, washed, and stained with 0.01% crystal violet at room temperature for 20 min. Each well was extensively washed with water and dried. The stained cells were lysed by adding 100 μl of lysis buffer (20% SDS and 50% *N,N*-dimethylformamide (pH 4.7)), and the cell number was then estimated by measuring the absorbance at 570 nm using a microplate reader.

Apoptosis Assay—Apoptosis was detected by flow cytometry with the terminal deoxynucleotidyltransferase-mediated dUTP nick end labeling (TUNEL) method (16) using an ApopTag Plus fluorescein *in situ* apoptosis detection kit (Intergen Co., Purchase, NY). Briefly, cells were harvested and fixed in 70% ethanol, treated with terminal deoxynucleotidyltransferase for 1 h and then with fluorescein isothiocyanate-conjugated anti-digoxigenin antibody for 1 h at room temperature, and washed with PBS containing 0.1% Triton X-100. Fluorescence intensity was measured at 530 nm using a flow cytometer (BD PharMingen). Apoptosis was also measured by flow cytometry as described (17). Briefly, the cells were washed with PBS and resuspended in PBS with 0.1% Triton X-100 and 50 μg/ml propidium iodide. The DNA content was analyzed by flow cytometry. Hypodiploid cells containing a smaller amount of DNA and a side scatter higher than that of G_0/G_1 cells were considered to be apoptotic. Caspase-3 activity was assayed by spectrophotometric detection of the chromophore *p*-nitroanilide after cleavage from the substrate DEVD-*p*-nitroanilide using a CPP32/caspase-3 colorimetric protease assay kit (Medical & Biological Laboratories, Nagoya, Japan). The *p*-nitroanilide light emission was quantified by measuring the absorbance at 405 nm.

Immunoblot Analysis—Cultured cells were harvested and lysed for 20 min at 4 °C in lysis buffer (20 mM Tris-HCl (pH 7.5), 130 mM NaCl, 1% Nonidet P-40, 10% glycerol, 0.4 mM sodium orthovanadate, 10 mM sodium pyrophosphate, and 10 mM sodium fluoride including protease inhibitors (20 μM amidinophenyl methanesulfonyl fluoride, 50 μM pepstatin, and 50 μM leupeptin)). The supernatants obtained on centrifugation at 8,000 × *g* for 10 min then were used in subsequent experiments. Protein samples were electrophoresed on 7.5, 10, or 12.5% SDS-polyacrylamide gels under reducing conditions and then transferred to nitrocellulose membrane as described (18). The membrane was blocked with 3% bovine serum albumin or 5% skim milk in Tris-buffered saline (10 mM Tris-HCl (pH 7.5) and 0.15 M NaCl) and incubated at room temperature for 2 h with the primary antibody in Tris-buffered saline containing 0.05% Tween 20. The blots were coupled with the peroxidase-conjugated secondary antibodies, washed, and then developed using the ECL chemiluminescence detection kit (Amersham Biosciences) according to the manufacturer's instructions.

Akt Activity Assay—Akt activity was assayed using an Akt assay kit (Cell Signaling Technology) according to the manufacturer's protocol. Briefly, Akt was immunoprecipitated from cell lysates using anti-Akt antibody, and the immunoprecipitates were then incubated at 30 °C for 30 min in an assay mixture containing an Akt substrate, GSK-3α/β fusion protein. Phosphorylated proteins were separated by 12.5% SDS-PAGE and then transferred to nitrocellulose membrane to detect phosphorylated GSK-3α/β using anti-phosphorylated GSK-3α/β ($Ser^{21/9}$) antibody.

Northern Blot Analysis—The full-length rat PP1αc and PP2Aαc cDNAs were generously provided by Dr. Kunimi Kikuchi (Hokkaido University, Hokkaido, Japan) (19, 20). A *PstI-SmaI* fragment of 600 bp and an *EcoRI-PvuII* fragment of 680 bp were prepared from the cDNAs of PP1αc and PP2Aαc, respectively, and used as cDNA probes. The probes were radiolabeled with ^{32}P using a random primer labeling kit (Takara Biomedicals, Shiga, Japan). The isolation of cytoplasmic RNA and Northern blotting were essentially performed as described by Sambrook *et al.* (21). Isolated RNAs (10 μg) were electrophoresed on a 1% agarose gel containing 0.6 M formaldehyde, transferred to a nylon membrane, and then hybridized with ^{32}P-labeled probes. Autoradiographed membranes were analyzed using a BAS5000 bioimage analyzer (Fuji Photo Film).

Protein Phosphatase Assay—Ser/Thr protein phosphatase activity was assayed photometrically using a Ser/Thr phosphatase assay kit (kit 1, Upstate Biotechnology, Inc.) according to the manufacturer's protocol. The phosphopeptide RKpTIRR and *p*-nitrophenyl phosphate were used as phosphatase substrates. Protein concentrations were determined using a BCA assay kit (Pierce).

Measurement of Intracellular Free Calcium—The intracellular free calcium concentration was measured using fura-2 essentially as described previously (22). Briefly, cells cultured on glass coverslips were loaded with 5 μM fura-2/AM (Dojindo, Kumamoto, Japan) for 20 min in Earle's balanced salt solution in the presence of 0.01% pluronic F-127. After four washes with Earle's balanced salt solution, the coverslip was positioned in a quarts cuvette containing 3.5 ml of fresh Earle's balanced salt solution at a 45° angle to both the excitation and emission light paths. The fura-2 fluorescence was determined at 37 °C using a Shimadzu RF-5000 spectrofluorophotometer operating at an emission wavelength of 505 nm with excitation wavelengths of 340 and 380 nm. The maximal signal (R_{max}) was obtained by adding ionomycin at a final concentration of 4 μM. Then, the minimal signal (R_{min}) was obtained by adding EGTA at a final concentration of 7.5 mM, followed by Tris-free base at a final concentration of 30 mM, to increase the pH to 8.3. *R* is the ratio (F1/F2) of the fluorescence of $Ex_{340\ nm}/Em_{505\ nm}$ (F1) to that of $Ex_{380\ nm}/Em_{505\ nm}$ (F2). The actual calcium concentration was calculated as $K_d \times (R - R_{min})/(R_{max} - R)$, with K_d equal to 224 nM (23).

RESULTS

Establishment of CRT Gene Overexpressers Using H9c2 Cells—To investigate the functional roles of CRT during cardiac differentiation, a CRT gene expression vector was constructed and transfected into rat cardiomyoblast H9c2 cells. After the screening of G418-resistant transfectants, the expression level of CRT was characterized immunologically. Two high expression transfectants (CRT-S2 and CRT-S8) were used in

* This work was supported in part by grants-in-aid from the Ministry of Education, Science, Sports, and Culture of Japan and by the Japan Foundation of Cardiovascular Research. The costs of publication of this article were defrayed in part by the payment of page charges. This article must therefore be hereby marked "*advertisement*" in accordance with 18 U.S.C. Section 1734 solely to indicate this fact.

¶ Both authors contributed equally to this work.
‖ To whom correspondence should be addressed. Tel.: 81-95-849-7099; Fax: 81-95-849-7100; E-mail: y-ihara@net.nagasaki-u.ac.jp.

[1] The abbreviations used are: CRT, calreticulin; ER, endoplasmic reticulum; PP, protein phosphatase; DMEM, Dulbecco's modified Eagle's medium; FCS, fetal calf serum; RA, all-*trans*-retinoic acid; PBS, phosphate-buffered saline; TUNEL, terminal deoxynucleotidyltransferase-mediated dUTP nick end labeling; GSK, glycogen synthase kinase; SAPK, stress-activated protein kinase; MAPK, mitogen-activated protein kinase; PI3K, phosphatidylinositol 3-kinase; BAPTA/AM, 1,2-bis(o-aminophenoxy)ethane-*N,N,N′,N′*-tetraacetic acid tetra(acetoxymethyl) ester; CRE, cAMP-responsive element.

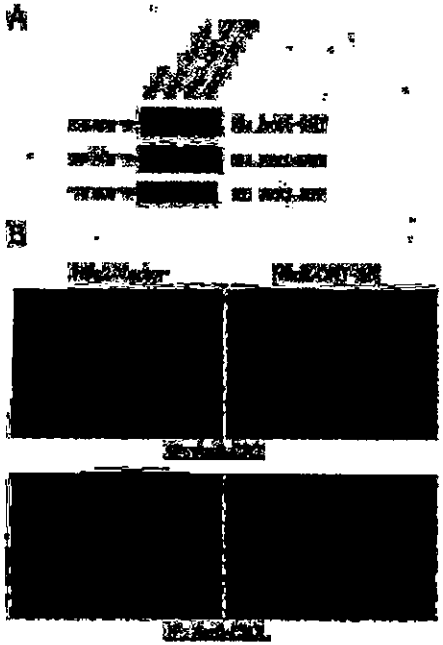

FIG. 1. *A*, calreticulin expression in control and CRT gene-transfected H9c2 cells. The expression levels for CRT, calnexin (*CNX*), and BiP were estimated by immunoblot analysis using specific antibodies as described under "Materials and Methods." The data represent three independent experiments. *B*, intracellular localization of CRT and calnexin in control and transfected H9c2 cells. The intracellular localization of CRT and calnexin was evaluated by indirect immunofluorescence (*IF*) microscopy using specific antibodies. The data represent two independent experiments.

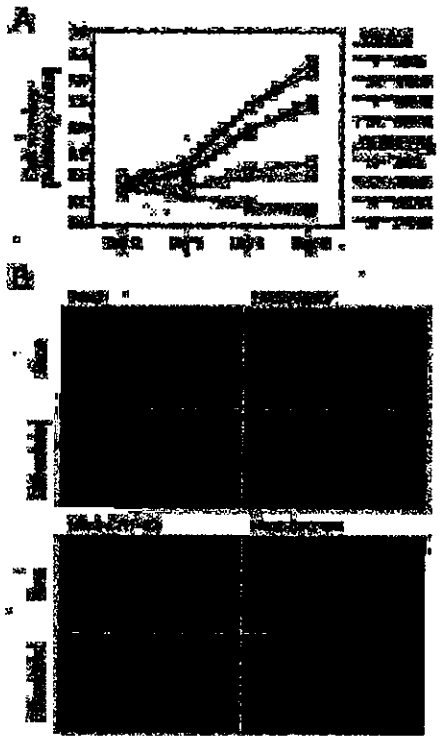

FIG. 2. *A*, proliferation of control and gene-transfected H9c2 cells treated with differentiation medium for 5 days. Cell proliferation was evaluated by measuring attached live cells photometrically after staining with crystal violet as described under "Materials and Methods." Each value represents the mean of four independent experiments, and the S.D. was always within 10% of the mean. *B*, morphological change in control and gene-transfected H9c2 cells during differentiation. The cells were cultured in differentiation medium for 5 days, and cell morphology was characterized microscopically. The results were reproducible in five independent experiments.

subsequent experiments. Fig. 1*A* shows that expression of CRT increased in the overexpressers to ~2.7-fold the level in the parental and mock-transfected (control) H9c2 cells. Transfection had no apparent effect on expression of other ER chaperones such as calnexin and BiP. The intracellular localization of CRT was examined by indirect immunofluorescence. As shown in Fig. 1*B*, immunoreactive signals showed a perinuclear reticular pattern in all cases, including the control and gene-transfected cells, although the signal intensity was increased in the transfectants compared with the control cells. Under non-permeabilized conditions, no significant increase in CRT expression on the cell surface was observed in the gene-transfected cells (data not shown). In the case of calnexin, the transfectants were similar to controls in the localization and intensity of immunoreactive signals.

Effect of Overexpression of CRT on the Differentiation of H9c2 Cells—The H9c2 cell acquires the cardiac phenotype under conditions of retinoic acid-induced differentiation (14). To test the effect of overexpressed CRT on cardiac differentiation, control and gene-transfected H9c2 cells were cultured with or without differentiation medium (1% FCS and 10 nM RA in DMEM), and cell proliferation and morphology were compared. As shown in Fig. 2*A*, after 5 days of culture in differentiation medium, cell proliferation was suppressed in control cells, but was only reduced in the transfectants. Cardiac differentiation was confirmed as described by Ménard *et al.* (14) by suppression of cell proliferation and increase in expression of specific differentiation markers such as L-type voltage-dependent calcium channel α1C and myosin heavy chain by immunoblot analysis (data not shown). Under normal culture conditions, cell proliferation in the gene transfectants was relatively reduced compared with the control cells. Fig. 2*B* shows that after 5 days of culture in differentiation medium, large and round differentiated cells were seen in the control cultures. The results are consistent with a previous report (14). In contrast, the transfectants were small and round and mostly detached from the plastic culture dish, suggesting they had been damaged by the treatment.

Overexpression of CRT Causes Apoptosis during the Cardiac Differentiation of H9c2 Cells—To examine whether apoptosis

contributed to the cell damage seen in the transfectants after the differentiation treatment, a TUNEL assay and analysis of DNA content with propidium iodide staining were carried out using cells treated with or without differentiation medium for 3 days. In the TUNEL assay (Fig. 3*A*), an increase in fluorescence intensity derived from DNA strand breaks was detected in the transfectants, but not in the control cells cultured in differentiation medium. Upon staining with propidium iodide (Fig. 3*B*), apoptotic cells appeared as a hypodiploid DNA peak preceding the narrow peak of diploid DNA from viable cells. In the transfectants, a hypodiploid DNA peak was detected after differentiation treatment. No such peak was seen in control cells. Next, the activity of caspase-3 was examined in the cells cultured with or without differentiation medium for 3 days. Caspase-3 activity was markedly elevated after the differentiation treatment in the transfectants compared with the control cells (Fig. 3*C*). These results indicate that apoptosis was promoted by overexpression of CRT in H9c2 cells during the experimentally induced differentiation.

Overexpression of CRT Suppresses Protein Kinase B/Akt Activity during the Cardiac Differentiation of H9c2 Cells—Apoptosis is known to be regulated by several signal transduction pathways, including the stress-activated protein kinase (SAPK), mitogen-activated protein kinase (MAPK), and protein kinase B/Akt pathways (24). To reveal whether overexpression of CRT affected the cell survival signaling of Akt during differentiation-induced apoptosis, the phosphorylation of Akt Ser^{473} was examined and compared between control cells and cells transfected with the CRT gene during differentiation (Fig. 4*A*). In controls, the levels of Ser^{473}-phosphorylated Akt were unchanged on day 1 of the differentiation treatment, but decreased to 37% of initial values on day 3. In contrast, in the transfectants, they decreased to 35% of the initial level on day 1 of treatment. Akt activity was also examined in the controls and transfectants after 24 h of treatment to induce differentiation. Fig. 4*B* shows that Akt activity was suppressed after 24 h of culture in differentiation medium in the transfectants, but not in the control cells. This is consistent with the finding that the level of phosphorylated Akt correlates well with the activity of Akt (25). The phosphorylation of BAD, a downstream signal of Akt, was examined. Despite the change in Akt activity, the level of phosphorylated BAD did not change significantly in either the control or transfected cells during differentiation (data not shown).

Differentiation Treatment-induced Apoptosis Is Enhanced in the Presence of Wortmannin and LY294002 in Both Control and CRT Gene-transfected H9c2 Cells—To clarify the significance of Akt signaling to anti-apoptotic functions, cells were treated with 1% FCS and RA for 24 h in the presence or absence of the phosphatidylinositol 3-kinase (PI3K) inhibitors wortmannin (300 nM) and LY294002 (10 μM), and apoptosis was then examined by TUNEL methods. Fig. 5*A* shows that the PI3K inhibitors enhanced apoptosis during treatment for 24 h in both control and transfected cells. Caspase-3 activity was also induced by the inhibitors (data not shown). Moreover, Fig. 5*B* shows that phosphorylation of Akt was suppressed by the PI3K inhibitors during treatment. Thus, suppression of Akt signaling by specific inhibitors enhanced the differentiation-induced apoptosis, suggesting that Akt signaling has a vital anti-apoptotic function in this differentiation model.

Protein Phosphatase 2A Is Up-regulated in H9c2 Cells Transfected with the CRT Gene—To establish whether overexpression of CRT affects the activity of PI3K, an upstream signaling molecule of Akt, we examined PI3K activity in control and gene-transfected cells treated with or without differentiation medium for 24 h. However, PI3K activity was not affected by overexpression of CRT during differentiation (data not shown). Next, to identify the molecules that suppressed Akt signaling in the transfectants upon the differentiation treatment, we focused on Ser/Thr phosphatases that could dephosphorylate Akt to suppress the signaling. Fig. 6*A* shows the protein levels for cytosolic Ser/Thr phosphatases (*i.e.* PP1αc, PP2A$c\alpha$, PP2B-Aα, and PP2Cα) determined by immunoblot analysis in control and gene-transfected cells with or without the differentiation treatment (1% FCS and RA for 24 h). In the case of both PP1αc and PP2B-Aα (calcineurin), there was no significant difference in the level of expression between the control and transfected cells, although the level increased slightly after the differentiation treatment. In contrast, the protein levels of PP2A$c\alpha$ increased significantly in the transfectants compared with the controls and increased during differentiation in both cases. Interestingly, for PP2Cα, protein levels were relatively suppressed in the transfectants. Moreover, no differentiation-induced increase in expression was observed, unlike for PP2A$c\alpha$. The mRNA expression levels for PP2A$c\alpha$ and PP1αc were examined by Northern blot analysis (Fig. 6*B*). The mRNA for PP2A$c\alpha$ increased significantly in the transfectants compared with the controls and following differentiation treatment in both cases. No such elevation in the basal level of mRNA was seen in the case of PP1αc. These results are consistent with the protein expression levels shown in Fig. 6*A*.

Next, we examined the enzymatic activity of total phosphatase and PP2A. Fig. 6*C* shows that PP2A activity was strengthened in the transfectants compared with the controls with or without the differentiation treatment, but no such significant difference in total phosphatase activity was seen between control and transfected cells cultured with or without differentiation medium. Collectively, these results suggest that the elevation of PP2A was responsible for suppression of Akt phosphorylation in the gene-transfected cells, leading to a greater susceptibility to apoptosis during differentiation.

PP2A Activity Is Related to the Regulation of Akt Activity in Gene-transfected Cells—To confirm that PP2A is involved in the dephosphorylation and inactivation of Akt, we examined the effect of a specific serine/threonine phosphatase inhibitor (calyculin A) on the phosphorylation and activity of Akt in the gene transfectants cultured in differentiation medium. The transfectants were cultured with 1% FCS and RA for 24 h and then treated with 5 nM calyculin A for 0, 10, or 30 min. Fig. 7*A* shows that the specific activity of PP2A was significantly reduced by the treatment with calyculin A. In contrast, the phosphorylation and specific activity of Akt were significantly increased by calyculin A in a time-dependent manner (Fig. 7, *B* and *C*). Taken together, these results suggest that the specific activity of PP2A is closely related to the regulation of Akt function in H9c2 cells.

Overexpression of CRT Increases the Intracellular Free Calcium Concentration in H9c2 Cells—CRT is a Ca^{2+} storage protein in the ER that functions in intracellular calcium homeostasis (1). We examined and compared the intracellular free Ca^{2+} contents of control and gene-transfected cells with or without the differentiation treatment (Table I). In the cells overexpressing CRT, the intracellular free Ca^{2+} concentration increased ~1.3-fold relative to the control value. This increase seems to be different from previous reports (26, 27). After 24 h of treatment to induce differentiation, intracellular free Ca^{2+} concentrations were up-regulated in both control and gene-transfected cells compared with the initial levels; but the concentration was always higher in the transfectants than in the controls, indicating that it was continuously elevated in cells overexpressing CRT.

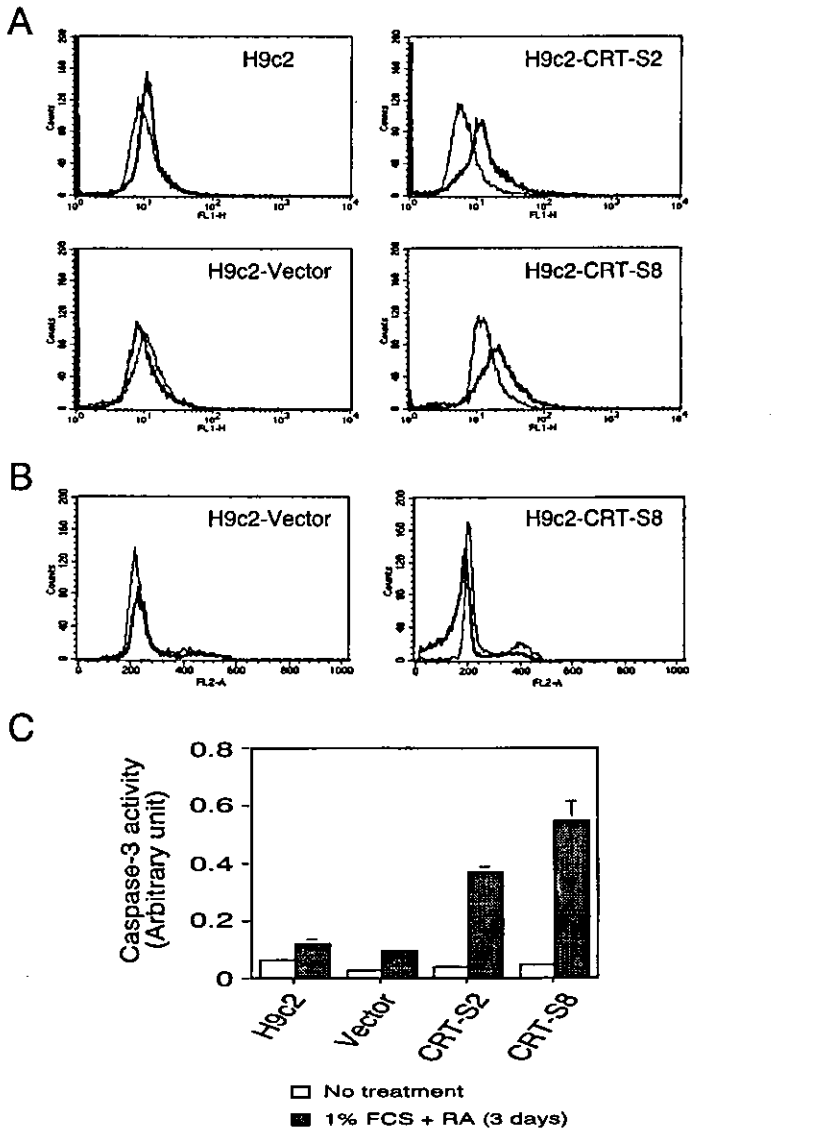

FIG. 3. *A*, TUNEL assay for control and gene-transfected H9c2 cells upon differentiation treatment. DNA double-strand breaks were detected by the TUNEL method as described under "Materials and Methods." Cells were treated with (*thick lines*) or without (*thin lines*) differentiation medium for 3 days. The data represent three independent experiments. *B*, flow cytometric analysis of DNA content in control and gene-transfected H9c2 cells upon differentiation treatment. Cells were treated with (*thick lines*) or without (*thin lines*) differentiation medium for 3 days. The data represent four independent experiments. *C*, caspase-3 activity in control and gene-transfected H9c2 cells upon differentiation treatment for 3 days. Caspase-3 activity was assayed photometrically as described under "Materials and Methods" using DEVD-*p*-nitroanilide as a substrate. Each value represents the mean ± S.D. of four independent experiments.

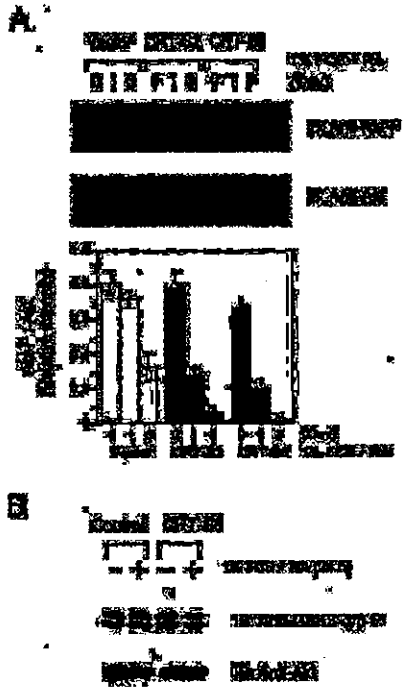

FIG. 4. *A*, phosphorylation of Akt in control and gene-transfected H9c2 cells upon differentiation treatment for 3 days. Ser^{473}-phosphorylated Akt and total Akt were detected by immunoblot (*IB*) analysis using specific antibodies as described under "Materials and Methods." The band intensity was estimated densitometrically, and the phosphorylation rate is expressed as the relative intensity of phosphorylated Akt (*Akt-P*/Akt. Each value represents the mean ± S.D. of four independent experiments. *B*, Akt activity in control and gene-transfected H9c2 cells upon differentiation treatment for 24 h. Akt activity was assayed as described under "Materials and Methods." Akt was immunoprecipitated from cell lysates (600 μg) using anti-Akt antibody, and Akt activity was then measured using GSK-3α/β as a substrate. Phosphorylated GSK-3α/β was detected by immunoblot analysis using anti-phosphorylated GSK-3α/β antibody (*Anti-GSK3-α/β-P*). The data represent three independent experiments.

Effect of Ca^{2+} Modulators on PP2Acα Expression and Akt Signaling—To examine whether intracellular Ca^{2+} levels could affect expression of the PP2Acα gene and change Akt signaling, the effect of Ca^{2+} modulators on PP2Acα expression and Akt signaling was investigated. To observe the effect of increased intracellular Ca^{2+} levels, control cells were treated with thapsigargin (5 μM) or ionomycin (1 μM) for specific periods, and the mRNA and protein expression levels of PP2Acα were then estimated by Northern blot analysis and immunoblot analysis, respectively (Fig. 8, *A* and *B*, *left panels*). Following the treatments, an increase in intracellular free Ca^{2+} was observed using a spectrofluorophotometer (data not shown). After 4 h of treatment with thapsigargin or ionomycin, both the mRNA and protein levels of PP2Acα significantly increased, suggesting that PP2Acα gene expression is regulated by intracellular Ca^{2+} levels. To confirm this, the CRT gene-transfected

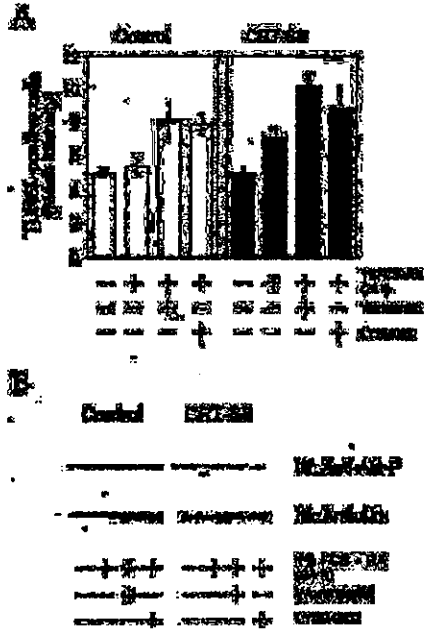

FIG. 5. **Effect of wortmannin and LY294002 on apoptosis and phosphorylation of Akt in control and gene-transfected H9c2 cells upon differentiation treatment.** *A*, TUNEL assay for control and transfected H9c2 cells upon differentiation treatment with or without wortmannin (300 nM) or LY294002 (10 μM) for 24 h. The number of apoptotic cells is expressed as a shift of the mean intensity in TUNEL-positive cells. Each value represents the mean ± S.D. of three independent experiments. *B*, phosphorylation of Akt in control and gene-transfected H9c2 cells upon differentiation treatment with or without wortmannin or LY294002 as described for *A*. Ser^{473}-phosphorylated Akt (*Akt-P*) and total Akt were detected by immunoblot (*IB*) analysis using specific antibodies as described under "Materials and Methods." The data represent three independent experiments.

cells were treated with BAPTA/AM (10 μM), a cell-permeable Ca^{2+} chelator, to decrease intracellular Ca^{2+} levels, and the mRNA and protein expression levels of PP2Acα were then estimated as described above (Fig. 8, *A* and *B*, *right panels*). After 2 h of treatment with BAPTA/AM, both the mRNA and protein levels of PP2Acα had significantly decreased. In parental H9c2 cells, BAPTA/AM showed a similar effect on PP2Acα expression (data not shown). The protein levels of PP2B-Aα showed no significant change upon treatment with such Ca^{2+} modulators. Together, these results strongly suggest that PP2Acα gene expression is regulated via intracellular Ca^{2+} homeostasis. Next, to clarify whether the change in PP2Acα expression caused by Ca^{2+} modulators reflects an alteration of Akt signaling, the phosphorylation and activity of Akt were investigated. In control cells treated with thapsigargin and ionomycin for 4 h, the phosphorylation and activity of Akt were significantly suppressed (Fig. 8*C*, *left panel*). In contrast, the gene-transfected cells treated with BAPTA/AM for 2 h showed an increase in the phosphorylation and activity of Akt (Fig. 8*C*, *right panel*). In parental cells, BAPTA/AM had similar effects on Akt signaling (data not shown). The results for Akt signal-

FIG. 6. **Protein phosphatase 2A is up-regulated in gene-transfected H9c2 cells.** *A*, immunoblot analysis of Ser/Thr protein phosphatases in control and gene-transfected H9c2 cells upon differentiation treatment for 24 h. The protein expression levels for cytoplasmic

ing were compatible with the change in PP2Acα expression caused by Ca^{2+} modulators. Collectively, these results indicate that PP2Acα expression is regulated via intracellular Ca^{2+} homeostasis, leading to the alteration of Akt signaling, suggesting that the change in PP2Acα expression and Akt signaling in CRT-overexpressing cells is mainly due to the altered regulation of intracellular Ca^{2+} levels.

DISCUSSION

In this study, we employed cardiomyoblast H9c2 cells to establish a cell line overexpressing CRT and then examined the effect of the overexpression on the cardiac differentiation of H9c2 cells. When cultured in a differentiation medium containing 1% FCS and 10 nM RA, the overexpressers showed a decrease in cell number and an increase in DNA double-strand breaks, indicating that they were highly susceptible to apoptosis compared with controls. We found that Akt signaling was significantly suppressed in the gene-transfected cells compared with the mock-transfected controls during differentiation. In control cells, the phosphorylation and activity of Akt showed a gradual decline during the culture. In contrast, the decline was significantly accelerated in the gene-transfected cells. Furthermore, in the transfectants, PP2A, a Ser/Thr protein phosphatase, was significantly up-regulated in response to the treatment, implying that suppression of Akt signaling was due to dephosphorylation of Akt caused by the up-regulated PP2A expression. Consequently, we conclude that overexpression of CRT promotes the differentiation-dependent apoptosis of H9c2 cells through suppression of the Akt signaling pathway via up-regulation of PP2A by altered Ca^{2+} homeostasis. This is the first report of the Akt-mediated cell survival signaling pathway being modulated by the introduction of the CRT gene.

Apoptosis is regulated by several signaling pathways, including the SAPK, MAPK, and protein kinase B/Akt pathways (24). The Akt signaling pathway is a well characterized anti-apoptotic signal for cell survival (28). Under conditions in which the PI3K/Akt pathway was suppressed by PI3K inhibitors, differentiation-induced apoptosis was significantly enhanced, and Akt phosphorylation was diminished in both control and CRT gene-transfected cells (Fig. 5). This indicates that Akt is an important cell survival and anti-apoptotic signal in differentiating H9c2 cells. To elucidate why Akt signaling was affected by overexpression of CRT, we compared the activity of PI3K, an upstream signal of Akt, between control and transfected cells. Surprisingly, there was no significant difference in the activity of PI3K between the cells, although differentiation-induced apoptosis was promoted in both cases by PI3K inhibitors (data not shown). In general, growth factor-induced activation of Akt is mediated by PI3K (28), but PI3K-independent activation of Akt was also reported to occur in response to specific stresses such as heat shock and hyperosmolarity (29). Therefore, in the case of H9c2 cells undergoing differentiation, Akt signaling might not be regulated solely by PI3K. Previously, PI3K and Akt signals were both

Ser/Thr protein phosphatases, including PP1cc, PP2Acα, PP2B-Aα (calcineurin), and PP2Cα, were estimated by immunoblot (*IB*) analysis using specific antibodies as described under "Materials and Methods." *B*, Northern blot analysis of PP2Ac and PP1cc in control and gene-transfected H9c2 cells upon differentiation treatment for 24 h. Total RNA (10 μg) was separated by electrophoresis on 1% agarose gel containing formaldehyde. After blotting onto nylon membrane, the membrane filter was hybridized with ^{32}P-labeled DNA probes for PP1cc and PP2Acα. Autoradiographed membranes were analyzed using a Fuji BAS5000 bioimage analyzer. *C*, enzymatic activities of PP2A and total phosphatase in control and gene-transfected H9c2 cells upon differentiation treatment for 24 h. The activities of total phosphatase and PP2A were assayed photometrically as described under "Materials and Methods" using *p*-nitrophenyl phosphate and RKpTIRR, respectively. Each value represents the mean ± S.D. of three independent experiments.

FIG. 7. **Calyculin A suppresses PP2A activity, leading to an increase in Akt phosphorylation and activity in gene-transfected H9c2 cells upon differentiation treatment.** *A*, effect of calyculin A on PP2A activity in gene-transfected H9c2 cells upon differentiation treatment. The transfectants were cultured with 1% FCS and RA for 24 h and then treated with 5 nM calyculin A for 0, 10, or 30 min. PP2A activity was assayed photometrically as described under "Materials and Methods" using RKpTIRR as a substrate. *B*, effect of calyculin A on Akt phosphorylation in gene-transfected H9c2 cells upon differentiation treatment. The transfectants were cultured with differentiation medium for 24 h and then treated with calyculin as described for *A*. Phosphorylated Akt and total Akt were detected by immunoblot analysis as described under "Materials and Methods" using specific antibodies. The phosphorylation rate of Akt is expressed as the relative intensity of phosphorylated Akt (*Akt-P*/Akt. *C*, effect of calyculin A on Akt activity in gene-transfected H9c2 cells upon differentiation treatment. The transfectants were cultured with differentiation medium for 24 h and then treated with calyculin as described for *A*. The activity of immunoprecipitated Akt was measured as described under "Materials and Methods" using GSK-3α/β as a substrate. Phosphorylated GSK-3α/β was detected by immunoblot analysis, and the band intensity was quantified densitometrically. Each value represents the mean ± S.D. of three to four independent experiments.

reported to be involved in the skeletal differentiation of H9c2 cells (30). The authors described that PI3K regulated cell differentiation mainly through an Akt-independent pathway. However, to our knowledge, there is no report that Akt functions in the apoptosis of H9c2 cells.

To identify other regulators of Akt activity and signaling, we focused on protein phosphatases that could regulate the activity by dephosphorylating phosphoseryl or phosphothreonyl residues of Akt. We found that the expression and activity of PP2A were significantly increased in the gene transfectants compared with the controls throughout the differentiation (Fig. 6).

TABLE I

Intracellular free calcium concentration in control and gene-transfected H9c2 cells upon differentiation treatment

Each value represents the mean ± S.D. of six experiments.

	Calcium conc upon.	
	No treatment	24-h treatment with 1% FCS and 10 nM RA
	nM	
H9c2	69.3 ± 7.9	97.3 ± 11.5
Vector	67.3 ± 12.3	97.3 ± 8.0
CRT-S2	88.3 ± 15.2	109.8 ± 11.0
CRT-S8	97.3 ± 16.3	121.3 ± 16.0

Ser/Thr-specific PP2A is present in most eukaryotic cells and functions in a variety of processes, including cell cycle regulation, cell differentiation, and signal transduction (31–33). PP2A is known to modulate the activities of several kinases *in vitro* and *in vivo* such as phosphorylase kinase (34), MAPKs, the calmodulin-dependent kinase, protein kinase A, protein kinase B/Akt, protein kinase C, p70 S6 kinase, IκB kinase, and cyclin-dependent kinases (35). Akt is inactivated *in vitro* by PP2A and is activated in cells upon treatment with okadaic acid (36–38) and calyculin A (37, 39), suggesting that Akt is a putative substrate for PP2A. We also observed that calyculin A inhibited PP2A activity to prevent the differentiation-induced dephosphorylation and inactivation of Akt in cells transfected with the CRT gene (Fig. 7). Collectively, these results strongly suggest that PP2A acted as a regulator for dephosphorylation and inactivation of Akt in the transfected H9c2 cells during their differentiation.

Recently, it was reported that CRT expression levels can modulate intracellular signaling, including the β-catenin pathway, by altering protein-tyrosine kinase or phosphatases (40). It was observed that overexpression of CRT in mouse L fibroblasts decreased protein phosphorylation at tyrosine and also that the dephosphorylated protein was β-catenin, although the mechanism of the CRT-dependent modulation of tyrosine dephosphorylation was not made clear. Similarly, in H9c2 cells overexpressing CRT, we too observed a decrease in protein phosphorylation at tyrosine compared with controls (data not shown). However, it is worth nothing that the phosphotyrosine levels and patterns for PI3K-associated proteins differed little between the control and gene-transfected cells (data not shown). PI3K is activated by binding through Src homology domain 2 to signaling proteins bearing phosphotyrosine (41). These findings suggest that the decrease in protein phosphorylation at tyrosine occurs selectively in cells overexpressing CRT, although the molecular mechanism involved is not known.

Recently, Nakamura *et al.* (42) reported that cells deficient in CRT are resistant to apoptosis compared with cells expressing CRT. Pinton *et al.* (43) have also shown that overexpression of CRT promotes ceramide-induced apoptosis in HeLa cells. These results seem to support our finding that CRT expression positively regulates the apoptotic process under specific cellular conditions such as during cell differentiation. However, Oyadomari *et al.* (44) reported that overexpression of CRT actually protects pancreatic β-cells from nitric oxide-induced apoptosis, whereas Zhu and Wang (45) found that CRT antisense oligonucleotides down-regulate CRT protein production and significantly increase the sensitivity to calcium ionophore-induced apoptosis. This discrepancy may be due to the different cell types, stress stimuli, and experimental models used, but further investigation is needed into the molecular mechanism of the apoptotic process in each of these experimental models.

Retinoids are potent regulators of cell proliferation and differentiation (46). CRT was reported to interfere with retinoid signals both *in vitro* and *in vivo* (47–50). Very recently, Holaska

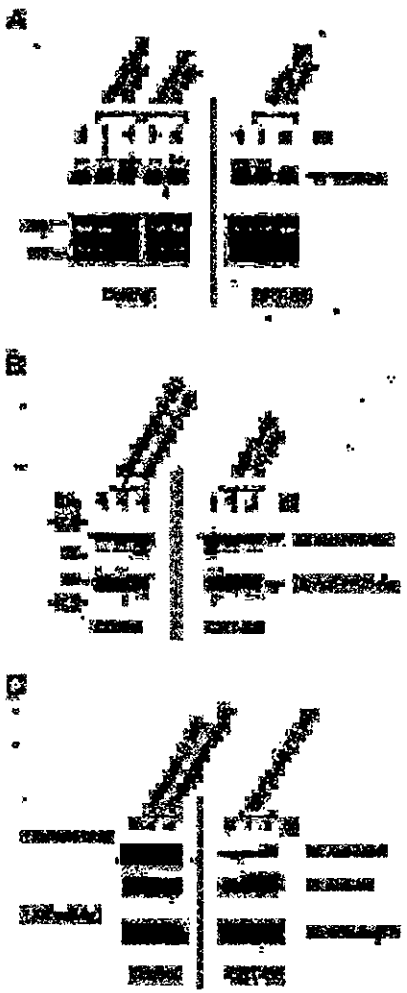

FIG. 8. **Effect of Ca^{2+} modulators on PP2Acα expression and Akt signaling.** Control H9c2 cells were treated with thapsigargin (5 μM) or ionomycin (1 μM) for the periods indicated (*left panels*). The CRT gene-transfected cells were treated with BAPTA/AM (10 μM) for the periods specified (*right panels*). After each treatment, cells were harvested and subjected to the following assays. *A*, shown are the results from Northern blot analysis of PP2Acα. Total RNA (10 μg) was separated by electrophoresis and then blotted onto nylon membrane. The membrane filter was hybridized with ^{32}P-labeled DNA probes for PP2Acα. Autoradiographed membranes were analyzed using a Fuji BAS5000 bioimage analyzer. *B*, shown are the results from immunoblot (*IB*) analysis of PP2Acα and PP2B-Aα. The protein expression levels for PP2Acα and PP2B-Aα were estimated by immunoblot analysis using specific antibodies. *C*, phosphorylated Akt (*Akt-P*) and total Akt were detected by immunoblot analysis using specific antibodies as described under "Materials and Methods." Akt activity was assayed as described under "Materials and Methods" using GSK-3α/β as a substrate. The enzymatic product of Akt, phosphorylated GSK-3α/β (*GSK-3α/β-P*), was detected by immunoblot analysis using anti-phosphorylated GSK-3α/β antibody. The data represent three independent experiments.

et al. (5) demonstrated that some CRT exists in the cytosol, where it functions as a nuclear export receptor for the glucocorticoid receptor by binding its DNA-binding domain, including the sequence KGFFKR. They suggested that retinoid receptors are also regulated by this nuclear export pathway because they contain an amino acid sequence highly similar to that of the glucocorticoid receptor. In the present study, RA was used to induce the cardiac differentiation of H9c2 cells. However, H9c2 cells are known to differentiate into skeletal myotubes in culture medium containing 1% FCS and no RA (14, 30). Similarly, in the CRT gene transfectants, differentiation-induced apoptosis was observed only when 1% FCS was present in the culture medium (data not shown). Moreover, Akt signaling was suppressed accompanying the up-regulation of PP2A in the transfectants only with 1% FCS (data not shown). Thus, these findings suggest that the differentiation-induced apoptosis promoted in the cells overexpressing CRT is not solely due to the alteration of retinoic acid signaling. In a previous report, the selective down-regulation of the catalytic β-subunit (but not α-subunit) of PP2A was observed during RA-induced differentiation of HL-60 cells (51), but the biological significance and molecular mechanism of this event are still not known.

A previous study indicates that enhanced expression of CRT increases the Ca^{2+} storage capacity of the ER (1). CRT also appears to modulate store-operated Ca^{2+} influx (26, 27, 52, 53) and to alter Ca^{2+} transport by the sarcoplasmic/endoplasmic reticulum Ca^{2+}-ATPase SERCA2b (54). In the present study, the intracellular free concentration Ca^{2+} was higher in the CRT gene transfectants than in the controls throughout differentiation. To elucidate whether altered Ca^{2+} homeostasis could affect PP2Acα expression and Akt signaling, the effect of Ca^{2+} modulators on PP2Acα expression and Akt signaling was tested (Fig. 8). The results showed that PP2Acα expression increased to suppress Akt signaling upon treatment with thapsigargin and ionomycin, which increased the level of intracellular Ca^{2+}. Furthermore, upon treatment with BAPTA/AM, which decreases intracellular Ca^{2+} levels, PP2Acα expression decreased to enhance Akt signaling. These results strongly suggest that PP2Acα gene expression is controlled by intracellular Ca^{2+} levels and homeostasis. The gene structure and regulation of PP2A have been elucidated in human and rat. In both PP2Acα genes, the promoter region is GC-rich and lacks TATA and CCAAT sequences, consistent with a housekeeping gene (55, 56). The PP2Acα gene contains several Sp1-binding sites and a potential cAMP-responsive element (CRE). CRE may be regulated by a calcium-regulated transcription factor (CRE-binding protein) through Ca^{2+}/calmodulin-dependent kinases (57), but the DNA-binding activity for CRE was suppressed in the CRT gene-transfected cells compared with control cells in the electrophoretic mobility shift assay (data not shown). Rather, the DNA-binding activity for Sp1 increased in the CRT gene-transfected cells compared with control cells (data not shown). Although the precise mechanism linking CRE, Sp1, and overexpression of CRT in H9c2 cells is still not clear, further investigation based on Ca^{2+} homeostasis will be required to understand the gene regulation by overexpression of CRT. Although elevations in Ca^{2+} act as a signal, a prolonged increase in the concentration of Ca^{2+} can be lethal (58). Moreover, transcription factors are activated differentially by the amplitude and duration of the response to Ca^{2+} (59). Therefore, overexpression of CRT may affect the transcriptional regulation of PP2Acα mainly via the regulation of Ca^{2+} homeostasis in H9c2 cells.

CRT functions as a molecular chaperone in the ER (60). It is widely believed that CRT and its membrane-bound homolog calnexin act as molecular chaperones for *N*-linked glycoproteins because they are associated predominantly with folding intermediates rather than fully folded glycoproteins *in vivo* (60, 61). It has also been confirmed that CRT and calnexin function as chaperones for both glycosylated and non-glycosylated proteins *in vitro* (62, 63) and *in vivo* (64). This chaperone function of CRT may also contribute to the differentiation-induced apoptosis of H9c2 cells overexpressing CRT by affecting the ER stress signaling pathway. When the ER is under stress, resident kinases such as IRE1 and PKR-like ER kinase are activated to produce stress signals through a change in the luminal environment, *e.g.* by accumulation of unfolded proteins in the ER (65). Another ER chaperone, BiP, has been reported to be involved in the regulation of IRE1 activation in the ER under stress conditions (66). Moreover, Urano *et al.* (67) demonstrated that IRE1 activates c-Jun N-terminal kinase in response to ER stress. This strongly suggests that endogenous signals initiated in the ER modulate cytoplasmic signal transduction cascades. Recently, Nakagawa *et al.* (68) reported that caspase-12 is activated in the ER specifically in response to ER stress. Therefore, it is also possible that a pathway containing caspase-12 is involved in the differentiation-induced apoptosis of H9c2 cells overexpressing CRT.

In conclusion, we have demonstrated that, when overexpressed, CRT modulates Akt signaling to promote differentiation-induced apoptosis in H9c2 cells. CRT is essential for cardiac development, and its expression is strictly down-regulated in mature cardiomyocytes. As CRT functions to promote apoptosis, it may have some important physiological function in the process of cardiogenesis. Although further investigation of the correlation between CRT expression and apoptotic signals is required, this study has revealed a novel pathway of cellular signaling for apoptosis and its regulation via a change in the ER luminal environment and Ca^{2+} homeostasis.

Acknowledgments—We thank Drs. Kunimi Kikuchi and Hiroshi Shima for generously providing the rat PP1cα and PP2Acα cDNAs. We also thank Noriko Sadakata, Satoko Mori, and Hiromi Setoguchi for technical assistance.

REFERENCES

1. Michalak, M., Corbett, E. F., Mesaeli, N., Nakamura, K., and Opas, M. (1999) *Biochem. J.* **344**, 281–292
2. Michalak, M., Milner, R. E., Burns, K., and Opas, M. (1992) *Biochem. J.* **285**, 681–692
3. Johnson, S., Michalak, M., Opas, M., and Eggleton, P. (2001) *Trends Cell Biol.* **11**, 122–129
4. Krause, K.-H., and Michalak, M. (1997) *Cell* **88**, 439–443
5. Holaska, J. M., Black, B. E., Love, D. C., Hanover, J. A., Leszyk, J., and Paschal, B. M. (2001) *J. Cell Biol.* **152**, 127–140
6. Imanaka-Yoshida, K., Aoitani, A., Ioshii, S. O., Koyabu, S., Yamakado, T., and Yoshida, T. (1996) *J. Mol. Cell. Cardiol.* **28**, 553–562
7. Srivastava, D., and Olson, E. N. (2000) *Nature* **407**, 221–226
8. Guo, L., Lynch, J., Nakamura, K., Fliegel, L., Kazahara, R., Izumo, S., Kozuru, I., Agellon. L. B., and Michalak, M. (2001) *J. Biol. Chem.* **276**, 2797–2801
9. Mesaeli, N., Nakamura, K., Zvaritch, E., Dickie, P., Dziak, E., Krause, K.-H., Opas, M., MacLennan, D. H., and Michalak, M. (1999) *J. Cell Biol.* **144**, 857–868
10. Rauch, F., Prud'homme, J., Arabian, A., Dedhar, S., and St-Arnaud, R. (2000) *Exp. Cell Res.* **258**, 105–111
11. Nakamura, K., Robertson, M., Liu, G., Dickie, P., Nakamura, K., Guo, J. Q., Duff, H. J., Opas, M., Kavanagh, K., and Michalak, M. (2001) *J. Clin. Invest.* **107**, 1245–1253
12. Kimes, B. W., and Brandt, B. L. (1976) *Exp. Cell Res.* **98**, 367–381
13. Hescheler, J., Meyer, R., Plant, S., Krautwurst, D., Rosenthal, W., and Schultz, G. (1991) *Circ. Res.* **69**, 1476–1486
14. Ménard, C., Pupier, S., Mornet, D., Kitzmann, M., Nargeot, J., and Lory, P. (1999) *J. Biol. Chem.* **274**, 29063–29070
15. Smith, M. J., and Koch, G. L. (1989) *EMBO J.* **8**, 3581–3586
16. Gevriali, Y., Sherman, Y., and Benn-Sasson, S. A. (1992) *J. Cell Biol.* **119**, 493–501
17. Nicoletti, I., Migliorati, G., Pagliacci, M. C., Grimgnani, F., and Riccardi, C. (1991) *J. Immunol. Methods* **139**, 271–279
18. Ihara, Y., Sakamoto, Y., Mihara, M., Shimizu, K., and Taniguchi, N. (1997) *J. Biol. Chem.* **272**, 9629–9634
19. Kitamura, K., Misuno, Y., Sasaki, A., Yasui, A., Tsuiki, S., and Kikuchi, K. (1991) *J. Biochem. (Tokyo)* **109**, 307–310
20. Kitagawa, Y., Tahara, T., Ikeda, I., Kikuchi, K., Tsuiki, S., Sugimura, T., and Nagao, M. (1988) *Biochim. Biophys. Acta* **951**, 123–129
21. Sambrook, J., Fritsch, E. F., and Maniatis, T. (1989) *Molecular Cloning: A Laboratory Manual*, 2nd Ed., pp. 7–39, Cold Spring Harbor Laboratory, Cold Spring Harbor, NY
22. Chen, Q., Jones, T. W., and Stevens, J. L. (1994) *J. Cell. Physiol.* **161**, 293–302
23. Grynkiewcz, G., Poenie, M., and Tsien, R. Y. (1985) *J. Biol. Chem.* **260**, 3440–3450
24. Ballif, B. A., and Blenis, J. (2001) *Cell Growth Differ.* **12**, 397–408
25. Alessi, D. R., Andjelkuvic, M., Caudwell, B., Cron, P., Morrice, N., Cohen, P., and Hemmings, B. A. (1996) *EMBO J.* **15**, 6541–6551
26. Bastianutto, C., Clementi, E., Codazzi, F., Podini, P., De Giorgi, F., Rizzuto, R., Meldolesi, J., and Pozzan, T. (1995) *J. Cell Biol.* **130**, 847–855
27. Mery, L., Mesaeli, N., Michalak, M., Opas, M., Lew, D. P., and Krause, K.-H. (1996) *J. Biol. Chem.* **271**, 9332–9339
28. Coffer, P. J., Jin, J., and Woodgett, J. R. (1998) *Biochem. J.* **335**, 1–13
29. Konishi, H., Matsuzaki, H., Tanaka, M., Ono, Y., Tokunaga, C., Kuroda, S., and Kikkawa, U. (1996) *Proc. Natl. Acad. Sci. U. S. A.* **93**, 7639–7643
30. Kim, J. M., Yoon, M.-Y., Kim, J., Kim, S. S., Kang, I., Ha, J., and Kim, S. S. (1999) *Arch. Biochem. Biophys.* **367**, 67–78
31. Mumby, M. C., and Walter, G. (1993) *Physiol. Rev.* **73**, 673–699
32. Mayer-Jaekel, R. E., and Hemmings, B. A. (1994) *Trends Cell Biol.* **4**, 287–291
33. Janssens, V., and Goris, J. (2001) *Biochem. J.* **353**, 417–439
34. Ramachandran, C., Goris, J., Waelkens, E., Merlevede, W., and Walsh, D. A. (1987) *J. Biol. Chem.* **262**, 3210–3218
35. Millward, T. A., Zolnierowicz, S., and Hemmings, B. A. (1999) *Trends Biochem. Sci.* **24**, 186–191
36. Andjelkovic, M., Jakubowicz, T., Cron, P., Ming, X.-F., Han, J.-W., and Hemmings, B. A. (1996) *Proc. Natl. Acad. Sci. U. S. A.* **93**, 5699–5704
37. Chen, D., Pucini, R. V., Olson, A. L., Hemmings, B. A., and Pessin, J. E. (1999) *Mol. Cell. Biol.* **19**, 4684–4694
38. Sato, S., Fujita, N., and Tsuruo, T. (2000) *Proc. Natl. Acad. Sci. U. S. A.* **97**, 10832–10837
39. Meier, R., Thelen, M., and Hemmings, B. A. (1998) *EMBO J.* **17**, 7294–7303
40. Fadel, M. P., Szewczenko-Pawlikowski, M., Leclerc, P., Dziak, E., Symonds, J. M., Blaschuk, O., Michalak, M., and Opas, M. (2001) *J. Biol. Chem.* **276**, 27063–27069
41. Songyang, Z., and Cantley, L. C. (1995) *Trends Biochem. Sci.* **20**, 470–475
42. Nakamura, K., Bossy-Wetzel, E., Burns, K., Fadel, M. P., Lozyk, M., Goping, I. S., Opas, M., Bleackley, R. C., Green, D. R., and Michalak, M. (2000) *J. Cell Biol.* **150**, 731–740
43. Pinton, P., Ferrari, D., Rapizzi, E., Virgilio, F. D., Pozzan, T., and Rizzuto, R. (2001) *EMBO J.* **20**, 2690–2701
44. Oyadomari, S., Takeda, K., Takiguchi, M., Gotoh, T., Matsumoto, M., Wada, I., Akira, S., Araki, E., and Mori, M. (2001) *Proc. Natl. Acad. Sci. U. S. A.* **98**, 10845–10850
45. Zhu, N., and Wang, Z. (1999) *Cancer Res.* **59**, 1896–1902
46. De Leca, L. M. (1991) *FASEB J.* **5**, 2924–2933
47. Dedhar, S., Rennie, P. S., Shago, M., Leung Hagesteijn, C.-Y., Yang, H., Filmus, J., Hawley, R. G., Bruchovsky, N., Cheng, H., Matsuik, R. J., and Giguere, V. (1994) *Nature* **367**, 480–483
48. Winrow, C. J., Miyata, K. S., Marcus, S. L., Burns, K., Michalak, M., Capone, J. P., and Rachubinski, R. A. (1995) *Mol. Cell. Endocrinol.* **111**, 175–179
49. Dessi, D., Michalak, M., Singh, N. K., and Nilles, R. M. (1996) *J. Biol. Chem.* **271**, 15153–15159
50. Shago, M., Flock, G., Leung Hagesteijn, C.-Y., Woodside, M., Grinstein, S., Giguere, V., and Dedhar, S. (1997) *Exp. Cell Res.* **230**, 50–60
51. Nishikawa, M., Omay, S. B., Toyoda, H., Tawara, I., Shima, H., Nagao, M., Hemmings, B. A., Mumby, M. C., and Deguchi, K. (1994) *Cancer Res.* **54**, 4879–4884
52. Fasolato, C., Pizzo, P., and Pozzan, T. (1998) *Mol. Biol. Cell* **9**, 1513–1522
53. Xu, W., Longo, F. J., Wintermantel, M. R., Jiang, X., Clark, R. A., and DeLisle, S. (2000) *J. Biol. Chem.* **275**, 36676–36682
54. John, L. M., Lechleiter, J. D., and Camacho, P. (1998) *J. Cell Biol.* **143**, 963–973
55. Khew-Goodall, Y., Mayer, R. E., Maurer, F., Stone, S. R., and Hemmings, B. A. (1991) *Biochemistry* **30**, 89–97
56. Kitagawa, Y., Shima, H., Sasaki, K., and Nagao, M. (1991) *Biochim. Biophys. Acta* **1089**, 339–344
57. West, A. E., Chen, W. G., Dalva, M. B., Dolmetsch, R. E., Kornhauser, J. M., Shaywitz, A. J., Takasu, M. A., Tao, X., and Greenberg, M. E. (2001) *Proc. Natl. Acad. Sci. U. S. A.* **98**, 11024–11031
58. Berridge, M. J., Bootman, M. D., and Lipp, P. (1998) *Nature* **395**, 645–648
59. Dolmetsch, R. E., Lewis, R. S., Goodnow, C. C., and Healy, J. I. (1997) *Nature* **386**, 855–858
60. Helenius, A., Trombetta, E. S., Hebert, D. N., and Simons, J. F. (1997) *Trends Cell Biol.* **7**, 193–200
61. Ellgaard, L., and Helenius, A. (2001) *Curr. Opin. Cell Biol.* **13**, 431–437
62. Saito, Y., Ihara Y., Leach, M. R., Cohen-Doyle, M. F., and Williams, D. B. (1999) *EMBO J.* **18**, 6718–6729
63. Ihara, Y., Cohen-Doyle, M. F., Saito, Y., and Williams, D. B. (1999) *Mol. Cell* **4**, 331–341
64. Danilczyk, U. G., and Williams, D. B. (2001) *J. Biol. Chem.* **276**, 25532–25540
65. Kaufman, R. J. (1999) *Genes Dev.* **13**, 1211–1233
66. Bertolotti, A., Zhang, Y., Hendershot, L. M., Harding, H. P., and Ron, D. (2000) *Nat. Cell Biol.* **2**, 326–332
67. Urano, F., Wang, X., Bertolotti, A., Zhang, Y., Chung, P., Harding, H. P., and Ron, D. (2000) *Science* **287**, 664–666
68. Nakagawa, T., Zhu, H., Morishima, N., Li, E., Xu, J., Yankner, B. A., and Yuan, J. (2000) *Nature* **403**, 98–103

ACADEMIC PRESS

Biochemical and Biophysical Research Communications 297 (2002) 353–360

BBRC

www.academicpress.com

Tyrosine phosphorylation of clathrin heavy chain under oxidative stress

Yoshito Ihara,[a] Chie Yasuoka,[a] Kan Kageyama,[a] Yoshinao Wada,[b] and Takahito Kondo[a,*]

[a] *Department of Biochemistry and Molecular Biology in Disease, Atomic Bomb Disease Institute, Nagasaki University School of Medicine, 1-12-4 Sakamoto, Nagasaki 852-8523, Japan*

[b] *Reaearch Institute, Osaka Medical Center for Maternal and Child Health, 840 Murodo-cho, Izumi, Osaka 594-1101, Japan*

Received 6 August 2002

Abstract

In mouse pancreatic insulin-producing βTC cells, oxidative stress due to H_2O_2 causes tyrosine phosphorylation in various proteins. To identify proteins bearing phosphotyrosine under stress, the proteins were affinity purified using an anti-phosphotyrosine antibody-conjugated agarose column. A protein of 180 kDa was identified as clathrin heavy chain (CHC) by electrophoresis and mass spectrometry. Immunoprecipitated CHC showed tyrosine phosphorylation upon H_2O_2 treatment and the phosphorylation was suppressed by the Src kinase inhibitor, PP2. The phosphorylation status of CHC affected the intracellular localization of CHC and the clathrin-dependent endocytosis of transferrin under oxidative stress. In conclusion, CHC is a protein that is phosphorylated at tyrosine by H_2O_2 and this phosphorylation status is implicated in the intracellular localization and functions of CHC under oxidative stress. The present study demonstrates that oxidative stress affects intracellular vesicular trafficking via the alteration of clathrin-dependent vesicular trafficking. © 2002 Elsevier Science (USA). All rights reserved.

Keywords: Clathrin heavy chain; H_2O_2; Oxidative stress; Pancreatic β-cell; Tyrosine phosphorylation

Pancreatic β-cells are more susceptible to oxidative stress than other cell types, perhaps because of the relatively low potential of their cellular anti-oxidant systems [1]. This would suggest that β-cells are easily damaged by oxidative stress caused by a variety of environmental factors, and this may be a factor in the β-cell dysfunction that contributes to the pathogenesis and development of diabetes. In this respect, it is important to investigate the effect of oxidative stress on β-cell signaling to understand the pathophysiology of β-cell dysfunction in diabetes.

The proliferation of pancreatic β-cells is known to be regulated by several growth factors, including growth hormone and insulin-like growth factor I [2]. In the case of insulin-like growth factor I signaling, tyrosine phosphorylation status is important in downstream adapter proteins such as the insulin receptor substrate family. The phosphorylation of adapter proteins leads to phosphatidylinositol 3-kinase-dependent downstream activation of protein kinase B/Akt and 70-kDa S6 kinase, which are important for β-cell growth and survival [3]. The tyrosine-phosphorylation status of signaling proteins is known to be influenced by oxidative stress via the altered regulation of kinases and tyrosine phosphatase [4], suggesting that oxidative stress modulates β-cell functions by affecting the tyrosine-phosphorylation status of various signaling proteins.

In the present study, we focused on the altered tyrosine-phosphorylation status of cellular proteins in pancreatic βTC cells under oxidative stress and found the clathrin heavy chain (CHC) to be phosphorylated by H_2O_2. The phosphorylation status of CHC under stress affected its intracellular localization and clathrin-dependent endocytosis. This is the first report which shows that CHC is phosphorylated at tyrosine by H_2O_2 and suggests a novel physiological regulation of β-cell function via altered CHC functions under conditions of oxidative stress.

Materials and methods

Antibodies and reagents. The anti-phosphotyrosine monoclonal antibody (PY99) and the anti-clathrin heavy chain polyclonal antibody (C-20) were purchased from Santa Cruz Technology (Santa Cruz, CA). The anti-clathrin heavy chain monoclonal antibody (Clone X22) [5] was purchased from Affinity Bioreagents (Golden, CO), and used for immunoprecipitation and immunofluorescence. The antibodies against Src and phosphorylated Src were from Upstate Biotechnology (Lake Placid, NY) and Biosource International (Camarillo, CA), respectively. The other reagents used in the study were of high quality grade and from Sigma (St. Louis, MO) or Wako Pure Chemicals (Osaka, Japan).

Cell culture. Mouse pancreatic insulinoma βTC cells were established from transgenic mice expressing the simian virus 40 large T antigen under the control of the rat insulin gene promoter [6]. βTC cells were cultured in Dulbecco's modified Eagle's medium (DMEM) containing 5.5 mM glucose, supplemented with 10% fetal calf serum (FCS), under a humidified atmosphere of 95% air and 5% CO_2. For stimulation, H_2O_2 was added in the culture medium to a final concentration of 100 μM and then the culture was continued for a given period.

Immunoprecipitation and immunoblot analysis. Cultured cells were harvested and lysed in lysis buffer [20 mM Tris–HCl (pH 7.2), 130 mM NaCl, 1% NP-40, 10% glycerol, 0.4 mM sodium orthovanadate, 10 mM sodium pyrophosphate, and 10 mM sodium fluoride including protease inhibitors (20 μM APMSF, 50 μM pepstatin, and 50 μM leupeptin)]. Cell lysates normalized with respect to protein levels were immunoprecipitated using the primary antibodies. After preclearing, the cell lysates were incubated with the primary antibodies at 4 °C for 2 h, followed by another 1 h with protein G–Sepharose beads (Amersham Pharmacia Biotechnology, UK). After a wash with the lysis buffer, the immunoprecipitates were subjected to immunoblotting. For immunoblot analysis, proteins were eluted from the beads by boiling with SDS-dye solution. Protein samples were electrophoresed on 7.5 or 10% SDS–polyacrylamide gels under reducing conditions and then transferred to nitrocellulose membranes as described before [7]. The membranes were blocked with 3% bovine serum albumin or 5% skim milk in TBS [10 mM Tris–HCl (pH 7.5), 0.15 M NaCl] and then incubated at room temperature for 2 h with the primary antibody in TBS containing 0.05% Tween 20. The blots were coupled with the peroxidase-conjugated secondary antibodies, washed, and then developed using the ECL chemiluminescence detection kit (Amersham Pharmacia Biotechnology) according to manufacturer's instructions.

Purification and identification of tyrosine-phosphorylated proteins. Cells (approximately 1×10^8) were treated at 37 °C with 100 μM H_2O_2 for 10 min, harvested, lysed with the lysis buffer described above, and then centrifuged at 8000*g* for 20 min to remove the debris. The supernatant was applied to the anti-phosphotyrosine antibody (PY20)-conjugated agarose column (1 mg IgG/0.5 ml gel: Transduction Laboratories) equilibrated with the lysis buffer. After a wash with the lysis buffer, proteins bound to the column were eluted with 10 mM NH_3 and neutralized with sodium acetate (pH 4.5). Eluted fractions were concentrated and the buffer was changed to 10 mM Tris–HCl (pH 7.5), 150 mM NaCl using a centricon-YM10 (Millipore). The purified protein sample was separated by 7.5% SDS–PAGE and visualized by silver staining. The silver-stained band was excised and subjected to in-gel digestion by trypsin. Peptide mass fingerprinting was performed as described elsewhere [8] using the obtained tryptic peptides. The protein was identified with the MASCOT (Matrix Science, London) searching algorithms using the non-redundant database [9].

Fluorescence microscopy. Cells (5×10^4/ml) were grown on Lab-Tek chamber slides for 24 h. They were fixed with 4% paraformaldehyde in phosphate-buffered saline (PBS, pH 7.2) and permeabilized for 10 min with PBS containing 0.1% Triton X-100. The cells were then blocked with 1% bovine serum albumin (BSA) in PBS, incubated at 4 °C with the antibody against CHC (X22) overnight, and washed with PBS containing 1% BSA. The immunoreactive primary antibody was visualized with fluorescein isothiocyanate (FITC)-conjugated anti-mouse immunoglobulin (Cappel). After a wash, the stained cells were mounted in the Vectashield medium. A Zeiss Axioskop2 (Carl Zeiss, Jena, Germanny), with epi-illumination for fluorescence, was used for the fluorescence microscopic analysis.

Preparation of plasma membrane and cytoplasmic fractions. The plasma membrane fraction was isolated by differential centrifugation essentially as described by Corvera [10]. Cells were homogenized in 20 mM sodium phosphate (pH 6.5), 1 mM EDTA, and 255 mM sucrose using a Dounce homogenizer. Cell homogenates were centrifuged at 3000*g* for 10 min and the supernatant was further centrifuged at 12,000*g* for 15 min. The plasma membrane was precipitated and separated from the cytoplasmic fraction (supernatant). Cell surface proteins from a test sample were biotinylated with sulfo-NHS-biotin (Pierce) according to manufacturer's protocol and the purity of the plasma membrane fraction was confirmed by immunoblot analysis using a peroxidase-conjugated avidin (Fig. 3B, inset). The plasma membrane pellet was solubilized in 100 mM Tris–HCl (pH 8.0) 8 M urea, and used for further analysis.

Quantification of internalization of dextran and transferrin. The uptake of both fluorescent dextran and transferrin by the cells was measured to assess bulk and clathrin-coated vesicle dependent endocytosis, respectively. The cells were treated with or without H_2O_2 (100 μM) for 10 min and washed with cold PBS after removal of the medium. Then, the cells were cultured at 37 °C for given periods in Earle's balanced salt solution containing 20 μg/ml of 70 kDa FITC-dextran or FITC-transferrin (Molecular Probes, Eugene, OR) with or without H_2O_2 (100 μM). To terminate the uptake, the cells were chilled and washed three times with cold PBS. Next they were lysed as described, the cell lysates were excited at 494 nm, and the emission at 520 nm was determined using a spectrofluorophotometer (Shimadzu RF-5000, Japan) to quantitate the internalized FITC-labeled molecules. In some experiments, the cells were precultured for 15 min with PP2 (1 μM) before H_2O_2 treatment and PP2 coexisted in the solution during subsequent culture. The uptake of FITC-transferrin was also visualized by fluorescence microscopy as described above.

Results and discussion

Purification and identification of CHC as a tyrosine-phosphorylated protein under oxidative stress with H_2O_2

To investigate the effect of oxidative stress on the tyrosine-phosphorylation of cellular proteins, proteins bearing phosphotyrosine were detected in βTC cells treated with H_2O_2 by immunoblot analysis using an anti-phosphotyrosine antibody. As shown in Fig. 1A, various proteins were detected and distinct signals of 180, 110, 90, 80, and 54 kDa were enhanced by 100 μM H_2O_2 treatment in a time-dependent manner.

To identify the proteins phosphorylated by H_2O_2, those bearing phosphotyrosine were affinity purified from lysate of cells treated with H_2O_2, using an anti-phosphotyrosine antibody-conjugated agarose column as described in Materials and methods. As shown in Fig. 1B, various proteins were purified and tyrosine-phosphorylated proteins were confirmed by immunoblot analysis using an anti-phosphotyrosine antibody. Among the purified proteins, we focused on one with a molecular size of 180 kDa. After SDS–PAGE followed by silver staining, the band corresponding to the location of the 180 kDa protein was excised and digested in-gel with trypsin, and then subjected to mass spect-

* Corresponding author. Fax: +81-95-849-7100.
E-mail address: kondo@net.nagasaki-u.ac.jp (T. Kondo).

PII: S0006-291X(02)02195-2

Fig. 1. Purification and identification of CHC as a tyrosine-phosphorylated protein under oxidative stress. (A) Tyrosine-phosphorylated proteins were characterized by immunoblot analysis using an anti-phosphotyrosine antibody in βTC cells treated with H_2O_2 (100 μM) for the periods indicated. Arrows show proteins in which phosphotyrosine signals are enhanced. (B) Tyrosine-phosphorylated proteins were affinity purified from the cells treated with H_2O_2 (100 μM, 10 min) with an anti-phosphotyrosine antibody-conjugated agarose column. Purified proteins were subjected to 7.5% SDS–PAGE, followed by silver staining or immunoblot analysis using an anti-phosphotyrosine antibody as described in Materials and methods. PP180 (arrow) was identified as CHC by peptide mass finger printing as described in Materials and methods. (C) CHC was immunoprecipitated from cells treated with or without H_2O_2 (100 μM, 10 min), using a specific antibody (X22) as described in Materials and methods. The immunoprecipitates were subjected to 7.5% SDS–PAGE, followed by immunoblot analysis using anti-CHC or anti-phosphotyrosine antibodies.

rometry. Seventeen peptide peaks were detected and peptide mass finger printing followed by a database search suggested that the protein of 180 kDa is clathrin heavy chain (CHC)(data not shown).

CHC is phosphorylated at tyrosine by H_2O_2

To confirm the phosphorylation of CHC by H_2O_2, CHC was immunoprecipitated from the cell lysates with and without H_2O_2 treatment, using a specific antibody, and then the samples were subjected to immunoblot analysis using an anti-phosphotyrosine antibody (Fig. 1C). The results indicated phosphorylation at tyrosine. Taken together, these results strongly support that CHC is a protein that is phosphorylated at tyrosine by H_2O_2. The phosphorylation has already been reported in chick embryo fibroblast cells transformed with Rous sarcoma virus [11]. In that report, pp60V-Src was suggested to be responsible for the in vivo phosphorylation of CHC. Goren et al. [12] also indicated that CHC was phosphorylated in vitro by insulin via the insulin receptor. However, the tyrosine-phosphorylation of CHC by oxidative stress has not been reported.

The phosphorylation of CHC by H_2O_2 was suppressed by the Src kinase inhibitor, PP2

Recently, it has been reported that CHC was phosphorylated at tyrosine 1477 by Src kinase on treatment with epidermal growth factor (EGF) and the phosphorylation was involved in the receptor-mediated endocytosis of clathrin-coated vesicles [13]. In the study, the endocytosis of the activated receptor was delayed when Src activity was inhibited. To investigate whether Src kinase is activated in βTC cells treated with H_2O_2, the phosphorylation status of Src was examined by immunoblot analysis using a specific antibody against phosphorylated Src. As shown in Fig. 2A, the phosphorylation of Src was enhanced by H_2O_2 treatment, indicating that Src kinase was activated by H_2O_2 in βTC cells. The results were consistent with previous reports that Src kinase is activated by oxidative stress [14–16]. To test whether Src kinase is involved in the phosphorylation of CHC by H_2O_2, the effect of PP2, a specific inhibitor for Src kinase, on the phosphorylation of CHC was examined. Fig. 2B shows that the phosphorylation of CHC by H_2O_2 was significantly suppressed in the presence of PP2. The results suggest that the phosphorylation of CHC by H_2O_2 is regulated by the Src kinase family as is the phosphorylation of CHC by EGF [13].

The phosphorylation of CHC by H_2O_2 affects the intracellular localization of CHC

Next to examine whether the phosphorylation of CHC by H_2O_2 affects the intracellular localization of CHC, intracellular CHC was detected immunologically

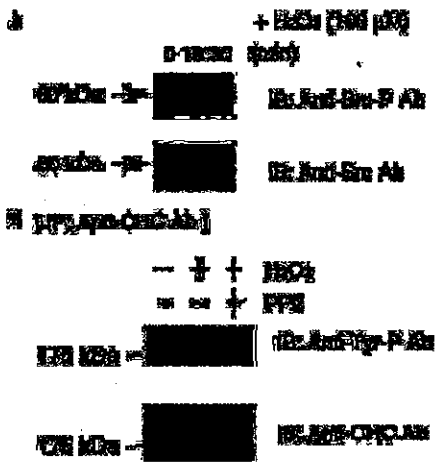

Fig. 2. Phosphorylation of CHC is regulated by the Src kinase family under oxidative stress. (A) The phosphorylation status of Src was characterized by immunoblot analysis using an anti-phosphorylated Src antibody in βTC cells treated with H_2O_2 (100 μM) for the periods indicated. (B) Effect of the Src kinase inhibitor PP2 on the phosphorylation of CHC by H_2O_2. The cells were pretreated with or without PP2 (1 μM, 15 min) and then treated with H_2O_2 (100 μM, 10 min) as described in Materials and methods. CHC was immunoprecipitated from each cell lysate with the specific antibody (X22) and subjected to 7.5% SDS–PAGE, followed by immunoblot analysis using anti-phosphotyrosine or anti-CHC antibodies.

by fluorescence microscopy. As shown in Fig. 3A, CHC exhibited a distinct perinuclear distribution in the non-stressed cells, suggesting localization in the trans-Golgi network [17]. After a 10 min treatment with H_2O_2, the perinuclear signals were diminished in intensity and spread in the cytoplasm. In contrast, in the presence of PP2, no significant change was seen with H_2O_2 treatment than without. To confirm that the intracellular localization of CHC is affected by H_2O_2, cells were treated under the same conditions and then the plasma membrane was isolated as described in Materials and methods. The distribution of CHC in the plasma membrane and cytoplasmic fractions was examined by immunoblot analysis. As shown in Fig. 3B, on treatment with H_2O_2, CHC was translocated from the plasma membrane to cytoplasm. However, in the presence of PP2, the translocation was suppressed, even with H_2O_2 treatment. Together, these results indicate that the intracellular distribution of CHC is altered by H_2O_2 treatment and the change is suppressed by a Src kinase inhibitor, PP2.

Oxidative stress is known to suppress the receptor-mediated endocytosis of several molecules, such as mannose [18], tumor necrosis factor-α [19], transferrin [20], and EGF [21,22]. Moreover, Malorni et al. [20] reported that CHC expression, which was mainly expressed in the plasma membrane region of control cells, was uniformly distributed in menadione-exposed K562 cells. Although the regulatory mechanism has yet to be clarified, the previous findings are consistent with the present results.

The phosphorylation of CHC by H_2O_2 affects the clathrin-dependent endocytosis of transferrin

Clathrin is known to play an important role in the receptor-mediated endocytosis of a variety of molecules, such as transferrin, EGF, nerve growth factor, and fibroblast growth factor [17]. To investigate the effect of phosphorylation by H_2O_2 on the functions of CHC, clathrin-dependent endocytosis was examined by estimating the internalization of FITC-transferrin under conditions of oxidative stress. Cells were pretreated with 100 μM H_2O_2 for 10 min and then incubated at 37 °C for given periods with the solution containing FITC-transferrin and H_2O_2. Then, FITC-transferrin was visualized microscopically or quantified photometrically as described in Materials and methods. As shown in Fig. 4A, in non-treated control cells, FITC-transferrin showed a diffuse cytoplasmic distribution at 5 min, but the signals were concentrated in spots at 30 min. In contrast, in the cells treated with H_2O_2, internalization of FITC-transferrin was significantly suppressed at 5 min, similar to the result after incubation at 4 °C for 30 min (negative control). However, after 30 min, concentrated spot-like signals of FITC-transferrin appeared in the cells treated with H_2O_2. These findings indicate that the uptake of FITC-transferrin was suppressed at an early phase and delayed by H_2O_2 treatment. In some experiments, cells were pretreated with 5 μM PP2 to see whether the phosphorylation status of CHC affects the clathrin-dependent endocytosis under oxidative stress. In the presence of PP2, the uptake of FITC-transferrin was slightly suppressed in every case, compared with non-treated controls. However, the suppression by H_2O_2 seen at 5 min was not significant in the case with PP2 as compared to without. In Fig. 4B, compared with non-treated controls, the uptake of FITC-transferrin was suppressed by H_2O_2 early, within 10 min, but was rather enhanced at 30 min. In the presence of PP2, the uptake was slightly suppressed both with and without H_2O_2 treatment, compared to non-treated controls. The H_2O_2-induced suppression of FITC-transferrin uptake was not significant in the presence of PP2. These results seem to be compatible with the microscopic findings. To assess the total bulk endocytosis, the uptake of FITC-dextran (70 kDa) was also examined (Fig. 4C). No significant difference was seen in the uptake of FITC-dextran with and without H_2O_2 and/or PP2 treatment,

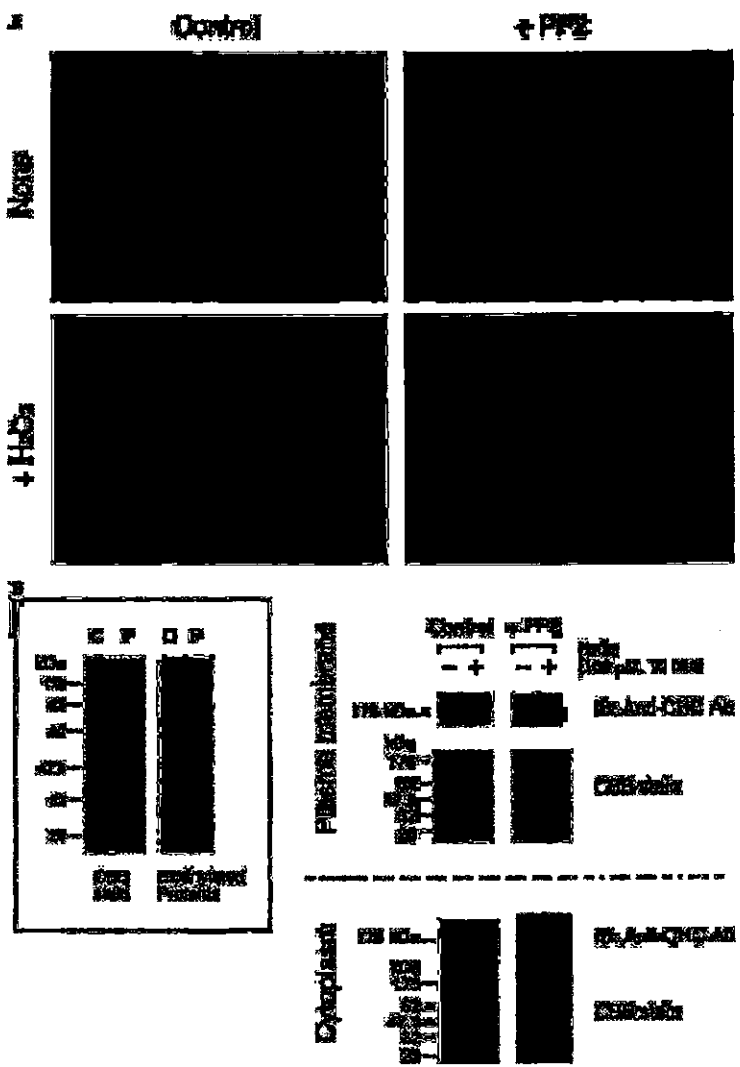

Fig. 3. Intracellular localization of CHC under oxidative stress. (A) Immunofluorescence microscopy for CHC. Cells were pre-treated with or without PP2 (1 μM) for 15 min and then treated with or without H_2O_2 (100 μM) for 10 min. After washing with cold PBS, cells were fixed and processed for CHC immunostaining with the specific antibody (X22) as described in Materials and methods. (B) Immunoblot analysis of CHC in the cytoplasmic and plasma membrane fractions. After the treatment as described in (A), the cells were homogenized and the plasma membrane fraction was isolated by differential centrifugation as described in Materials and methods. CHC was detected by immunoblot analysis using the anti-CHC-antibody (C20). Cell surface proteins from a test sample were biotinylated with sulfo-NHS-biotin as described in Materials and methods and the purity of the plasma membrane fraction was confirmed by immunoblot analysis using a peroxidase-conjugated avidin (inset). C, cytoplasm; P, plasma membrane. Data represent three independent experiments.

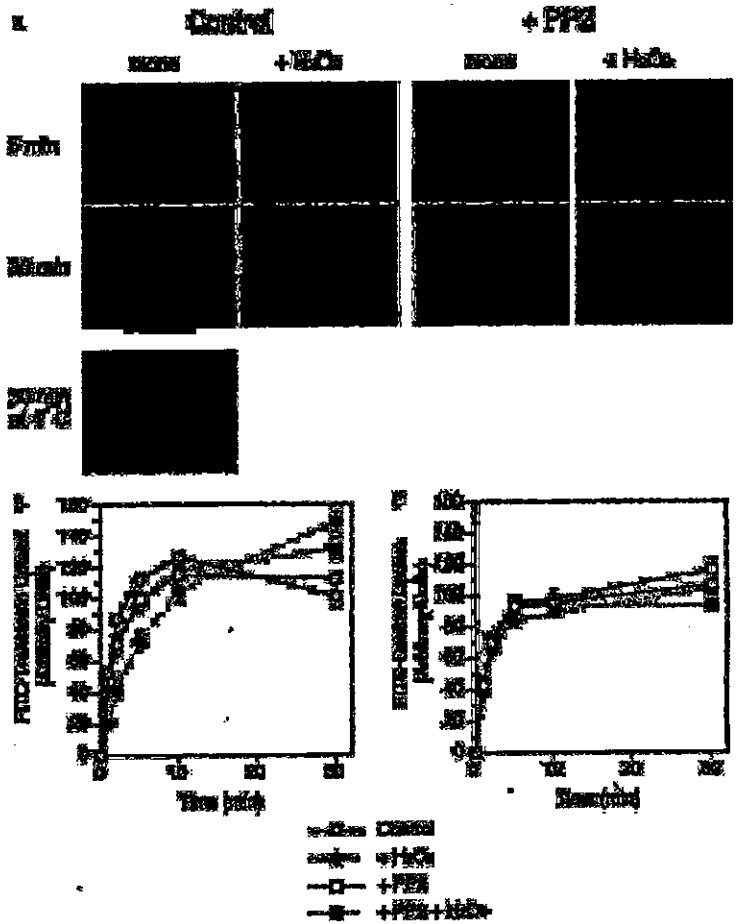

Fig. 4. Clathrin-dependent vesicular trafficking under oxidative stress. (A) The uptake of FITC-transferrin was examined microscopically to investigate clathrin-dependent endocytosis. The cells were pre-treated with or without PP2 (1 μM) for 15 min and then treated with or without H_2O_2 (100 μM) for 10 min. After a wash, the cells were cultured for the periods indicated in Earle's balanced salt solution containing 20 μg/ml FITC-transferrin with or without H_2O_2 (100 μM). After a wash with cold PBS, cells were fixed and then the uptake of FITC-transferrin was visualized by fluorescence microscopy as described in Materials and methods. As a negative control, non-treated cells were incubated at 4 °C for 30 min with the FITC-transferrin solution. (B) Quantification of FITC-transferrin uptake by the cells. The cells were treated as described in (A) and lysed after extensive washing with cold PBS. The cell lysates were excited at 494 nm and the emission at 520 nm was determined using a spectrofluorophotometer to quantitate the internalized FITC-labeled molecules. The value shows fluorescence intensity/mg protein in arbitrary units and represents three independent experiments. (C) Quantification of FITC-dextran uptake by the cells. To assess the effect of oxidative stress on total bulk endocytosis, the cells were treated as described in (A) and the uptake of FITC-dextran (70 kDa) (20 μg/ml) was measured as described in (B). The value represents three independent experiments.

suggesting that oxidative stress specifically influenced clathrin-dependent endocytosis but not total bulk endocytosis. The result that oxidative stress suppressed clathrin-dependent endocytosis was consistent with previous findings on the endocytosis of the transferrin receptor [20] and EGF-receptor [21,22]. Recently, Sorkina et al. [23] have reported the effect of tyrosine kinase inhibitors on clathrin-dependent vesicular trafficking of the EGF-receptor. In the study, a moderate suppression of the internalization of the EGF-receptor was observed in the presence of PP2, similar to our findings (Fig. 4B). However, the authors suggested that PP2 might inhibit not only the Src kinase family but also other kinases, because SU6656, a more specific inhibitor for Src kinase, showed no suppression of EGF-receptor internalization [23]. In this respect, further investigation of the mechanism of CHC phosphorylation under oxidative stress is required. Moreover, it is noteworthy that, in cells treated with EGF or nerve growth factor, phosphorylated CHC is redistributed to the plasma membrane [13,24]. In contrast, in H_2O_2-treated βTC cells, CHC is phosphorylated but redistributed from the plasma membrane to cytoplasm (Fig. 3B). The difference between the results obtained with growth factors and H_2O_2 suggests that the intracellular localization of CHC is affected by the phosphorylation status of CHC, but the cellular destination of CHC is not regulated simply by the phosphorylation. Although the precise mechanism is not known, the cell functional significance of CHC phosphorylation may be covered by other side effects of H_2O_2 on cellular signaling and regulation [4]. To address this, the effect of oxidative stress on the functions of other CHC-related adaptors [17] and regulatory mechanisms must also be clarified.

In conclusion, we identified CHC as a tyrosine-phosphorylated protein in βTC cells under oxidative stress. The phosphorylation status in the stressed cells altered the intracellular localization of CHC and downmodulated clathrin-dependent endocytosis, suggesting that the phosphorylation status of CHC is part of the regulatory mechanism for clathrin-dependent vesicular trafficking under conditions of oxidative stress. In EGF signaling during oxidative stress, H_2O_2 inhibited EGF-receptor internalization by inhibiting the ubiquitination of proteins involved in EGF-receptor-mediated endocytosis [22], but the mechanism related to the phosphorylation of CHC was not examined. Moreover, Howe et al. [25] have recently reported that, in nerve growth factor signaling, clathrin-coated vesicles function as a platform for the Ras-MAPK pathway, suggesting a novel function for CHC in the signal transduction. In this respect, under oxidative stress, the modulated CHC functions and vesicular trafficking may cause an aberrant regulation of cellular signaling related to cell growth. Although further investigation is needed to elucidate the relation between CHC function and cellular signaling, the present study has revealed a novel response to oxidative stress by β-cells via the altered function of CHC and suggests an as yet uncovered pathological mechanism of β-cell dysfunction in diabetes.

Acknowledgments

We are grateful to Noriko Sadakata and Hiroaki Kawano for the technical assistance. This work was supported in part by a grant-in-aid for scientific research on priority areas from the Ministry of Education, Science, Sports, and Culture of Japan.

References

[1] S. Lenzen, J. Drinkgern, M. Tiedge, Low antioxidant enzyme gene expression in pancreatic islets compared with various other mouse tissues, Free Radic. Biol. Med. 20 (1996) 463–466.
[2] C.J. Rhodes, IGF-I and GH post-receptor signaling mechanism for pancreatic β-cell replication, J. Mol. Endocrinol. 24 (2000) 303–311.
[3] R.L. Tuttle, N.S. Gill, W. Pugh, J.-P. Lee, B. Koeberlein, E.E. Furth, K.S. Polonsky, A. Naji, M.J. Birnbaum, Regulation of pancreatic β-cell growth and survival by the serine/threonine protein kinase Akt1/PKBα, Nat. Med. 7 (2001) 1133–1137.
[4] T. Finkel, Oxygen radicals and signaling, Curr. Opin. Cell Biol. 10 (1998) 248–253.
[5] F.M. Brodsky, Clathrin structure characterized with monoclonal antibodies. I. Analysis of multiple antigenic sites, J. Cell Biol. 101 (1985) 2047–2054.
[6] S. Efrat, S. Linde, H. Kofod, β-Cell lines derived from transgenic mice expressing a hybrid insulin gene-oncogene, Proc. Natl. Acad. Sci. USA 85 (1988) 9037–9041.
[7] Y. Ihara, Y. Sakamoto, M. Mihara, K. Shimizu, N. Taniguchi, Overexpression of *N*-acetylglucosaminyltransferase III disrupts the tyrosine phosphorylation of Trk with resultant signaling dysfunction in PC12 cells treated with nerve growth factor, J. Biol. Chem. 272 (1997) 9629–9634.
[8] Y. Wada, K. Matsumori, T. Terachi, O. Ogawa, Measurement of polymorphic repeats in the androgen receptor gene by matrix-assisted laser desorption/ionization time-of-flight mass spectrometry, J. Mass Spectrom. 34 (1999) 885–888.
[9] D.N. Perkins, D.J. Pappin, D.M. Creasy, J.S. Cottrell, Probability-based protein identification by searching sequence databases using mass spectrometry data, Electrophoresis 20 (1999) 3551–3567.
[10] S. Corvera, Insulin stimulates the assembly of cytosolic clathrin onto adipocyte plasma membranes, J. Biol. Chem. 265 (1990) 2413–2416.
[11] J. Martin-Perez, D. Bar-Zvi, D. Branton, R.L. Erikson, Transformation by rous sarcoma virus induces clathrin heavy chain phosphorylation, J. Cell Biol. 109 (1989) 577–584.
[12] H.J. Goren, M.J. Mooibroek, D. Boland, In vitro, insulin receptor catalyses phosphorylation of clathrin heavy chain and plasma membrane 180,000 molecular weight protein, Cell. Signal. 3 (1991) 523–536.
[13] A. Wilde, E.C. Beattie, L. Lem, D.A. Riethof, S.-H. Liu, W.C. Mobley, P. Soriano, F.M. Brodsky, EGF receptor signaling stimulates SRC kinase phosphorylation of clathrin, influencing clathrin redistribution and EGF uptake, Cell 96 (1999) 677–687.
[14] Y. Devary, R.A. Gottlieb, T. Smeal, M. Karin, The mammalian ultraviolet response is triggered by activation of Src tyrosine kinase, Cell 71 (1992) 1081–1091.

[15] J.-I. Abe, M. Takahashi, M. Ishida, J.-D. Lee, B.C. Berk, c-Src is required for oxidative stress-mediated activation of big mitogen-activated kinase 1 (BMK1), J. Biol. Chem. 272 (1997) 20389–20394.
[16] K.-I. Sato, K. Ogawa, A.A. Tokmakov, T. Iwasaki, Y. Fukami, Hydrogen peroxide induces Src family tyrosine kinase-dependent activation of Xenopus eggs, Dev. Growth Differ. 43 (2001) 55–72.
[17] F.M. Brodsky, C.-Y. Chen, C. Knuehl, M.C. Towler, D.E. Wakeham, Biological basket weaving: formation and function of clathrin-coated vesicles, Annu. Rev. Cell Dev. Biol. 17 (2001) 517–568.
[18] P.M. Bozeman, J.R. Hoidal, V.L. Shepherd, Oxidant-mediated inhibition of ligand uptake by the macrophage mannose receptor, J. Biol. Chem. 263 (1988) 1240–1247.
[19] L. Baud, H. Affres, J. Perez, R. Ardaillou, Reduction in tumor necrosis factor binding and cytotoxicity by hydrogen peroxide, J. Immunol. 145 (1990) 556–560.
[20] W. Malorni, U. Testa, G. Rainaldi, E. Tritarelli, C. Peschle, Oxidative stress leads to a rapid alteration of transferrin receptor intravesicular trafficking, Exp. Cell Res. 241 (1998) 102–116.
[21] R. De Wit, A. Capello, J. Boonstra, A.J. Verkleij, J.A. Post, Hydrogen peroxide inhibits epidermal growth factor receptor internalization in human fibroblasts, Free Radic. Biol. Med. 28 (2000) 28–38.
[22] R. De Wit, M. Makkinje, J. Boonstra, A.J. Verkleij, J.A. Post, Hydrogen peroxide reversibly inhibits epidermal growth factor (EGF) receptor internalization and coincident ubiquitination of the EGF receptor and Eps15, FASEB J. 15 (2000) 306–308.
[23] T. Sorkina, F. Huang, L. Beguinot, A. Sorkin, Effect of tyrosine kinase inhibitors on clathrin coated pit recruitment and internalization of epidermal growth factor receptor, J. Biol. Chem. 277 (2002) 27433–27441.
[24] E.C. Beattie, C.L. Howe, A. Wilde, F.M. Brodsky, W.C. Mobley, NGF signals through TrkA to increase clathrin at the plasma membrane and enhance clathrin-mediated membrane trafficking, J. Neurosci. 20 (2000) 7325–7333.
[25] C.L. Howe, J.S. Valletta, A.S. Rusnak, W.C. Mobley, NGF signaling from clathrin-coated vesicles: evidence that signaling endosomes serve as a platform for the Ras-MAPK pathway, Neuron 32 (2001) 801–814.

THE JOURNAL OF BIOLOGICAL CHEMISTRY
Vol. 279, No. 49, Issue of December 3, pp. 51182–51192, 2004
Printed in U.S.A.

Antiapoptotic Activity of Akt Is Down-regulated by Ca^{2+} in Myocardiac H9c2 Cells

EVIDENCE OF Ca^{2+}-DEPENDENT REGULATION OF PROTEIN PHOSPHATASE 2Ac*

Received for publication, June 28, 2004, and in revised form, September 3, 2004
Published, JBC Papers in Press, September 16, 2004, DOI 10.1074/jbc.M407225200

Chie Yasuoka‡§¶, Yoshito Ihara‡¶‖, Satoshi Ikeda§, Yoshiyuki Miyahara§, Takahito Kondo‡, and Shigeru Kohno§

From the ‡Department of Biochemistry and Molecular Biology in Disease, Atomic Bomb Disease Institute and the §Second Department of Internal Medicine, Nagasaki University Graduate School of Biomedical Sciences, Nagasaki 852-8523, Japan

Cell survival signaling of the Akt/protein kinase B pathway was influenced by a change in the cytoplasmic free calcium concentration ($[Ca^{2+}]_i$) for over 2 h via the regulation of a Ser/Thr phosphatase, protein phosphatase 2Ac (PP2Ac), in rat myocardiac H9c2 cells. Akt was down-regulated when $[Ca^{2+}]_i$ was elevated by thapsigargin, an inhibitor of the endoplasmic reticulum Ca^{2+}-ATPase, but was up-regulated when it was suppressed by 1,2-bis(o-aminophenoxy)ethane-*N,N,N′,N′*-tetraacetic acid tetra(acetoxymethyl)ester (BAPTA-AM), a cell permeable Ca^{2+} chelator. The inactivation of Akt was well correlated with the susceptibility to oxidant-induced apoptosis in H9c2 cells. To investigate the mechanism of the Ca^{2+}-dependent regulation of Akt via the regulation of PP2A, we examined the transcriptional regulation of PP2Acα in H9c2 cells with Ca^{2+} modulators. Transcription of the *PP2Acα* gene was increased by thapsigargin but decreased by BAPTA-AM. The promoter activity was examined and the cAMP response element (CRE) was found responsible for the Ca^{2+}-dependent regulation of PP2Acα. Furthermore, phosphorylation of CRE-binding protein increased with thapsigargin but decreased with BAPTA-AM. A long term change of $[Ca^{2+}]_i$ regulates *PP2Acα* gene transcription via CRE, resulting in a change in the activation status of Akt leading to an altered susceptibility to apoptosis.

Calcium (Ca^{2+}) plays a signaling role in many important cellular functions, such as fertilization, embryonic pattern formation, differentiation, proliferation, contraction, secretion, and metabolism (1). The versatility of the Ca^{2+}-signaling mechanism in terms of speed, amplitude and spatio-temporal patterning enables elevations of Ca^{2+} to regulate many processes of cell activity. Ca^{2+} exhibits cross-talk between a variety of signaling pathways (1). Ca^{2+} affects the protein kinase A pathway by regulating the metabolism of cAMP. It also activates nitric-oxide (NO) synthase to generate NO, which in turn activates the cGMP pathway through the activation of guanylyl cyclase. The Ras/mitogen-activated protein kinase (MAPK)[1] and Ca^{2+}/calmodulin/calmodulin kinase (CaMK) pathways are also controlled by Ca^{2+} (1, 2).

On the other hand, a cellular Ca^{2+} overload or the perturbation of intracellular Ca^{2+} compartmentalization can cause cytotoxicity and trigger apoptosis or necrosis (3, 4). Under such circumstances, various Ca^{2+}-dependent signaling cascades with kinases and phosphatases directly or indirectly influence cellular signaling. Protein kinase C family has been proposed to play an important role in the Ca^{2+}-mediated signaling of apoptosis (5). Calcineurin/PP2B, a Ca^{2+}-dependent Ser/Thr phosphatase (6), also appears to be involved in apoptosis (7). Together, these findings show that Ca^{2+} has a pivotal role in the regulatory mechanism of signaling pathways in cell survival and death, although the precise mechanism of Ca^{2+}-dependent cross-talk has not been fully clarified.

Akt/protein kinase B is a pleckstrin homology domain-containing Ser/Thr kinase (8, 9, 10). Akt is presently recognized as a cell survival or an antiapoptotic cellular signaling mediator. Akt is activated through a growth factor receptor-mediated activation of the phosphatidylinositol 3-kinase (PI3K) pathway (10). With growth factor signals, Akt is recruited to the plasma membrane and is activated through phosphorylation at Ser-473 and Thr-308 by phosphatidylinositol 3-phosphate-dependent protein kinase-1 (PDK1) or integrin-linked kinase (9, 10). Akt can phosphorylate Bad, caspase-9, and forkhead-related transcription factors, leading to their inactivation and to enhanced cell survival (8, 9, 10). Inhibitor of nuclear factor κB (IκB) kinase is also phosphorylated by Akt leading to an up-regulation of its activity and resulting in a promotion of the nuclear factor κB (NFκB)-mediated inhibition of apoptosis (8, 11, 12)

Akt has been found to be involved in cell death following the withdrawal of extracellular signaling factors, oxidative and osmotic stress, irradiation, treatment with drugs and ischemic stress (10). However, in spite that a variety of cellular stressors influence cells through Ca^{2+} signaling, the number of studies on Akt signaling and Ca^{2+} is limited. As for Akt, Ca^{2+}-dependent activation was reported in several studies (13, 14). On the other hand, there was a report that the activation of Akt is independent of Ca^{2+} (15). In contrast, we found that Akt was suppressed by an elevation of $[Ca^{2+}]_i$ in myocardiac H9c2 cells overexpressing the calreticulin gene (16). In the cells overexpressing calreticulin, protein phosphatase 2A (PP2A) was up-regulated by Ca^{2+} to decrease the phosphorylation level of Akt, and the inactivated status of Akt was well correlated with the susceptibility to apoptosis in H9c2 cells under conditions for differentiation induced by retinoic acid. Collectively, these results suggest that the Ca^{2+}-dependent regulatory mechanism of Akt signaling may be important to a variety of apoptotic signaling mechanisms, although how has not been fully clarified.

In the present study, to investigate the mechanism of the Ca^{2+}-dependent regulation of Akt signaling, we examined the influence of a change of $[Ca^{2+}]_i$ on susceptibility to oxidative stress-induced cell injury and on the Akt signaling pathway in myocardiac H9c2 cells. We show that the Ca^{2+}-dependent regulation of *PP2Acα* gene transcription is controlled through the cAMP responsive element (CRE), resulting in a change in the activation status of Akt leading to an altered susceptibility to apoptosis.

MATERIALS AND METHODS

Antibodies and Reagents—Antibodies against Akt, phospho-Akt (Ser-473), and phospho-Akt (Thr-308), CRE-binding protein (CREB), and phospho-CREB (Ser-133) were purchased from Cell Signaling Technology (Beverly, MA). The antibody against Sp1 was purchased from Santa Cruz Biotechnology (Santa Cruz, CA). The reagents used in the study were all of high grade and from Sigma or Wako Pure Chemicals (Osaka, Japan).

Cell Culture—H9c2 cells from embryonic rat heart (16, 17) were obtained from American Type Culture Collection (CRL-1446). H9c2 cells were cultured in Dulbecco's modified Eagle's medium supplemented with 10% fetal bovine serum in a humidified atmosphere of 95% air and 5% CO_2 at 37 °C. Before reaching confluence, the cells were split, and plated at low density in culture medium containing 10% fetal bovine serum.

Measurement of Cytoplasmic Free Ca^{2+}—The cytoplasmic free Ca^{2+} concentration, $[Ca^{2+}]_i$, was measured using Fura-2-AM essentially as described previously (16). Briefly, cultured cells on glass coverslips were loaded with 5 μM Fura-2-AM (Dojindo, Kumamoto, Japan) for 20 min in Earle's balanced salt solution (EBSS) in the presence of 0.01% pluronic acid F-127. After four washes with EBSS, the cover glass was positioned in a quartz cuvette containing 3.5 ml of fresh EBSS at a 45° angle to both excitation and emission light paths. The fura-2 fluorescence was determined at 37 °C using a spectrofluorophotometer operating at an emission wavelength of 505 nm with an excitation wavelength of 340 and 380 nm. The maximal signal (R_{max}) was obtained by adding ionomycin at a final concentration of 4 μM. Then the minimal signal (R_{min}) was obtained by adding EGTA at a final concentration of 7.5 mM, followed by Tris-free base to a final concentration of 30 mM, to increase the pH to 8.3. R is the ratio (F1/F2) of the fluorescence of Ex 340 nm, Em 505 nm (F1) to that of Ex 380 nm, Em 505 nm (F2). The actual Ca^{2+} concentration was calculated as $K_d \times (R - R_{min})/(R_{max} - R)$ with the K_d equal to 224 nM (18).

Lactate Dehydrogenase (LDH) Release Assay—After 4 h of treatment with 5 μM thapsigargin or 10 μM BAPTA-AM or not, cells were incubated with 75 μM hydrogen peroxide (H_2O_2) for 0–120 min. The LDH activity was assayed by using a MTX LDH kit (Kyokuto Seiyaku, Tokyo, Japan) according to the manufacturer's instructions. Briefly, 50 μl of supernatant was transferred to a 96-well plate, then 50 μl of coloring reagent was added and incubated for 45 min at room temperature. After 100 μl of stop solution was added, absorbance was measured at 560 nm with a microplate reader. The LDH release was shown as a rate of LDH released in the medium to total cellular LDH.

TUNEL Assay—Apoptosis was detected flow cytometrically by the terminal deoxynucleotidyltransferase-mediated dUTP nick-end labeling (TUNEL) method (19) using an ApopTag Plus Fluorescein *in situ* Apoptosis Detection kit (Serologicals, Norcross, GA). Briefly, cells were harvested and fixed in 70% ethanol, treated with terminal deoxynucleotidyl transferase for 1 h, and then with fluorescein isothiocyanate (FITC)-conjugated antidigoxigenin for 1 h at room temperature, and washed with phosphate-buffered saline (pH 7.0) (PBS) containing 0.1% Triton X-100. The fluorescence intensity was measured at 530 nm using a flow cytometer (BD Biosciences, San Jose, CA).

Northern Blot Analysis—The full-length rat PP1α catalytic subunit and PP2A catalytic α cDNAs were generously provided by Dr. Kunimi Kikuchi (Hokkaido University, Japan) (20, 21). A PstI-SmaI fragment of 600 bp and EcoRI-PvuII fragment of 680 bp were prepared from the cDNAs of PP1α and PP2Acα, respectively, and used as cDNA probes. The probes were labeled with ^{32}P using a Random Primer Labeling kit (Takara Biomedicals, Shiga, Japan). The isolation of cytoplasmic RNA and Northern blotting were essentially performed as described before (16). Isolated RNAs (10 μg) were electrophoresed on a 1% agarose gel containing 0.6 M formaldehyde, transferred to a nylon membrane, and then hybridized with ^{32}P-labeled probes. Autoradiographed membranes were analyzed using a BAS5000 bioimage analyzer (Fuji Photo Film).

Immunoblot Analysis—Cultured cells were harvested and lysed for 20 min at 4 °C in lysis buffer (20 mM Tris-HCl, pH 7.5, 130 mM NaCl, 1% Nonidet P-40, and 10% glycerol including protease inhibitors (20 μM amidinophenylmethanesulfonyl fluoride, 50 μM pepstatin, and 50 μM leupeptin)). The supernatants obtained on centrifugation at 8,000 × *g* for 10 min were used in subsequent experiments. Protein samples were subjected to 10% SDS-PAGE under reducing conditions and then transferred to nitrocellulose membrane as described (22). The membrane was blocked with 5% skim milk or 3% bovine serum albumin in Tris-buffered saline (pH 7.5) containing 0.05% Tween 20. The blots were coupled with the peroxidase-conjugated secondary antibodies, washed, and then developed using the ECL chemiluminescence detection kit (Amersham Biosciences) according to the manufacturer's instructions.

Akt Activity Assay—Akt acitivity was assayed using an Akt assay kit (Cell Signaling Technology) according to the manufacturer's protocol. Briefly, Akt was immunoprecipitated from cell lysates using the anti-Akt antibody, and then the immunoprecipitates were incubated at 30 °C for 30 min in an assay mixture containing an Akt substrate, GSK-3α/β fusion protein. Phosphorylated proteins were separated by 12.5% SDS-PAGE and then transferred to nitrocellulose membrane to detect phosphorylated GSK-3α/β using an anti-phosphorylated GSK-3α/β (Ser-21/9) antibody.

Protein Phosphatase Assay—Protein Ser/Thr phosphatase activity was assayed photometrically using Ser/Thr phosphatase assay kit 1 (Upstate Biotechnology, Lake Placid, NY), according to the manufacturer's directions. The activity was assayed in the presence or absence of 10 nM okadaic acid, and the okadaic acid-sensitive activity was estimated as PP2A-specific activity. The phosphopeptide (RK(pT)IRR) was used as a phosphatase substrate. Protein concentrations were determined using a BCA assay kit (Pierce).

Generation of Luciferase Reporter Constructs—A ~1.6-kb fragment of rat *PP2Acα* gene promoter (−1350 to +258) (23) was amplified with rat genome by PCR using *Pfu* turbo DNA polymerase (Stratagene). The primers used are as follows; a forward primer (5′-GATCTCAGGTACTT-TCTTCCGGAACACTAG-3′) and a reverse primer (5′-GTCCAGCTCCT-TGGTGAACAACTTC-3′). The PCR product was subcloned into pUC18 to obtain pUC18-pro-PP2Ac. The nucleotide sequence was confirmed by sequencing with an ALFexpress II system (Amersham Biosciences). pUC18-pro-PP2Ac was digested with HindIII, and the resulting fragment containing the promoter region from −1209 to +258 was inserted into the HindIII site of the reporter vector pGL3-Basic (Stratagene) to give pGL3-pro-PP2Ac. To generate deleted mutants of the luciferase reporter construct, pGL3-pro-PP2Ac was digested with SacI and XhoI, and deletion mutants were made using a deletion kit for kilo sequence (Takara Biomedicals).

Site-directed Mutagenesis for Luciferase Vectors—*In vitro* mutagenesis was performed with pGL3-pro-PP2Ac-del (−279 to +258) and del (−145 to +258) as templates by using a QuikChange site-directed mutagenesis kit (Stratagene). Oligonucleotides used are as follows: GC box (−155), 5′-CCCTCCCCGCGGGAGGACCACAACCCAAAAGCGAA-GCCACTTCC-3′; CRE (−26), 5′-CCTGACGCCGGCGTGTGGTCACCA-CGCCGGGCGGCCGCCATTAC-3′. The nucleotide sequences were confirmed by sequencing with an ALFexpress II system (Amersham Biosciences).

Luciferase Activity Assay—Each vector was transfected into H9c2 cells by using Lipofectamine2000 (Invitrogen) according to the manufacturer's instructions. After 24 h of transfection, cells were treated with thapsigargin (5 μM) or BAPTA-AM (10 μM), or left untreated for the periods indicated in the text. Then luciferase activity was assayed with cellular extracts by using a dual-luciferase reporter assay system (Promega).

* This work was supported in part by grants-in-aid from the Japanese Ministry of Education, Culture, Sports, Science, and Technology through the 21st Century COE program, and by a grant provided by the Ichiro Kanehara Foundation. The costs of publication of this article were defrayed in part by the payment of page charges. This article must therefore be hereby marked "*advertisement*" in accordance with 18 U.S.C. Section 1734 solely to indicate this fact.

The nucleotide sequence(s) reported in this paper has been submitted to the GenBank™/EBI Data Bank with accession number(s) AY749432.

¶ Both authors contributed equally to this work.

‖ To whom correspondence should be addressed: Dept. of Biochemistry and Molecular Biology in Disease, Atomic Bomb Disease Institute, Nagasaki University Graduate School of Biomedical Sciences, 1-12-4 Sakamoto, Nagasaki 852-8523, Japan. Tel.: 81-95-849-7099; Fax: 81-95-849-7100; E-mail: y-ihara@net.nagasaki-u.ac.jp.

[1] The abbreviations used are: MAPK, mitogen-activated protein kinase; BAPTA-AM, 1,2-bis (o-aminophenoxy) ethane-*N,N,N′,N′*-tetraacetic acid tetra (acetoxymethyl) ester; CRE, cAMP response element; CREB, CRE-binding protein; ER, endoplasmic reticulum; FITC, fluorescein isothiocyanate; PBS, phosphate-buffered saline; PI3K, phosphatidylinositol 3-kinase; LDH, lactate dehydrogenase; CaMK, calmodulin kinase; TUNEL, terminal deoxynucleotidyltransferase-mediated dUTP nick end-labeling; EMSA, electrophoretic mobility shift assay.

Electrophoretic Mobility Shift Assay—The electrophoretic mobility shift assay (EMSA) for the GC box and CRE was performed as described previously (24). Briefly, oligonucleotides were labeled with [γ-^{32}P]ATP using T4 polynucleotide kinase and then annealed to double-strand oligonucleotides. Specific oligonucleotides for the GC box and CRE were prepared according to the nucleotide sequences of the rat *PP2Acα* promoter region. Oligonucleotides used are as follows: GC box (−155), 5′-CGGGAGGACCACGCCCCAAAAGCGAAGC-3′; GC box (−155)-Mt, 5′-CGGGAGGACCACAACCCAAAAGCGAAGC-3′; CRE (−26), 5′-GACGCCGGCCTGACGTCACCACGCC-3′; CRE (−26)-Mt, 5′-GACGCCGGCCTGTGGTCACCACGCC -3′. Binding reactions were carried out in 15 μl of reaction mixture (25 mM Tris, pH 7.0, 6.25 mM $MgCl_2$, 0.5 mM EDTA, 0.5 mM dithiothreitol, 50 mM KCl, and 10% glycerol) containing 10 μg of nuclear extract, and 25 ng of labeled oligonucleotide. For the supershift assay, specific antibodies were added to the reaction mixture during the 30-min binding reaction.

Indirect Immunofluorescence Microscopy—After treatment with 5 μM thapsigargin or 10 μM BAPTA-AM for 2 h, cells incubated on Lab-Tek chamber slides (Nunc) were fixed with 3% paraformaldehyde for 20 min at room temperature and washed three times with PBS. Cells were permeabilized in 1% Triton X-100 in PBS for 10 min and washed three times with PBS. They were blocked with 1% bovine serum albumin in PBS for 30 min at room temperature, washed three times with PBS, and then incubated with antiphospho-CREB (Ser-133) overnight at 4 °C. Cells were washed with PBS four times and incubated with FITC-labeled anti-rabbit IgG antibody for 30 min in a dark room. The immunoreactive signals were visualized by indirect immunofluorescence microscopy.

RESULTS

Elevation of $[Ca^{2+}]_i$ Gradually Accelerates Cell Damage and Apoptosis in H9c2 Cells—To modify the level of $[Ca^{2+}]_i$ in H9c2 cells, the cells were treated with 5 μM thapsigargin (25), an inhibitor for sarcoplasmic/endoplasmic reticulum Ca^{2+} ATPase to increase $[Ca^{2+}]_i$, or with 10 μM BAPTA-AM (26), a cell permeable Ca^{2+} chelator to decrease $[Ca^{2+}]_i$, for 0–4 h. As shown in Fig. 1*A*, with thapsigargin, $[Ca^{2+}]_i$ shows a transient increase within the first 10 min. It then decreases to the basal level till 30 min, but again increases and retains elevated until 120 min, before gradually decreasing to the initial level. In contrast, with BAPTA-AM, $[Ca^{2+}]_i$ shows a continuous lowering during the treatment. To investigate the influence of the long term change of $[Ca^{2+}]_i$ on susceptibility to oxidative stress-induced cell injury, cells were treated with Ca^{2+} modulators (*i.e.* thapsigargin and BAPTA-AM) for 4 h then exposed to 75 μM hydrogen peroxide (H_2O_2) for 0–120 min, and cell damage was examined at predetermined times using the LDH release assay as described in the methods. In Fig. 1*B*, the release of LDH by H_2O_2 was observed only at 120 min in the medium of untreated cells. However, the release by H_2O_2 was initially observed at 60 min and increased at 120 min in the cells treated with thapsigargin. In contrast, BAPTA-AM treatment completely suppressed the release of LDH by H_2O_2 throughout the 120 min. Next, to investigate whether apoptosis is involved in the mechanism of thapsigargin-induced cell damage, cells were treated with Ca^{2+} modulators for 4 h then exposed to H_2O_2 (75 μM) for 2 h, and apoptosis was examined. Fig. 1*C* shows that TUNEL-positive fluorescence intensity was increased slightly by H_2O_2 (*upper*), but was significantly enhanced after the pretreatment with thapsigargin (*middle*). In contrast, no change was observed in the fluorescent intensity of the BAPTA-AM-treated cells with or without H_2O_2 (*lower*). Collectively, these results indicate that the susceptibility to apoptosis was enhanced with a long term elevation of $[Ca^{2+}]_i$, but was suppressed with the lowering of $[Ca^{2+}]_i$ in the cells under oxidative stress with H_2O_2, suggesting that the continuous change of $[Ca^{2+}]_i$ influences the susceptibility to apoptosis.

The Long Term Change of $[Ca^{2+}]_i$ Influences Akt Signaling in H9c2 Cells—To know the role of $[Ca^{2+}]_i$ in cell survival signaling, we focused on the effect of Ca^{2+} modulators on Akt signaling. Previously, we found that the Akt signaling pathway is responsible for the cytoprotective mechanism in H9c2 cells under conditions of stress such as serum starvation with retinoic acid (16), and oxidative stress with hydrogen peroxide (27). Although elevations in Ca^{2+} act as a signal, a prolonged increase in the concentration of Ca^{2+} can be lethal (1). Moreover, cell signaling molecules including transcription factors are activated differentially by the amplitude and duration of the response to Ca^{2+} (28). In the present study, H9c2 cells were treated with Ca^{2+} modulators such as thapsigargin (5 μM) and BAPTA-AM (10 μM) for over 2 h to induce a long term change of $[Ca^{2+}]_i$. After the treatments, the phosphorylation levels of Ser-473 and Thr-308 of Akt were examined. The phosphorylation of Thr-308 located in the kinase catalytic domain of Akt is necessary for the activation, and the phosphorylation of Ser-473 located in the regulatory domain of Akt supports the activation. As shown in Fig. 2, *A* (*right*) and *B*, the treatment with BAPTA-AM increased the phosphorylation of Akt both at Ser-473 and Thr-308, and the phosphorylation level increased to a maximum at 2 h, and was sustained thereafter till 4 h. In contrast, the phosphorylation of Akt decreased in a time-dependent manner with thapsigargin (Fig. 2, *A* (*left*) and *B*). Next we examined whether Ca^{2+} modulators also have an effect on the kinase activity of Akt. Fig. 2*C* shows that Akt activity is suppressed after the treatment with thapsigargin, but increased with BAPTA-AM. These results were consistent with the change in the phosphorylation status of Akt on treatment with Ca^{2+} modulators such as thapsigargin and BAPTA-AM. Together, Akt signaling was suppressed by the long term elevation of $[Ca^{2+}]_i$ with thapsigargin, but was enhanced by the long term lowering of $[Ca^{2+}]_i$ with BAPTA-AM. This suggests a Ca^{2+}-dependent regulation of Akt signaling in H9c2 cells. Furthermore, the Ca^{2+}-induced suppression of Akt signaling was compatible with the enhanced susceptibility to apoptosis in H9c2 cells treated with H_2O_2 (Fig. 1, *B* and *C*).

The Expression of PP2Acα Is Transcriptionally Regulated by Ca^{2+} Modulators—3-Phosphoinositide-dependent protein kinase (PDK1) is known to be responsible for phosphorylating Akt at Thr-308, and is activated by both phosphatidylinositol (3,4,5)-trisphosphate and phosphatidylinositol (3,4,)-bisphosphate, products of PI3K (9, 10). To investigate whether the upstream kinases are involved in the regulation of Akt by the change of $[Ca^{2+}]_i$, the activities for PI3K and PDK1 were measured in the cells treated with Ca^{2+} modulators. However, neither activities showed any significant change even if the cells were treated with thapsigargin or BAPTA-AM for 0–4 h (data not shown). Therefore, we focused on Ser/Thr protein phosphatases that could dephosphorylate and inactivate Akt to regulate the Akt signaling pathway (7). To investigate whether $[Ca^{2+}]_i$ levels affect the expression of protein Ser/Thr phosphatases, the cells were treated with 5 μM thapsigargin or 10 μM BAPTA-AM for 0–4 h, and transcriptional levels were estimated by Northern blot analysis for protein phosphatase 2A catalytic subunit α (PP2Acα) and protein phosphatase 1α catalytic subunit (PP1cα). In Fig. 3*A*, the level of PP2Acα mRNA was increased by thapsigargin but decreased by BAPTA-AM. In contrast, the mRNA level of PP1cα was not significantly changed by the Ca^{2+} modulators. In the immunoblot analysis, the protein level of PP2Acα was increased by thapsigargin but decreased by BAPTA-AM (Fig. 3*B*). However, the protein level of PP1cα was not influenced by thapsigargin or BAPTA-AM. The protein level of calcineurin/PP2B was not influenced by thapsigargin or BAPTA-AM either (data not shown). These results were consistent with results of the change of transcriptional levels for the phosphatases in the cells treated with each Ca^{2+} modulator. The enzymatic activity

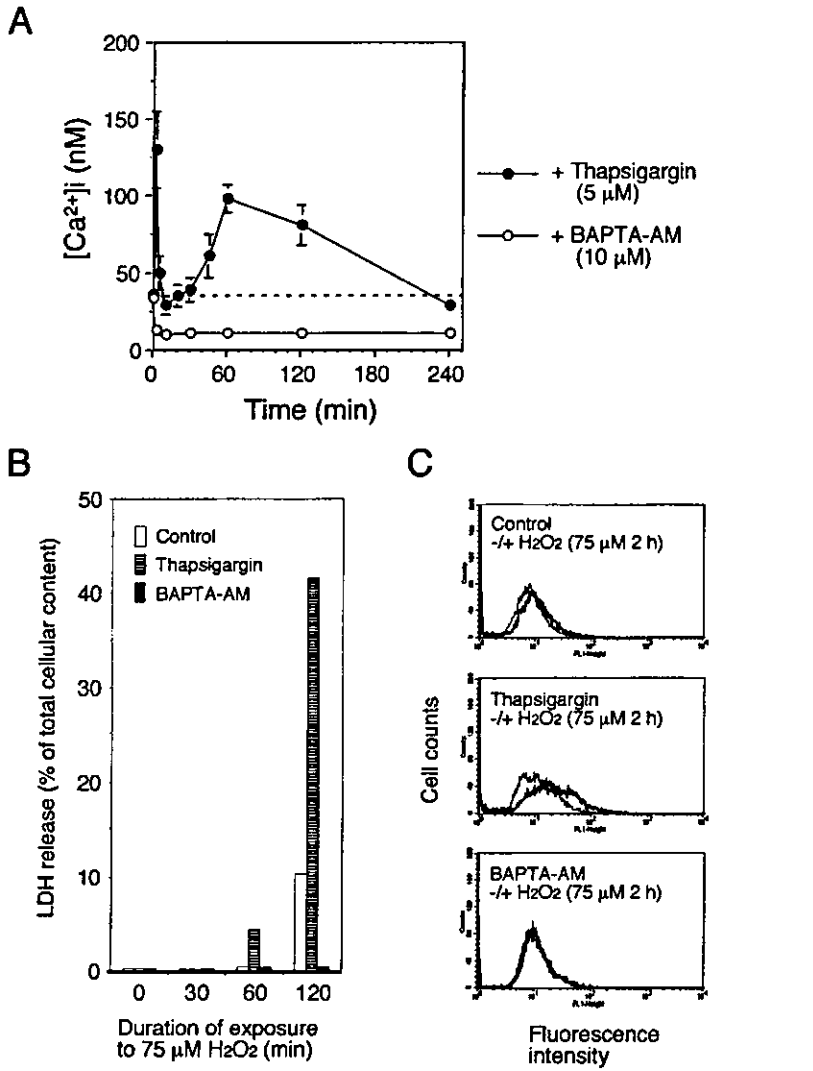

FIG. 1. **The long term elevation of $[Ca^{2+}]_i$ accelerates apoptosis in H9c2 cells under oxidative stress with H_2O_2.** *A*, H9c2 cells were treated with thapsigargin (5 μM) or BAPTA-AM (10 μM) for the periods indicated, and $[Ca^{2+}]_i$ was measured using Fura-2-AM as described under "Materials and Methods." Each value represents the mean ± S.D. of four independent experiments. *B*, after 4 h of treatment with thapsigargin (5 μM) or BAPTA-AM (10 μM) or not, the cells were incubated with H_2O_2 (75 μM) for the periods indicated. Cell injury was estimated by measuring the release of LDH in the culture medium as described under "Materials and Methods." The LDH release is shown as the proportion of total cellular LDH in the medium to total cellular LDH. Each value represents the mean of three experiments, and the S.D. was always within 10% of the mean. *C*, DNA double-stranded breaks were detected by the TUNEL method as described under "Materials and Methods." Cells were treated with either thapsigargin (5 μM) or BAPTA-AM (10 μM) for 4 h and untreated cells were prepared as a control. Then the cells were treated with (*thick lines*) or without (*thin lines*) H_2O_2 (75 μM) for 2 h. The results were reproducible in three independent experiments.

FIG. 2. **Ca^{2+} modulators influence the phosphorylation and kinase activity of Akt in H9c2 cells.** H9c2 cells were cultured in the presence of either thapsigargin (5 μM) or BAPTA-AM (10 μM) for the periods indicated. *A*, Akt phosphorylation was detected in the cell lysates by immunoblot analysis (*IB*) with anti-phospho-Akt (Ser-473), anti-phospho-Akt (Thr-308), and anti-Akt antibodies. *B*, quantitative data for the phosphorylation status of Akt shown in *A*. The band intensity was estimated densitometrically, and the phosphorylation rate is expressed as the relative intensity of the phosphorylated Akt (Akt-P/Akt. Each value represents the mean ± S.D. of four independent experiments. *C*, Akt kinase activity was assayed as described under "Materials and Methods" using GSK-3α/β as a substrate. Phosphorylated GSK-3α/β (Ser-21/9), the enzymatic products of Akt, was detected by immunoblot analysis using specific antibody. The data represent three independent experiments.

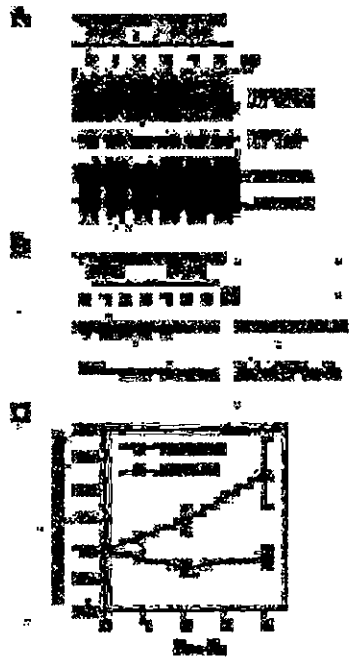

FIG. 3. **The expression and phosphatase activity of PP2Acα are regulated by Ca^{2+} modulators in H9c2 cells.** H9c2 cells were treated with thapsigargin (5 μM) or BAPTA-AM (10 μM) for the periods indicated. *A*, transcriptional levels of PP2Acα and PP1cα were evaluated by Northern blot analysis as described under "Materials and Methods." An EcoRI-PvuII fragment of 680 bp and a PstI-SmaI fragment of 600 bp were prepared from cDNAs for PP2Acα and PP1cα, respectively, and were used as cDNA probes after labeling with [α-^{32}P]dCTP. *B*, protein levels for PP2Acα and PP1cα were estimated by immunoblot analysis using specific antibodies. The data represent three independent experiments. *C*, protein phosphatase activity was assayed photometrically as described under "Materials and Methods." Each value represents the mean ± S.D. of four independent experiments.

of PP2A was also assayed in the cells treated with thapsigargin or BAPTA-AM for 0–4 h. As shown in Fig. 3*C*, the activity of PP2A increased with thapsigargin by ~2-fold compared with that of untreated cells. In contrast, the activity was slightly suppressed after 2 h treatment with BAPTA-AM. Collectively, these results indicate that PP2Acα expression is transcriptionally regulated by the long term change of $[Ca^{2+}]_i$ to control the phosphorylation status of target molecules including Akt.

Inhibition of PP2A Activity by Okadaic Acid Enhanced the Phosphorylation of Akt—Okadaic acid, a polyether toxin from the marine black sponge *Halichondria okadai* is a highly selective inhibitor of PP2A (29). To establish a link between Akt and PP2A, the influence of okadaic acid on Akt signaling was investigated with cells treated with okadaic acid. The cells were treated with okadaic acid (100 nM) for 0–30 min. The phosphorylation level of Akt was estimated by immunoblot analysis using specific antibodies. Akt kinase and PP2A activities were measured as described above. As shown in Fig. 4*A*, okadaic acid reduced the activity of PP2A by ~30%, and increased the phosphorylation level of Akt (both Thr-308 and Ser-473) and Akt kinase activity. Next, we examined whether the decrease in phosphorylation of Akt caused by thapsigargin could be reversed by okadaic acid. The cells were preincubated with thapsigargin (5 μM) for 4 h, and treated with or without okadaic acid (100 nM) for another 30 min, then the phosphorylation level of Akt was examined as described above. As shown in Fig. 4*B*, okadaic acid suppressed PP2A activity, and this reversed the decrease in phosphorylation of Akt with thapsigargin. Okadaic acid enhanced the phosphorylation of Akt at concentrations higher than 50 nM (data not shown). These results indicate that the function of PP2A can regulate the phosphorylation status of Akt in H9c2 cells.

Inhibition of PP2A Activity by Okadaic Acid Suppressed Apoptotic Cell Damage in H9c2 Cells Treated with Thapsigargin and H_2O_2—To establish a link between PP2A and Ca^{2+}-dependent enhancement of apoptosis, the influence of okadaic acid on apoptosis was investigated using cells treated with okadaic acid. In Fig. 5*A*, cells were treated with or without

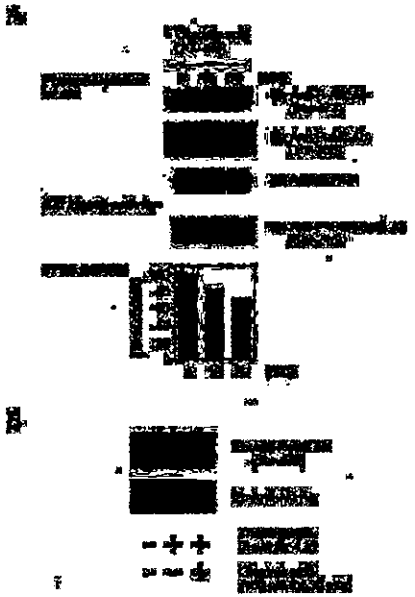

FIG. 4. **Inhibition of PP2A activity by okadaic acid enhances the phosphorylation of Akt in H9c2 cells.** *A*, H9c2 cells were incubated with 100 nM okadaic acid for 0–30 min. The phosphorylation level of Akt was estimated by immunoblot analysis using specific antibodies. The activities for Akt and PP2A were measured as described under "Materials and Methods." The data for PP2A activity represent the mean of three independent experiments. *B*, cells were preincubated with thapsigargin (5 μM) for 4 h then treated with or without okadaic acid (100 nM) for 30 min. The phosphorylation level of Akt (Ser-473) was examined by immunoblot analysis as described above. The data represent three independent experiments.

thapsigargin (5 μM) for 4 h then treated with okadaic acid (200 nM) for 30 min. Then cells were exposed to H_2O_2 (75 μM) for 0–2 h, and cell damage was examined at predetermined times using LDH release assay. The results showed that treatment with okadaic acid suppressed the Ca^{2+}-dependent enhancement of cell damage in cells treated with thapsigargin and H_2O_2. Fig. 5*B* shows a dose-dependent effect of okadaic acid on the Ca^{2+}-dependent enhancement of cell damage. Cells were treated with thapsigargin (5 μM) for 4 h then treated with different concentrations of okadaic acid (0–500 nM) for 30 min. Thereafter, cells were exposed to H_2O_2 (75 μM) for 2 h, and cell damage was examined using LDH release assay. Okadaic acid showed maximal cytoprotective effects at a limited concentration range around 100–200 nM. The protective effect of okadaic acid was rather diminished at concentrations higher than 500 nM (data not shown). Fig. 5*C* shows the effect of okadaic acid on Ca^{2+}-dependent enhancement of apoptosis. Cells were treated with thapsigargin (5 μM) for 4 h then treated with or without okadaic acid (100 nM) for 30 min. Then cells were exposed to H_2O_2 (75 μM) for 2 h, and apoptosis was examined by the TUNEL method. After thapsigargin treatment without okadaic acid, TUNEL-positive fluorescence intensity was significantly increased by H_2O_2 (Figs. 1*C* and 5*C*, Tg(+)OA(−)H_2O_2(+)). In contrast, okadaic acid reduced the TUNEL-positive fluorescence intensity even in the cells treated with thapsigargin and H_2O_2 (Fig. 5*C*, Tg(+)OA(+)H_2O_2(+)) compared with that of cells treated with thapsigargin and H_2O_2 without okadaic acid. Okadaic acid did not solely affect the fluorescence intensity in cells with thapsigargin without H_2O_2 (Fig. 5*C*, Tg(+)OA(−) and Tg(+)OA(+)). However, it is noteworthy that okadaic acid shows an antiapoptotic effect at a limited concentration range around 100 nM. At concentrations above 500 nM, the antiapoptotic effect of okadaic acid was diminished or rather it showed enhancement of apoptosis in the cells treated with thapsigargin and H_2O_2 (data not shown). This may be explained by the dualistic effect of inhibiting the effects of PP1 and PP2A on both apoptosis and cell proliferation in cells exposed to okadaic acid or microcystin-LR (30). Together, these results indicate that okadaic acid, a specific inhibitor of PP2A, inhibits apoptotic cell damage in H9c2 cells treated with thapsigargin and H_2O_2, and strongly suggests that PP2A up-regulates the Ca^{2+}-dependent enhancement of apoptosis by dephosphorylating Akt to inhibit cell survival signaling.

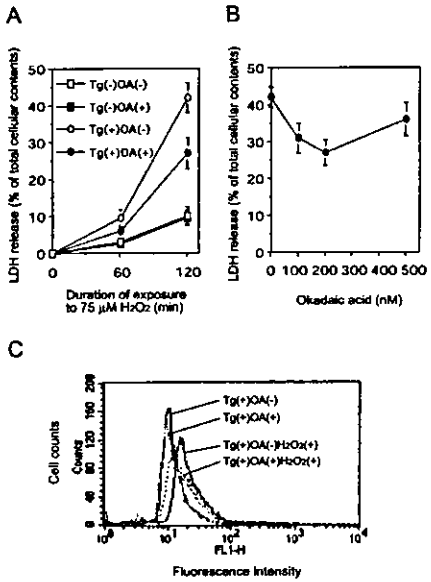

FIG. 5. **Inhibition of PP2A activity by okadaic acid suppresses apoptosis in H9c2 cells treated with thapsigargin and H_2O_2.** *A*, H9c2 cells were preincubated with or without thapsigargin (*Tg*, 5 μM) for 4 h then treated with or without okadaic acid (*OA*, 200 nM) for 30 min. Then the cells were treated with H_2O_2 (75 μM) for the periods indicated. Cell injury was estimated by measuring the release of LDH in the culture medium as described in Fig. 1*B*. Each value represents the mean ± S.D. of four independent experiments. *B*, cells were preincubated with thapsigargin (5 μM) for 4 h then treated with different concentrations of okadaic acid (0–500 nM) for 30 min. Then the cells were incubated with H_2O_2 (75 μM) for the periods indicated. Cell injury was estimated by measuring the release of LDH in the culture medium as described above. Each value represents the mean ± S.D. of four independent experiments. *C*, DNA double-stranded breaks were detected by the TUNEL method as described in Fig. 1*C*. Cells were treated with thapsigargin (5 μM) for 4 h then treated with or without okadaic acid (100 nM). Thereafter, the cells were treated with or without H_2O_2 (75 μM) for 2 h. The results were reproducible in three independent experiments.

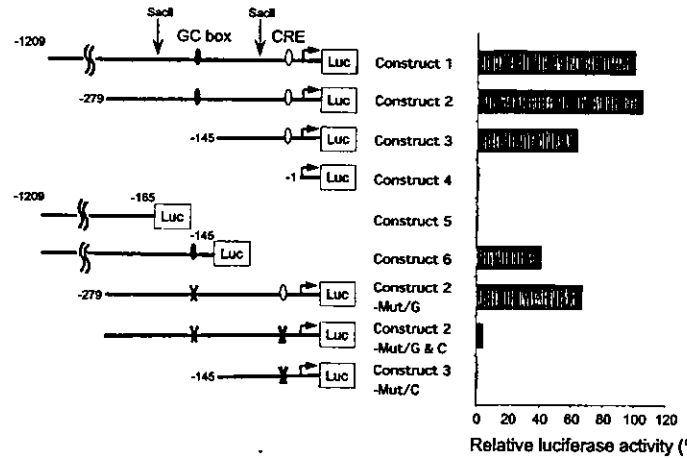

FIG. 6. **Both the GC box and CRE are important for basal activity of the PP2Acα promoter in H9c2 cells.** *Left*, schematic representation of luciferase vector constructs for the rat PP2Acα promoter. Each luciferase vector construct was generated as described under "Materials and Methods." A putative GC box site (−155) was mutated in Constructs 2-Mt/G and 2-Mt/G&C. The CRE site (−26) was mutated in Constructs 3-Mt/C and 2-Mt/G&C. *Arrows* show the transcription initiation site reported by Kitagawa *et al.* (23). *Right*, luciferase activity of the vector constructs for the rat *PP2Acα* gene promoter in H9c2 cells. The cells were transiently transfected with the *PP2Acα* promoter-luciferase gene fusion plasmids. After 24 h of transfection, luciferase activity was assayed with cellular extracts as described under "Materials and Methods." Each value represents the mean of at least three independent experiments, and the S.D. was always within 10% of the mean.

Characterization of PP2Acα Gene Promoter—To investigate the mechanism of the transcriptional regulation of PP2Acα expression, we used the 1.6-kb genomic fragment containing the promoter region of PP2Acα inserted into a luciferase vector, pGL3 Basic. The transcriptional initiation site (nucleotide +1) was denoted in accordance with the report of Kitagawa *et al.* (23) (Fig. 6, *arrows*). The promoter region contains neither a TATA box nor a consensus CAAT sequence. The promoter region contains various transcription factor binding sites such as, CRE at position −26, GC box for Sp1 (31) at positions −155 and −10, and binding sites for receptor-related orphan receptor α (RORα) (32) at positions −778 and −553.

Both CRE and Sp1 Contribute to the Basal Expression of the PP2Acα Gene—In the report by Kitagawa *et al.* (23), a fragment of 118 bp (−162 to −44) was defined as the essential region for the gene expression of *PP2Acα*. As shown in Fig. 6, the deletion fragments of the gene promoter were made from the HindIII-digested fragment (−1209 to +258, full-length) (*Construct 1*), and subcloned into a pGL3 Basic vector. Then, the activity of luciferase was assayed with the cells transfected with each deletion mutant vector. The activity was fully maintained in the 537-bp fragment (−279 to +258) (*Construct 2*), but it decreased to ~65% of the full activity in the 403-bp fragment (−145 to +258) (*Construct 3*) containing the CRE site. In the upstream fragment of 1064-bp (−1209 to −145) (*Construct 6*) containing the GC box, the activity decreased to ~40% of the full activity. However, the activity was almost lost in the upstream fragment of 1044 bp (−1209 to −165) (*Construct 5*) and the downstream fragment of 259 bp (−1 to +258) (*Construct 4*). The results indicated that the full promoter activity was located in the sequence between −279 and −1. To examine whether the CRE and GC box contribute to the full promoter activity, disabled mutants were generated for the consensus sequences of CRE at −26 and GC box at −155 in the luciferase vector containing the 537-bp Construct 2. In Construct 2-Mt/G containing a CRE but no GC box, the activity decreased to ~70% of the full activity, and the level was similar to that of Construct 3. In Construct 2-Mt/G&C, the activity was significantly suppressed to less than 5% of full activity by both mutations. Furthermore, by the mutation with CRE, the activity was completely lost in Construct 3-Mt/C. Taken together, these results indicate that both the CRE and GC box contribute to the basal expression of the *PP2Acα* gene in H9c2 cells.

Thapsigargin Enhanced Protein-CRE Complex Formation—To examine if a DNA-binding protein like Sp1 or CREB could interact with the *PP2Acα* promoter, EMSA was performed with nuclear extracts from the cells treated with 5 μM thapsigargin or 10 μM BAPTA-AM using ^{32}P-labeled oligonucleotides designed for the GC box at −155 and CRE at −26. In the case of the CRE, a major band appeared but it disappeared in the presence of an excess of unlabeled probe (not shown) or ^{32}P-labeled probe with the disabled-mutant for CRE (Fig. 7, *A* and *C*). The intensity of shifted band for CRE significantly increased with the nuclear extracts treated with thapsigargin for 1–2 h (Fig. 7*A*, *left*). In contrast, the intensity decreased with the nuclear extracts treated with BAPTA-AM for 1–2 h (Fig. 7*A*, *right*). In the case of the GC box, a major band appeared but it too disappeared in the presence of an excess of unlabeled probe (not shown) or ^{32}P-labeled probe with the disabled mutant for GC box (Fig. 7, *B* and *C*). However, the band intensity was not influenced by the treatment with thapsigargin or BAPTA-AM (Fig. 7). In the case of the GC box-like site at −10, no major band was observed in EMSA, suggesting that the site is nonfunctional (data not shown). In the case of the RORα site at −553, a gel shift was observed but was not changed by the treatment with Ca^{2+} modulators such as thapsigargin and BAPTA-AM (data not shown). Furthermore, there was no gel-shift observed with the probe for the RORα site at −778 in EMSA, suggesting that the site is nonfunctional (data not shown). Together, these results indicate that the DNA

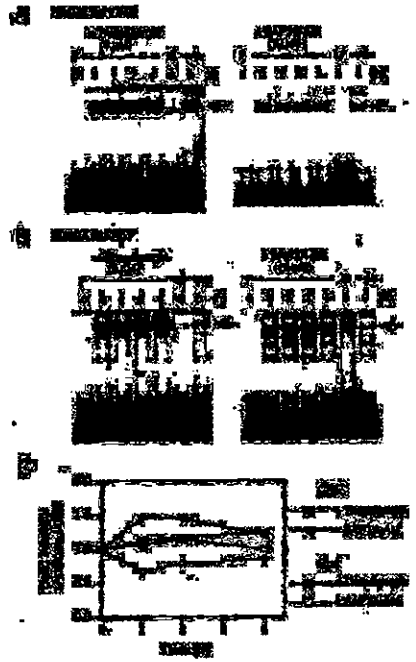

FIG. 7. **Ca^{2+} modulators influence DNA binding to CRE in EMSA.** H9c2 cells were incubated with thapsigargin (5 μM) or BAPTA-AM (10 μM) for the periods indicated, then the nuclear extracts were prepared as described under "Materials and Methods." ^{32}P-labeled oligonucleotides specific to CRE (−26) (*A*) and GC box (−155) (*B*) of the *PP2Acα* gene promoter were prepared and incubated with each nuclear extract, and then subjected to a 6% nondenatured PAGE. In *line F*, nuclear extract is free. In *line M*, ^{32}P-labeled mutant oligonucleotides were used for the original ones. In *line +Ab*, specific antibodies were added to the reaction mixture during the binding reaction for the supershift assay. *C*, quantitative data for the DNA binding to CRE and GC box shown in *A* and *B*. The intensity of gel-shift bands (*arrows*) was estimated densitometrically. Each value represents the mean of three experiments, and the S.D. was always within 10% of the mean.

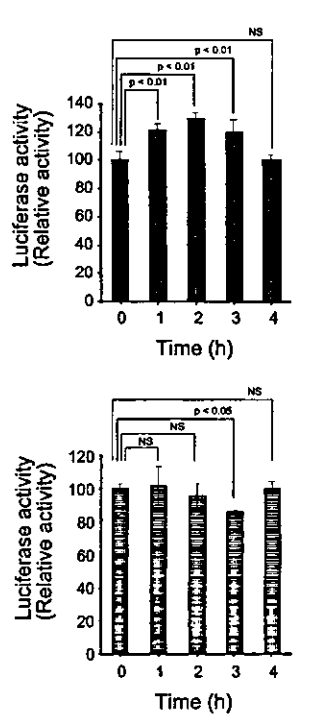

FIG. 8. **Ca^{2+} modulators influence the promoter activity of the rat *PP2Acα* gene in H9c2 cells.** H9c2 cells were transiently transfected with the *PP2Acα* promoter luciferase gene fusion plasmid (−145 to +258) (*Construct 3* in Fig. 6) containing CRE but no GC box. After 24 h of transfection, cells were treated with 5 μM thapsigargin (*A*) or 10 μM BAPTA-AM (*B*) for the periods indicated. Then luciferase activity was assayed with cell nuclear extracts as described under "Materials and Methods." Each value represents the mean ± S.D. of at least three experiments. The statistical analysis was performed with a factorial analysis of variance test.

binding activity involves both the CRE at −26 and GC box at −155, but it is specifically influenced by Ca^{2+} modulators, such as thapsigargin and BAPTA-AM, especially in the CRE at −26.

The Gene Promoter Activity of PP2Acα Is Regulated by Ca^{2+} Modulators via CRE—To confirm the CRE-dependent regulation of the gene expression of PP2Acα by Ca^{2+} modulators, the gene promoter activity was examined by assaying the luciferase activity as describe above. The cells were transfected with luciferase vector construct 3 (−145 to +258) (Fig. 6), which contains a CRE but no GC box. After 24 h of transfection, the cells were treated with 5 μM thapsigargin or 10 μM BAPTA-AM for predetermined periods, and the cell lysates were prepared and subjected to the assay for luciferase activity. As shown in Fig. 8*A*, the activity increased with thapsigargin to ~130% of the initial activity. The increase was not observed in the case of the disabled mutant for CRE with thapsigargin (data not shown). In contrast, with BAPTA-AM, the gene promoter activity decreased to ~85% of the initial level after 3 h of treatment, but returned to the initial level after 4 h (Fig. 8*B*). In the disabled mutant of CRE (*Construct 3-Mut/C* in Fig. 6), the promoter activity was lost and no activity was observed even on treatment with thapsigargin or BAPTA-AM (data not shown). Collectively, the results indicate that the gene expression of PP2Acα is transcriptionally regulated by the change of intracellular Ca^{2+} via CRE, and are consistent with the results of the EMSA for CREB binding (Fig. 6).

The Phosphorylation and Intracellular Localization of CREB Is Regulated by Ca^{2+} Modulators in H9c2 Cells—CREB is a pivotal transcription factor for the regulation of cellular survival, and its activation is mediated by phosphorylation at a specific residue, Ser-133 (33). To investigate the effect of Ca^{2+} modulators on the phosphorylation status of CREB, the level of CREB phosphorylated at Ser-133 was examined by immunoblot analysis using specific antibodies in the cells treated with thapsigargin or BAPTA-AM. As shown in Fig. 9*A*, the phosphorylation level of CREB increased on treatment with thapsigar-